Title
Distributed Control and Synchronization of Diffusively Coupled Systems

Author
Shafi, Sayed Yusef

Publication Date
2014

Peer reviewed|Thesis/dissertation

Distributed Control and Synchronization of Diffusively Coupled Systems

by

Sayed Yusef Shafi

A dissertation submitted in partial satisfaction of the

requirements for the degree of

Doctor of Philosophy

in

Engineering – Electrical Engineering and Computer Sciences

in the

Graduate Division

of the

University of California, Berkeley

Committee in charge:

Professor Murat Arcak, Chair
Professor Laurent El Ghaoui
Professor Andrew Packard

Spring 2014

Distributed Control and Synchronization of Diffusively Coupled Systems

Abstract

Distributed Control and Synchronization of Diffusively Coupled Systems

by

Sayed Yusef Shafi

Doctor of Philosophy in Engineering – Electrical Engineering and Computer Sciences

University of California, Berkeley

Professor Murat Arcak, Chair

Diffusively coupled networks, in which different components of a network adjust their behavior according to the local sum of differences between their own and neighbors' states, are a ubiquitous class of spatially-distributed models appearing in engineered and biological systems, and produce surprisingly rich dynamics. In this dissertation, we develop analysis methods and distributed algorithms that exploit the local structure of the network as well as individual component dynamics in order to guarantee the desirable operation of the aggregate network system in the absence of centralized coordination.

We begin by formulating network design problems to guarantee coordination of multi-agent systems by imposing constraints on the underlying structure of the diffusive coupling graph linking agents. The resulting constraint-derived linear matrix inequalities may then be iteratively solved using convex semidefinite programming, resulting in significant performance gains in several multi-agent systems problems. Our approach furthermore identifies critical nodes and edges in a network, and aids in developing strategies to enhance connectivity and robustness.

Next considering the case where desired steady-state trajectories may be time-varying, we derive conditions to determine whether limit cycle oscillations synchronize in diffusively coupled systems. Conversely, we highlight cases of diffusion-driven instability, a phenomenon widely hypothesized as a mechanism behind pattern formation in biological systems, in which sufficiently large diffusive coupling may destabilize a spatially homogeneous periodic orbit. The analytical and numerical conditions we derive lend insight to designing distributed laws where the local behavior about a specific attractor is of interest.

We then turn to the problem of developing distributed laws that guarantee spatially uniform behavior globally in diffusively coupled systems. We first study systems with spatially-

dependent diffusive coupling, and subsequently examine the case where the network itself has dynamics and adapts according to the agents' states. We develop adaptive laws to guarantee synchronization in systems with spatially-dependent coupling, and apply these results to a number of problems of interest arising from multi-agent systems and cooperative control. We finally address the case where the dynamics of the agents may be subject to spatially-varying input disturbances, and derive distributed laws to guarantee synchronization in the presence of such heterogeneities.

To Kay,
who has walked with me on each
step of this journey,

and

To Dadi,
who sacrificed her own dissertation
for the sake of her family.

Contents

Acknowledgments

First and foremost I thank my wife, Kay, whose steadfast love, encouragement, patience, support, and positive attitude have made it possible for me to reach this point. I am immeasurably blessed to share my life with her. I am also deeply indebted to my parents, Susan and Nadeem, for their overflowing support, high expectations, and kind words, even when I did not deserve them.

Crucial and fundamental to my graduate studies and research has been my advisor, Murat Arcak. Of course, he is an outstanding scholar and mentor, but what I am most grateful for is his constant willingness to sacrifice his time and discuss any research question. I will be forever thankful for his encouragement, confidence, and patience throughout my studies, especially when I did not believe in myself.

I especially enjoyed many spirited and fruitful research conversations with Andy Packard, one of my committee members. Ending a prolonged period of frustration following some successes in my first two years, our early discussions were vital in getting me out of what was becoming a deep morass, and for that I am truly grateful. I don't think I have ever left his office without gaining some key insight on a problem I had previously seen as intractable.

Working with Laurent El Ghaoui, another committee member and my qualifying exam chair, was a special privilege to have during my initial studies. I am thankful for his early advice to work on problems that would be interesting to anyone, although it has not always been easy to follow. Most recently I worked with him as the GSI for his optimization models in finance course, and it was a treat to put together an effective and fun course.

I am grateful to Claire Tomlin for the excellent foundation for my studies and her valuable feedback during my qualifying exam. I am deeply thankful for very smooth collaborations with Mihailo Jovanović and He Bai that helped shape my studies. I am sincerely appreciative to the outstanding staff in the EECS department, including Shirley Salanio, Xuan Quach, and Rosita Alvarez-Croft.

Graduate school is inherently about learning and working together, and I cannot express enough gratitude for the friendships I developed during my time here. Considering our research group, I am thankful to Sam Coogan, Ana S.R. Ferreira, Jansen Sheng, Justin Hsia, John Maidens, and Erin Summers, and recently Jon Tu and Eric Kim: I have really enjoyed their wit, charm, and good humor, and am excited to hear about their upcoming adventures. I am grateful for getting to know each of the many individuals I have had the good fortune to meet in and around EECS: I have never known such a simultaneously talented and kind community. In particular, fellow Albany residents and board game geeks Shangliang Jiang and Matt Weiner; Alan Malek, climbing, cocktail, coffee, and culinary connoisseur; Achintya Madduri; Elói Pereira; Kelvin So; Aude Hofleitner; and Ryan Herring have each brightened my days in Berkeley.

Life in Berkeley is not restricted to Cory Hall: I am thankful for the people of Berkeley Methodist United Church for welcoming Kay and me as family and for nurturing our growth, as well as for the support and friendship of Fangfang Xing, Michele Wang, Elizabeth Jensen, and the many Bruins on whom I have relied in my transition to and life in Northern California. I am grateful to the team at Bosch Energy Storage Solutions for giving me the opportunity to contribute to a new area of clean technology, which I hope will one day bring broad benefits to people and the planet. I am thankful also for the company and encouragement of friends, especially Andrew Rubin, and family who have visited me in and near Berkeley.

I may only hope that I can pay forward even a fraction of the abundance that each of you has shared with me. I conclude this thanksgiving with the words of Reverend Mark Nakagawa: Thanks be to God. Amen.

Chapter 1

Introduction

Spatially distributed models with diffusive coupling constitute a fundamental class of systems crucial to understanding the dynamical behavior of a range of engineered and biological systems. Diffusive coupling encompasses, among others, feedback laws for coordination of multi-agent systems [36, 59, 6, 2], electromechanical coupling of synchronous machines in power systems [9, 17], local update laws in distributed agreement algorithms [106, 11, 93, 73], and the interaction of chemical concentrations in biological networks [71, 20, 75]. Synchronization in diffusively coupled models is itself an active and rich research area [50], with applications spanning these areas and beyond. Conversely, developing conditions that rule out synchrony is also important, as such conditions facilitate the study of spatial pattern formation. One of the major ideas behind pattern formation in cells and organisms is based on diffusion-driven instability [86, 96], which occurs when higher-order spatial modes in a reaction-diffusion partial differential equation (PDE) are destabilized by diffusion [71, 20, 75, 61, 57]. Diffusion-driven instability with space-dependent coupling coefficients has also been used in developing realistic textures and patterns for computer graphics [105].

In this dissertation, we develop distributed algorithms that guarantee spatially uniform behavior in diffusively coupled systems by exploiting local network structure as well as the dynamics of the individual components of the subsystems. In doing so, we derive analysis and design tools that lend insight to the structure and behavior of diffusively coupled systems. Our methods apply both to the study of local behavior near a specific attractor, as well as that of global behavior of the full nonlinear dynamics.

We first consider the problem of designing distributed coordination laws for multi-agent systems. We propose a convex optimization framework making use of linear matrix inequalities for determining the weights of the nodes and the edges representing the coupling graph linking agents. We demonstrate the effectiveness of the strategy on several multi-agent systems problems, including formation control algorithms to achieve desired equilibrium configurations when agent dynamics can be destabilized by high gain feedback. We also study the

problem of guaranteeing synchronization of trajectories near a limit cycle. We develop numerical and analytical conditions to determine whether oscillations synchronize, and highlight cases of diffusion-driven instability.

In the remainder of the dissertation, we develop distributed laws that guarantee spatially uniform behavior when global behavior is of interest. We first discuss the case of space-dependent diffusive coupling, and then develop adaptive algorithms in which the weights of the coupling graph are adapted according to local disagreement between agents with the goal of reducing time to synchrony. We also consider the case where individual agents may be subject to disturbances. Throughout the dissertation, we present results both for compartmental systems of ODEs, in which each compartment represents a well-mixed spatial domain wherein like components in adjacent compartments are coupled by diffusion, and reaction-diffusion PDEs with Neumann boundary conditions, the spatial continuum analogue of the former setting. In Section 1.1 of this chapter, we first outline the contributions of the dissertation. We then introduce fundamental concepts that we employ throughout the dissertation in Section 1.2.

1.1 Overview of the Dissertation

Local Coordination through Coupling Weight Optimization

In Chapter 2, we study distributed control of diffusively coupled agents through the use of relative sensing information, and specifically consider the problem of guaranteeing fast convergence to a desired equilibrium formation. A well-examined tool for characterizing the interconnection topology of a network of diffusively coupled agents is the graph Laplacian matrix [18]. In particular, the spectrum of the Laplacian contains useful information about the dynamics of the network. For example, the smallest positive eigenvalue of a Laplacian, known as the algebraic connectivity, or Fiedler eigenvalue [37], is a common measure of how well connected a network is [36, 59, 73, 88]. On the other hand, the largest eigenvalue must be sufficiently small for stability of discrete-time consensus algorithms [59, 2], and for continuous-time formation control algorithms when agent dynamics can be destabilized by high gain feedback [6].

We present a scheme to enforce constraints on the Laplacian spectrum (ordered from least to greatest) by treating both node and edge weights as decision variables. Our goal is to achieve individual upper and lower bounds for several Laplacian eigenvalues simultaneously. We show how these bounds can be recast as linear matrix inequality constraints [12] that can be applied using semidefinite programming. We then study the case of larger graphs by deriving dual formulations of the optimization framework that we have developed. As demonstrated in the chapter, joint tuning of node and edge weights is an especially powerful tool that goes beyond the commonly-used edge weighting strategies for achieving spectral

constraints. Our framework furthermore addresses the problem of time-scale separation in networks in which groups of densely-connected nodes are sparsely connected with each other.

Synchronization of Limit Cycle Oscillations

Synchronization in diffusively coupled systems is essential to understanding the dynamical behavior of a range of engineered and biological systems. In Chapter 3, we study diffusively coupled nonlinear systems that exhibit limit cycles in the absence of diffusion. We develop analytical and numerical tools to determine whether diffusion stabilizes the spatially homogeneous limit cycle trajectories, thereby synchronizing the oscillations across the spatial domain. Our methods apply to reaction-diffusion PDEs conditions as well as compartmental ODEs.

In the case of sufficiently small or large diffusion, we use Floquet theory to decompose the linearized system into fast and slow time scales, and present results using *two-time scale averaging theory* [83, 94] that guarantee synchrony. In the case of diffusion coefficients of intermediate strength, we turn to a numerical approach, in which we use *harmonic balance* [101, 110] to represent the linearized system as an infinite-dimensional linear time invariant system. We make use of the structured singular value (SSV) [76] to determine stability of the linearized system in the presence of diffusion coefficients spanning a given finite interval. We apply our tests to a relaxation oscillator system and find that large enough diffusion indeed leads to loss of synchrony. Unlike standard examples of diffusion-driven instability of a homogeneous steady-state [86, 96, 71], this example demonstrates destabilization of a spatially homogeneous periodic orbit by diffusion.

Synchronization under Space-Dependent Diffusive Coupling

In Chapter 4, we present a condition that guarantees synchronization in diffusively coupled compartmental ODEs. Each set of like components has its own weighted undirected graph describing the topology of the interconnection between compartments. The condition makes use of the Jacobian of the vector field of the uncoupled dynamics as well as the Laplacian eigenvalues of each of the interconnection graphs. We present linear matrix inequalities that can be used to numerically verify the condition guaranteeing spatial uniformity, and apply the result to a coupled oscillator network. Next we turn to reaction-diffusion PDEs with diffusion terms that vary by species and in space, and derive an analogous condition guaranteeing spatial homogenization of solutions. The main contribution of the chapter is a relaxed condition to check synchronization that allows individual components to have their own specific diffusion terms and corresponding interconnection structures that may vary spatially.

Adaptive Synchronization of Diffusively Coupled Systems

In Chapter 5, we consider the case where the coupling network in addition to the nodes has dynamics. We present an adaptive algorithm that guarantees synchrony in diffusively coupled nonlinear systems using an incremental output-feedback passivity property [104, 85, 87] of the agents. A similar property was employed in [84] for static networks without adaptation. A related condition that restricts the Jacobian of the vector field describing the uncoupled dynamics was used in [1] to guarantee spatial homogeneity in reaction-diffusion PDEs, and generalized to heterogeneous diffusion in Chapter 4. Using these results as a starting point, here we first consider compartmental models and derive adaptive laws that update interconnection strengths locally to achieve sufficient connectivity for synchronization. We next consider reaction-diffusion PDEs, and show that a similar control law that adapts the strength of diffusion coefficients guarantees spatial homogeneity. We present numerical examples that demonstrate the effectiveness of adaptation in enhancing synchrony and that lend insight to understanding the structure and bottleneck edges of the network.

Synchronization under space and time-dependent heterogeneities

While the previous chapters have considered the case where each subsystem in the diffusively coupled network is identical, in Chapter 6, we consider synchronization in the presence of heterogeneities. We study diffusively coupled systems in which the nominal identical subsystems satisfy an incremental passivity property and are subject to a class of disturbance inputs including constants and sinusoids. Building on the robust DAC estimator in [7], we propose a distributed control law that achieves output synchronization in the presence of disturbances by defining an internal model subsystem at each node corresponding to the disturbance inputs. We next consider reaction-diffusion PDEs and present a distributed control law that achieves spatial homogenization in the presence of space and time-dependent disturbances. Our controller applies to systems with multiple input and output channels and allows non-identical disturbances to enter each channel.

1.2 Preliminaries

We introduce the following preliminaries of which we will make repeated use in the dissertation.

Spectral Graph Theory

We first review notions from spectral graph theory that are essential to this dissertation. A graph $\mathcal{G}$ is a collection of nodes and a corresponding set of edges, each consisting of a pair of nodes. In this dissertation, we consider undirected graphs, where two nodes are connected when there exists an edge incident to both. A graph itself is connected if there exists a sequence of edges connecting any pair of nodes in the graph.

Next, we assign an arbitrary orientation to the edges of the undirected graph $\mathcal{G}$, label the edges $\ell = 1, \ldots, M$, and introduce the $N \times M$ incidence matrix:

$$E_{i\ell} = \begin{cases} 1 & \text{if node } i \text{ is the head of edge } \ell \\ -1 & \text{if node } i \text{ is the tail of edge } \ell \\ 0 & \text{if node } i \text{ is not connected to edge } \ell. \end{cases} \tag{1.1}$$

We note that the incidence matrix is not unique for an undirected graph, and choice of orientation does not change our results.

We define the $N \times N$ graph Laplacian matrix L by

$$L = EE^T. \tag{1.2}$$

We next recall key facts about Laplacian matrices [18]. Clearly, L is symmetric positive semidefinite. Moreover, it has least one eigenvalue at zero corresponding to an eigenvector $\mathbf{1}_N = \frac{1}{\sqrt{N}}[1 \ldots 1]^T$. If the graph represented by L is connected, then L has exactly one eigenvalue at zero.

Self-Adjoint Elliptic Operators

We now turn to the spatial continuum analogue of the graph Laplacian matrix. Consider a bounded, connected domain $\Omega \subseteq \mathbb{R}^r$ with smooth boundary $\partial\Omega$, spatial variable $\chi \in \Omega$, and outward normal vector $\hat{n}(\chi)$ for $\chi \in \partial\Omega$. We consider self-adjoint elliptic operators $\mathcal{L}$ given by:

$$\mathcal{L}(\cdot) = -\nabla \cdot (d(\chi)\nabla(\cdot)), \quad d(\cdot) : \Omega \to \mathbb{R}^{r \times r}, \tag{1.3}$$

where $\nabla\cdot$ is the divergence operator and ∇ represents the gradient with respect to the spatial variable χ, the matrix-valued function $d(\chi)$ is symmetric with $d(\chi) = d(\chi)^T$ for all χ and bounded and $\exists \alpha > 0$ such that for all $\chi \in \Omega$ and for all $\zeta = (\zeta_1, \zeta_2, \ldots, \zeta_r) \in \mathbb{R}^r$, $\sum_{i,j}^r d_{ij}(\chi)\zeta_i\zeta_j \geq \alpha|\zeta|^2$.

We will make use of a Lemma following from the Poincaré principle [54, Equation (1.37)]:

Lemma 1 *Let λ_2 denote the second smallest of the Neumann eigenvalues $0 = \lambda_1 \leq \lambda_2 \leq \cdots$ of the operator $L = -\nabla \cdot (d(\chi)\nabla(\cdot))$ defined as in (1.3) on the connected, bounded domain Ω*

with smooth boundary $\partial\Omega$ and spatial variable $\chi \in \Omega$. Let $u(t,\chi)$ be a function not identically zero in $L_2(\Omega)$ with derivatives $\frac{\partial u}{\partial \chi_i} \in L_2(\Omega)$ that satisfies the Neumann boundary condition $\nabla u(t,\chi) \cdot \hat{n}(\chi) = 0$ where "$\cdot$" is the inner product in $\mathbb{R}^r$ and $\int_\Omega u(t,\chi)\, d\chi = 0$. Then the following inequality holds:

$$\int_\Omega \nabla u(t,\chi) \cdot (d(\chi)\nabla u(t,\chi))\, d\chi \geq \lambda_2 \int_\Omega u(t,\chi)^2\, d\chi. \tag{1.4}$$

□

Incremental Output-Feedback Passivity

We introduce a fundamental input-output property that characterizes several of the systems we consider in this dissertation. Consider a dynamical system H defined by:

$$H: \quad \dot{x} = f(x) + g(x)u \tag{1.5}$$
$$y = h(x), \tag{1.6}$$

in which $x \in \mathbb{R}^n$, $u \in \mathbb{R}^p$, $y \in \mathbb{R}^p$, and $f(\cdot) : \mathbb{R}^n \to \mathbb{R}^n$, $g(\cdot) : \mathbb{R}^n \to \mathbb{R}^{n\times p}$, and $h(\cdot) : \mathbb{R}^n \to \mathbb{R}^p$ are continuously differentiable maps. H_i is said to satisfy an incremental output-feedback passivity property [91, 84] if there exist a positive definite storage function $S : \mathbb{R}^n \to \mathbb{R}$ and a scalar $\theta \in \mathbb{R}$ such that for any two solution trajectories $x_a(t)$ and $x_b(t)$ of H with input-output pairs $u_a(t), y_a(t)$ and $u_b(t), y_b(t)$:

$$\frac{d}{dt}S(\delta x) =: \dot{S}(\delta x) \leq \theta \delta y^T \delta y + \delta u^T \delta y, \tag{1.7}$$

with $\delta x = x_a(t) - x_b(t)$, $\delta u = u_a(t) - u_b(t)$, and $\delta y = y_a(t) - y_b(t)$. When $\theta \leq 0$, H is called incrementally passive, and when $\theta < 0$, H is called output-strictly incrementally passive.

Chapter 2

Local Coordination through Coupling Weight Optimization

A well-studied tool for characterizing the interconnection topology of a network of distributed agents is the graph Laplacian matrix [18]. In particular, the spectrum of the Laplacian contains useful information about the dynamics of the network. For example, the smallest positive eigenvalue of a Laplacian, known as the algebraic connectivity, or Fiedler eigenvalue [37], is a common measure of how well connected a network is [36, 59, 73, 88]. On the other hand, the largest eigenvalue must be sufficiently small for stability of discrete-time consensus algorithms [59, 2], and for continuous-time formation control algorithms when agent dynamics can be destabilized by high gain feedback [6].

We present a scheme to enforce constraints on the Laplacian spectrum by treating both node and edge weights as decision variables. Let λ_i be the ith-smallest eigenvalue of the Laplacian, whose eigenvalues are ordered from least to greatest. Given $m \in \{2, \ldots, n\}$ and $\underline{\lambda}_m > 0$, the lower eigenvalue bound assignment problem is to guarantee $\lambda_m \geq \underline{\lambda}_m$. Likewise, given $p \in \{2, \ldots, n\}$ and $\overline{\lambda}_p > 0$, the upper eigenvalue bound assignment problem is to guarantee $\lambda_p \leq \overline{\lambda}_p$. Our goal is to achieve individual upper and lower bounds for several Laplacian eigenvalues simultaneously. We show how these bounds can be recast as linear matrix inequality constraints [12] that can be applied using semidefinite programming.

Convex optimization solutions to several graph problems are well-documented in the literature, including fastest distributed linear averaging (FDLA) [106], minimization of total effective resistance on a graph [46], fastest mixing Markov chains [11] and processes [93], and Fiedler eigenvalue maximization through vertex positioning [68]. In FDLA [106], a particular interconnection structure for a discrete system with symmetric interconnections is specified. The number of iterations required for linear averaging is minimized by finding a particular weight distribution that assigns iterative update laws for each node's state. The goal in many resistor network problems [46] is to minimize the total effective resistance on a graph

by assigning different weights representing resistances to the edges connecting the nodes of an electrical network. The aim for fastest mixing Markov chains [11] and processes [93] is to find the optimal transition probabilities between states to reach a stationary distribution as quickly as possible. Finally, vertex positioning [68] aims to find the optimal locations of vertices, corresponding to edge weights, in order to maximize the Fiedler eigenvalue.

Our approach is unique when compared to previous literature on optimization of the Laplacian spectrum because it is applicable to any selection of eigenvalues, and assigns weights independently to both nodes and edges. As demonstrated in the chapter, joint tuning of node and edge weights is an especially powerful tool that goes beyond the commonly-used edge weighting strategies for achieving spectral constraints.

The remainder of the chapter is organized as follows. Section 2.1 introduces preliminary results in linear algebra and spectral graph theory that are necessary for our analysis. Section 2.2 outlines a general optimization framework that enables upper and lower bounds on several Laplacian eigenvalues simultaneously based on node and edge weighting. Section 2.3 presents sample problems that can be formulated and solved using the methods of Section 2.2. Section 2.4 explores applications to multi-agent systems. Larger graphs are addressed in Section 2.5 with dual formulations of the optimization framework developed in Sections 2.2 and 2.3. We conclude in Section 2.6.

2.1 Linear Algebra Preliminaries

We review the following results from linear algebra, which we will use in Section 2.2. The first result concerns the eigenvalues of a product of two matrices ([56], Theorem 1.3.20):

Lemma 2 *Let $A \in \mathbb{R}^{r\times q}$, $B \in \mathbb{R}^{q\times r}$, and $r \geq q$. Then AB and BA have identical nonzero eigenvalues and AB has $r - q$ additional eigenvalues at zero.* □

The next lemma follows from the Courant-Fischer theorem, which characterizes the eigenvalues of a symmetric matrix ([56], Corollary 4.3.23):

Lemma 3 *If $A \in \mathbb{R}^{n\times n}$ is symmetric and if $x^TAx \geq 0$ for all vectors $x \in \mathbb{R}^n$ in a k-dimensional subspace, then A has at least k nonnegative eigenvalues.* □

Definition 1 *The square matrices A and B are* **congruent** *if $B = SAS^T$ for some square, nonsingular S.*

The following lemma is known as Sylvester's Law of Inertia ([56], Theorem 4.5.8):

Lemma 4 *Let A, $B \in \mathbb{R}^{n\times n}$ be symmetric matrices. A and B are congruent if and only if A and B have the same* inertia*, i.e., the same number of positive, negative, and zero eigenvalues.* □

An inequality due to Sylvester characterizes the relationship between the eigenvalues of two matrices and their products ([43], Section 3.5):

Lemma 5 *Given two matrices $A \in \mathbb{R}^{r\times n}$ and $B \in \mathbb{R}^{n\times q}$, the following inequality holds:*

$$rank(A) + rank(B) - n \leq rank(AB) \leq \min\{rank(A), rank(B)\}.$$

□

Next, consider an undirected graph $\mathcal{G}$. We denote by $L = EE^T$ the $n \times n$ graph Laplacian matrix where E is an incidence matrix of $\mathcal{G}$ as defined in (1.1). We define by $L_e = EKE^T$ the *edge-weighted Laplacian*, where $K \succeq 0$ is the diagonal *edge weighting matrix*. We denote by $L_g = M^{-1}EKE^T$ the *node- and edge- weighted graph Laplacian* (henceforth *weighted Laplacian*), where $M \succ 0$ is the diagonal *node weighting matrix*. Note that L_e retains the properties of L in Section 1.2. Although L_g is not symmetric in general, its eigenvalues possess properties similar to those of L and L_e:

Lemma 6 *Every eigenvalue of $L_g = M^{-1}EKE^T$ is real and nonnegative. If L_g represents a connected graph, then all eigenvalues of L_g, excepting one at zero, are positive.* □

Proof: A similarity transformation brings L_g to the symmetric form $M^{-1/2}L_eM^{-1/2}$, and so all eigenvalues of L_g are real. Furthermore, the symmetric matrices $M^{-1/2}L_eM^{-1/2}$ and L_e are congruent, and hence Lemma 4 guarantees that all eigenvalues of L_g are nonnegative. When L_e represents a connected graph, and, thus, has only one eigenvalue at zero, Lemma 4 implies that all eigenvalues of L_g, excepting one at zero, are positive.

2.2 Convex Characterizations of Upper and Lower Eigenvalue Constraints

Our goal is to find node and edge weighting matrices M and K, respectively, to assign individual lower and upper bounds for several eigenvalues of L_g simultaneously. Let $\lambda_k(L_g)$ denote the k-th smallest eigenvalue of L_g. Given $a, b \leq N$, define the sets of indices $\{m_i\}_{i=1}^a$ and $\{p_i\}_{i=1}^b$ with each $2 \leq m_i \leq N$ and $2 \leq p_j \leq N$ an integer contained in $\{2, N\}$. Define the sets of positive scalars $\{\underline{\lambda}_{m_i}\}_{i=1}^a$ and $\{\overline{\lambda}_{p_j}\}_{j=1}^b$. We wish to see if there exist M and K that satisfy the constraints in the following problem:

$$\begin{array}{ll} \text{Find} & M,\, K \\ \text{subject to} & \lambda_{m_i}(L_g) \geq \underline{\lambda}_{m_i},\, i = 1, \ldots, a \\ & \lambda_{p_j}(L_g) \leq \overline{\lambda}_{p_j},\, j = 1, \ldots, b. \end{array} \tag{2.1}$$

A. Bounding Eigenvalues from Below

Given $m < N$ and $\underline{\lambda}_m > 0$, we wish to design node and edge weights M and K, respectively, such that $\lambda_m(L_g) \geq \underline{\lambda}_m$. We note that by itself, the lower eigenvalue bound $\lambda_m(L_g) \geq \underline{\lambda}_m$ can be enforced by scaling M by $\frac{\lambda_m(L)}{\underline{\lambda}_m}$ or K by $\frac{\underline{\lambda}_m}{\lambda_m(L)}$. However, when the graph optimization problem also imposes upper eigenvalue constraints as in (2.1) or objective functions, this approach would likely be infeasible. In contrast, our results make it possible to apply several upper and lower eigenvalue bounds at once. To begin, we construct a linear matrix inequality enforcing the eigenvalue constraint, making use of the following lemma:

Lemma 7 *Suppose that $m < N$, $Q_m \in \mathbb{R}^{N \times (N-m+1)}$ is a full column rank matrix whose columns are orthogonal, and S is a symmetric matrix. If $Q_m^T S Q_m \succeq 0$, then $\lambda_m(S) \geq 0$.* □

Proof: The result follows immediately from Lemma 3: the subspace spanned by the columns of Q_m is $N - m + 1$ dimensional, so $\lambda_m(S) \geq 0$. □

The next theorem provides a sufficient condition in the form of a linear matrix inequality constraint to enforce lower eigenvalue bounds:

Theorem 2 *Let Q_m be as in Lemma 7. The constraint*

$$Q_m^T(L_e - \underline{\lambda}_m M)Q_m \succeq 0 \tag{2.2}$$

implies that $\lambda_m(L_g) \geq \underline{\lambda}_m$. □

Proof: First, we note by Lemma 7 that if (2.2) holds, then the matrix $L_e - \underline{\lambda}_m M$ has at most $m - 1$ negative eigenvalues. By congruence, $M^{-1/2} L_e M^{-1/2} - \underline{\lambda}_m I$ has at most $m - 1$ negative eigenvalues, which means that the symmetric positive semidefinite matrix $L_s \triangleq M^{-1/2} L_e M^{-1/2}$ has at most $m - 1$ eigenvalues less than $\underline{\lambda}_m$. Similarity of L_g to L_s implies that L_g has at most $m - 1$ eigenvalues less than $\underline{\lambda}_m$, implying that $\lambda_m(L_g) \geq \underline{\lambda}_m$. □

We now present a convex feasibility program that enforces the lower eigenvalue bound sufficient linear matrix inequality condition of Theorem 2:

$$\begin{array}{ll} \text{Find} & M,\, K \\ \text{subject to} & Q_m^T(EKE^T - \underline{\lambda}_m M)Q_m \succeq 0 \\ & M \succ 0,\, K \succeq 0;\, M,\, K \text{ diagonal.} \end{array} \tag{2.3}$$

Theorem 2 provides only a sufficient condition to imply $\lambda_m(L_g) \geq \underline{\lambda}_m$, because the choice of Q_m is arbitrary. We now present a necessary and sufficient condition enabled by a specific choice of Q_m:

Theorem 3 *The inequality $\lambda_m(L_g) \geq \underline{\lambda}_m$ holds if and only if $\mathcal{Q}_m^T(L_e - \underline{\lambda}_m M)\mathcal{Q}_m \succeq 0$, where $\mathcal{Q}_m \in \mathbb{R}^{N\times(N-m+1)}$ is the matrix whose columns are the eigenvectors corresponding to the $N-m+1$ largest eigenvalues of $L_e - \underline{\lambda}_m M$.* □

Proof: Necessity follows from Theorem 2. To prove sufficiency, suppose that $\lambda_m(L_g) \geq \underline{\lambda}_m$. By similarity, $L_s = M^{-1/2}L_eM^{-1/2}$ has the same spectrum as L_g. Then $L_s - \underline{\lambda}_m I$ has at most $m-1$ negative eigenvalues. By congruence, so does $L_e - \underline{\lambda}_m M$. Considering the projection matrix $\mathcal{Q}_m\mathcal{Q}_m^T$, it follows that $(L_e - \underline{\lambda}_m M)\mathcal{Q}_m\mathcal{Q}_m^T$ must have exclusively nonnegative eigenvalues. Lemma 2 then implies that $\mathcal{Q}_m^T(L_e - \underline{\lambda}_m M)\mathcal{Q}_m \succeq 0$. □

Theorem 3 is the basis for an iterative procedure presented in Section 2.3-A that allows for improved performance when the constraints of (2.3) are paired with an objective.

B. Bounding Eigenvalues from Above

Given $p \leq N$ and $\overline{\lambda}_p \geq 0$, we wish to design node and edge weights M and K, respectively, such that $\lambda_p(L_g) \leq \overline{\lambda}_p$. We construct a linear matrix inequality enforcing this eigenvalue constraint. The analysis is similar to that of the previous section, and so the proofs are omitted.

Theorem 4 *Let $U_p \in \mathbb{R}^{N\times p}$ be a full column rank matrix whose columns are orthogonal. The constraint*

$$U_p^T(\overline{\lambda}_p M - L_e)U_p \succeq 0 \tag{2.4}$$

implies that $\lambda_p(L_G) \leq \overline{\lambda}_p$. □

We now present a convex feasibility program that enforces the upper eigenvalue bound sufficient linear matrix inequality condition of Theorem 4:

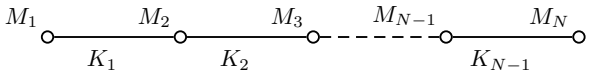

Figure 2.1: A chain graph with N nodes.

$$\begin{array}{ll} \text{Find} & M,\, K \\ \text{subject to} & U_p^T(\overline{\lambda}_p M - EKE^T)U_p \succeq 0 \\ & M \succ 0,\, K \succeq 0;\, M,\, K \text{ diagonal.} \end{array} \tag{2.5}$$

As in the case of bounding eigenvalues from below, Theorem 4 provides only a sufficient condition to imply $\lambda_p(L_g) \leq \overline{\lambda}_p$. The following theorem gives a necessary and sufficient condition enabled by a specific choice of U_p:

Theorem 5 *The inequality $\lambda_p(L_g) \leq \overline{\lambda}_p$ holds if and only if $\mathcal{U}_p^T(\overline{\lambda}_p M - L_e)\mathcal{U}_p \succeq 0$, where $\mathcal{U}_p \in \mathbb{R}^{N\times p}$ is the matrix whose columns are the eigenvectors corresponding to the p smallest eigenvalues of $\overline{\lambda}_p M - L_e$.* □

An iterative procedure presented in Section 2.3-B employs Theorem 5 and allows for improved performance when the constraints of (2.3) and (2.5) are paired with an objective. A special case of Theorem 5 is when $p = N$. In this case, the $\mathcal{U}_p$ that satisfies Theorem 5 is a square, orthogonal matrix, and thus the eigenvalues of $\mathcal{U}_p^T(\overline{\lambda}_p M - EKE^T)\mathcal{U}_p$ and $\overline{\lambda}_p M - EKE^T$ are equal by Lemma 2. Theorem 5 therefore simplifies to the following corollary:

Corollary 1 *The inequality $\lambda_N(L_g) \leq \overline{\lambda}_N$ holds if and only if $\overline{\lambda}_N M - L_e \succeq 0$.* □

2.3 Examples of Graph Design Problems

We provide two sample problems that can be addressed by combining (2.3) and (2.5), demonstrating the flexibility of our formulation to impose individual constraints on several eigenvalues simultaneously. In our numerical examples, we require that all node and edge weights be contained in $[\epsilon, \epsilon^{-1}]$, where $\epsilon < 1$ is a small positive parameter that guarantees that the largest and smallest weights do not have too great a relative difference. Smaller values of ϵ increase the number of feasible M and K matrices, making it more likely that any given constraint set is feasible, but run the risk of numerical loss of precision with very large differences in individual node and edge weightings. We perform our numerical examples using `CVX`, a package for *disciplined convex programming* [48] [49], and the SDPT3 interior point solver [95].

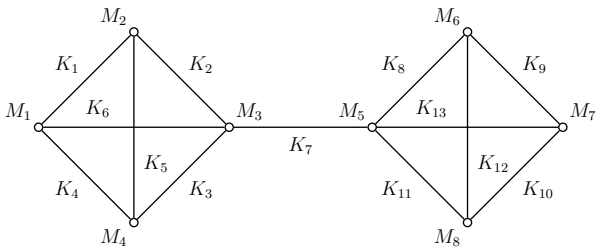

Figure 2.2: An eight node graph with two clusters.

A. Minimizing the Largest Eigenvalue Given a Minimum Connectivity Constraint

In formation control problems (see, e.g., Section 2.4), it is desirable to have a lower bound on λ_2 to ensure adequate convergence time while at the same time imposing an upper bound on λ_N for stability. We present the problem of minimizing the largest eigenvalue $\lambda_N(L_g)$ of a graph given the requirement $\lambda_2(L_g) \geq \underline{\lambda}_2$, making use of (2.3) and (2.5) as well as including upper and lower bounds on the entries of M and K:

$$\begin{aligned} \underset{\kappa,M,K}{\text{minimize}} \quad & \kappa \\ \text{subject to} \quad & \kappa\underline{\lambda}_2 M - EKE^T \succeq 0 \\ & Q_2^T(EKE^T - \underline{\lambda}_2 M)Q_2 \succeq 0 \\ & \epsilon^{-1}I \succeq M \succeq \epsilon I, \epsilon^{-1}I \succeq K \succeq \epsilon I;\ M,\ K \text{ diagonal.} \end{aligned} \tag{2.6}$$

The problem is quasiconvex for any $Q_2 \in \mathbb{R}^{N\times(N-1)}$. To find the optimal $\kappa = \frac{\lambda_N(L_g)}{\underline{\lambda}_2}$ for the problem, we perform a bisection on the interval $[\underline{\lambda}_2, \lambda_N(L)]$, where in each iteration, a convex feasibility problem is solved for the value of κ given by the bisection. As discussed in Section 2.2-A, an arbitrary choice of Q_2 may lead to conservatism in the optimal κ achieved. To improve the value of κ, we propose Algorithm 1, which makes use of Theorem 3 and updates Q_2.

Algorithm 1 Iterative Updates for Q_2

1: $M \Leftarrow I$, $K \Leftarrow I$, $\mu > 0$.
2: **repeat**
3: Set Q_2 to be the matrix whose columns are the eigenvectors corresponding to the $N-1$ largest eigenvalues of $EKE^T - \underline{\lambda}_2 M$.
4: Solve (2.6) and update M, K.
5: **until** $|\kappa_i - \kappa_{i-1}| \leq \mu$ OR ($\max(M) = \epsilon^{-1}$ AND $\min(M) = \epsilon$) OR ($\max(K) = \epsilon^{-1}$ AND $\min(K) = \epsilon$).

We note that when M and K are identity and Q_2 is initialized as in Algorithm 1, the columns of Q_2 are orthogonal both to each other and to $\mathbf{1}_n$. In our implementation, we choose μ to be very small, and the effective stopping criteria are the conditions on M and K involving ϵ. The parameter ϵ can be tuned by being made smaller or larger to achieve improved or worsened values of κ with the resulting difference $|\kappa_i - \kappa_{i-1}|$ relatively smaller or larger, respectively, when the algorithm terminates.

Numerical Example: For an unweighted chain graph with twenty nodes obeying the structure of Figure 2.1, we have $\lambda_2(L) = 0.025$ and $\kappa = \frac{\lambda_{20}(L)}{\lambda_2(L)} = 161.602$. We set $\epsilon = 10^{-2}$, and apply our method to reduce κ. For the first three experiments, (2.6) was solved with Q_2 set to be a matrix whose $N-1$ columns are orthogonal to $\mathbf{1}_N$. The lower eigenvalue bound was set to be $\underline{\lambda}_2 = \lambda_2(L)$. Solving for edges only, with nodes weighted to identity, produced no re-weighting of edges, and so κ was unchanged. In contrast, solving for nodes only, with edges weighted to identity, resulted in $\kappa = 123.529$. Simultaneous optimization with both the nodes and edges as decision variables produced a marked improvement to $\kappa = 52.862$. Allowing Q_2 to vary in accordance with Algorithm 1 described above resulted in $\kappa = 13.050$. By setting $\epsilon = 10^{-3}$, we achieved $\kappa = 6.302$.

B. Minimizing the Gap between λ_p and λ_{p+1}

We consider graphs with *clusters*, that is, groupings of densely connected nodes with sparse external edges. The Laplacian of a graph with p clusters exhibits, in addition to the first eigenvalue at zero, $p-1$ additional eigenvalues close to zero. Thus, in such graphs, there is a gap between the first p eigenvalues and the rest. Examples of systems obeying the clustered structure have been studied in building sensor networks [66] and power systems [17], where distributed estimation algorithms are increasingly prevalent. The gap in the eigenvalues may be undesirable because it leads to a two-time-scale behavior in the convergence of these algorithms [9].

To obtain uniform convergence rates for nodes in different clusters, we maximize λ_2 while requiring $\lambda_{p+1} \leq \overline{\lambda}_{p+1}$, and in so doing, minimize the gap between $\lambda_p(L_g)$ and $\lambda_{p+1}(L_g)$. Additionally, we fix $\lambda_N(L_g) \leq \overline{\lambda}_N$, so that the rest of the spectrum of the weighted Laplacian does not deviate far from its original location. The problem is solved with a bisection to maximize κ on the interval $[\lambda_2(L), \overline{\lambda}_{p+1}]$. We impose upper and lower bounds on the entries of M and K, and introduce $Q_2 \in \mathbb{R}^{N\times(N-1)}$ and $U_{p+1} \in \mathbb{R}^{N\times(p+1)}$ defined according to Theorems 2 and 4, respectively. We now write the quasiconvex problem, with $\kappa = \frac{\overline{\lambda}_{p+1}}{\lambda_2(L_g)}$:

$$\begin{array}{ll} \underset{\kappa,M,K}{\text{maximize}} & \kappa \\ \text{subject to} & \overline{\lambda}_N M - EKE^T \succeq 0 \\ & Q_2^T(EKE^T - \kappa M)Q_2 \succeq 0 \\ & U_{p+1}^T(\overline{\lambda}_{p+1} M - EKE^T)U_{p+1} \succeq 0 \\ & \epsilon^{-1} I \succeq M \succeq \epsilon I,\ \epsilon^{-1} I \succeq K \succeq \epsilon I,\ M,\ K \text{ diagonal.} \end{array} \tag{2.7}$$

We can realize significant improvements in reducing the gap between $\lambda_p(L_g)$ and $\lambda_{p+1}(L_g)$ by employing Algorithm 2, an iterative procedure similar to Algorithm 1 of Section 2.3-A.

Algorithm 2 Iterative Updates for Q_2, U_{p+1}

1: $M \Leftarrow I$, $K \Leftarrow I$, $\mu > 0$.
2: **repeat**
3: Set Q_2 to be the matrix whose columns are the eigenvectors corresponding to the $N-1$ largest eigenvalues of $EKE^T - \underline{\lambda}_2 M$.
4: Set U_{p+1} to be the matrix whose columns are the eigenvectors corresponding to the $p+1$ smallest eigenvalues of $\overline{\lambda}_{p+1} M - EKE^T$.
5: Solve (2.7) and update M, K.
6: **until** $|\kappa_i - \kappa_{i-1}| \leq \mu$ OR $(\max(M) = \epsilon^{-1}$ AND $\min(M) = \epsilon)$ OR $(\max(K) = \epsilon^{-1}$ AND $\min(K) = \epsilon)$.

Numerical Example: Consider the eight node graph with two clusters in Figure 2.2. Such a graph, with identical weights, exhibits a significant gap between λ_2 and λ_3. We have the relation $\frac{\lambda_3(L)}{\lambda_2(L)} = 11.293$, with the eigenvalues of the unweighted graph at $\{0.000,\ 0.354,\ 4.000,\ 4.000,\ \ldots,\ 4.000,\ 5.646\}$. Our goal is to reduce the gap $\frac{\lambda_3(L)}{\lambda_2(L)}$ by increasing the second eigenvalue while bounding the third and eighth eigenvalues from above. To do so, we employ Algorithm 2, iteratively updating both Q_2 and U_3 while requiring $\lambda_3(L_g) \leq 4.000$ and $\lambda_N(L_g) \leq 5.646$ and setting $\epsilon = 10^{-2}$. We find the optimal value $\lambda_2(L_g) = 4.000$, with $\frac{\lambda_3(L_g)}{\lambda_2(L_g)} = 1$.

2.4 Application to Multi-Agent Systems

We now apply the results of Section 2.3-A to multi-agent systems whose feedback structure is described by a graph Laplacian.

Each of the N subsystems possesses identical dynamics:

$$H_i : \left\{ \begin{array}{rcl} \dot{x}_i &=& Ax_i + Bu_i \\ y_i &=& Cx_i. \end{array} \right. \tag{2.8}$$

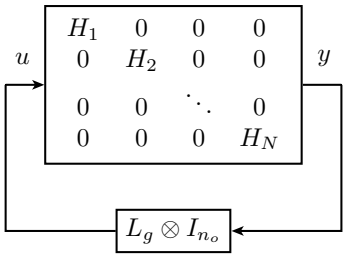

Figure 2.3: Block diagram of the multi-agent system (2.8-2.9).

and is controlled according to the feedback law:

$$u_i = -M_i^{-1} \sum_{j \in \mathcal{N}_i} K_j (y_i - y_j), \tag{2.9}$$

where $A \in \mathbb{R}^{n \times n}$, $B \in \mathbb{R}^{n \times n_o}$, and $C \in \mathbb{R}^{n_o \times n}$, with n and n_o the dimension of the state space and input and output, respectively. The set $\mathcal{N}_i$ consists of the neighbors j of agent i, that is, the other agents whom agent i senses. We assume that the individual plants are stable or can be stabilized by local state feedback (see the numerical example below). Therefore, we assume that A is Hurwitz. M_i and K_j denote entries i and j of the diagonal node and edge weighting matrices M and K, respectively. The block diagram of the system is shown in Figure 2.3, with each subsystem H_i having input given by (2.9). We let $x = [x_1^T, \ldots, x_N^T]^T$, and rewrite (2.8) and (2.9) as:

$$\dot{x} = [I_N \otimes A - L_g \otimes (BC)]x. \tag{2.10}$$

As a consequence of the identical dynamics of each subsystem, the system can be decoupled into n identical subsystems by a change of coordinates using the basis of eigenvectors of L_g [36]. Let U be the orthogonal change-of-coordinates matrix that diagonalizes L_g and let Λ be the diagonal matrix of eigenvalues of L_g. Then $\Lambda = U^{-1} L_g U$. Now let $V = U \otimes I$, and let $\tilde{x} = V^{-1} x$. In the new coordinates, the dynamics are given by:

$$\dot{\tilde{x}} = [I_N \otimes A - \Lambda \otimes (BC)]\tilde{x}, \tag{2.11}$$

and, thus, the eigenvalues are determined from the characteristic polynomials of $A - \lambda_i(L_g)BC$, $i = 1, \ldots, N$. This means that the multi-agent system can be analyzed as n decoupled feedback systems with constant gain $\lambda_i(L_g)$, $i = 1, \ldots, N$. In particular, larger Laplacian eigenvalues imply higher gains for these decoupled systems, which is often undesirable. For example, if the transfer function $C(sI - A)^{-1}B$ has non-minimum phase zeros or relative degree higher than two, high gain will result in right half plane poles, rendering the multi-agent system unstable. The largest eigenvalue minimization method of Section 2.3-A can

mitigate this instability by finding a node and edge weighting such that the spectrum of L_g spectrum falls within a range specified by design requirements.

Numerical Example: We consider formation control for four planar vertical takeoff and landing, or PVTOL, aircraft, as described in [82]. We model the state of the aircraft by its lateral position, x, vertical position y, and its roll, θ. The equations of motion, in input-output linearized form, are given by the following:

$$\begin{aligned} \ddot{x} &= u_1 \\ \ddot{y} &= u_2 \\ \ddot{\theta} &= \epsilon^{-1}(\sin\theta + \cos\theta u_1 + \sin\theta u_2). \end{aligned} \tag{2.12}$$

The zero dynamics of the system are unstable and the system is non-minimum phase:

$$\ddot{\theta} = \epsilon^{-1}\sin\theta. \tag{2.13}$$

We assume that the aircraft are in hover operation and are stabilized vertically, so we discard y and u_2, the vertical thrust input. We set $\epsilon = 0.1$ and see that the linearized dynamics around $x = 0$, $\theta = 0$ are:

$$\tilde{A} = \begin{bmatrix} 0 & 1 & 0 & 0 \\ 0 & 0 & 0 & 0 \\ 0 & 0 & 0 & 1 \\ 0 & 0 & 10 & 0 \end{bmatrix} \quad B = \begin{bmatrix} 0 \\ 1 \\ 0 \\ 10 \end{bmatrix} \quad C = \begin{bmatrix} -1 \\ 0 \\ 0 \\ 0 \end{bmatrix}^T. \tag{2.14}$$

The input to each aircraft is dictated by the input term of (2.8), with the graph structure of a four node chain. We choose a state feedback $J = [\ 0 \quad -90.616 \quad 42.147 \quad 13.216\ ]$, which renders $A = \tilde{A} - BJ$ Hurwitz. To achieve a reasonable response time and to maintain stability, we wish to contain the eigenvalues of the weighted Laplacian in the interval $[50, 125]$. In particular, the upper bound of this interval guarantees a damping ratio greater than 0.6. For the unweighted Laplacian, we have $\kappa = \frac{\lambda_4(L)}{\lambda_2(L)} = 5.828$, which means that scaling the Laplacian by a constant $\alpha = \frac{50}{\lambda_2(L)}$ to meet the lower eigenvalue constraint $\lambda_2(\alpha L) \geq 50$ will violate the upper eigenvalue constraint $\lambda_4(\alpha L) \leq 125$ and lead to instability as illustrated in Figure 2.4. In contrast, applying the node and edge weights found by applying Algorithm 1 results in an improvement to $\kappa = 1.020$. We show simulation results with the new weights in Figure 2.5.

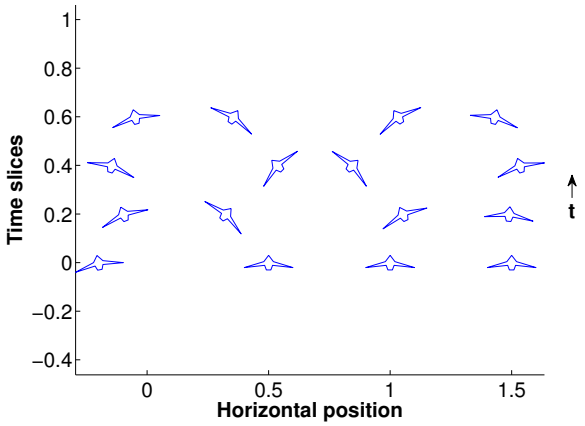

Figure 2.4: PVTOL formation of four aircraft with unweighted, scaled graph. Each row represents a snapshot in time in ascending order. Each aircraft's maximum roll angle and amplitude of deviation from the desired relative position increases in time, indicating instability.

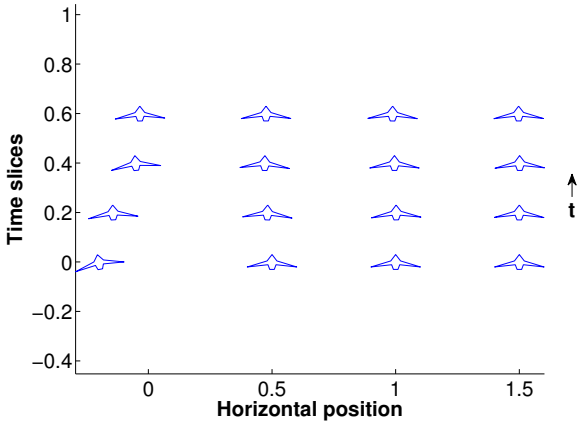

Figure 2.5: PVTOL formation of four aircraft with weighted graph. Each row represents a snapshot in time in ascending order. Each aircraft's maximum roll angle and amplitude of deviation from the desired relative position of the aircraft decrease in time as it converges to formation.

2.5 Dual Formulation of the Largest Eigenvalue Minimization Problem

Popular interior point methods, such as SDPT3 [95], when applied to the convex problems derived Section 2.3, are limited as to the size of graph they can handle, breaking down for many graphs with more than several tens of nodes. We show how using Lagrangian dual formulations enables our eigenvalue optimization framework to accommodate graphs with several hundred nodes and edges. In the following exposition, we derive the dual of the largest eigenvalue minimization problem of Section 2.3-A.

We begin with the convex problem solved as part of the solution to the largest eigenvalue minimization problem. We denote by $\langle \cdot, \cdot \rangle$ the trace inner product of two matrices of appropriate dimension. We set $Q \in \mathbb{R}^{N \times (N-1)}$ to be a matrix with columns orthogonal to each other and to $\mathbf{1}_n$. The convex problem we dualize is:

$$\begin{array}{ll} \text{Find} & K, M \\ \text{subject to} & \kappa M - EKE^T \succeq 0 \\ & Q^T(EKE^T - M)Q \succeq 0 \\ & M \succeq \epsilon I,\ K \succeq 0; M,\ K \text{ diagonal.} \end{array} \tag{2.15}$$

To derive the dual problem, we note that the Lagrangian function is:

$$\begin{aligned} L(K, M, Z, R, v, w) = &- \langle Z, \kappa M - EKE^T \rangle \\ &- \langle R, Q^T(EKE^T - M)Q \rangle \\ &- v^T(\text{diag}(M) - \epsilon \mathbf{1}_N) - w^T \text{diag}(K). \end{aligned} \tag{2.16}$$

We seek to obtain a finite minimization of the Lagrangian function with respect to M and K. Thus, minimizing (2.16) with respect to M yields the constraint:

$$\text{diag}(\tilde{R} - \kappa Z) = v, \tag{2.17}$$

where we have defined a new variable $\tilde{R} = QRQ^T$, from which we observe that $\tilde{R}\mathbf{1}_n = 0$. Likewise, minimizing the Lagrangian with respect to K yields the constraint:

$$\text{diag}(E^T(Z - \tilde{R})E) = w. \tag{2.18}$$

To express the nullspace constraint on $\tilde{R}$ as a single equality constraint, we begin by defining the matrix $E \in \mathbb{R}^{N \times N}$ to be $E = \mathbf{1}_N \mathbf{1}_N^T$, and state and prove the following lemma:

Lemma 8 *Let G be a positive semidefinite matrix. Then $G\mathbf{1}_N = 0$ if and only if $\langle G, E \rangle = 0$.* □

Table 2.1: Random Graphs with N Nodes and m Edges

N, m, κ	Primal Runtime (s)	Dual Runtime (s)
50, 100, 3	16.066	4.594
50, 500, 1.5	48.666	7.986
100, 200, 3	141.267	11.724
100, 1000, 1.5	N/A	27.186
200, 400, 3	N/A	32.980

Proof: $G\mathbf{1}_N = 0 \iff \mathbf{1}_N^T G \mathbf{1}_N = 0 \iff \mathrm{tr}(\mathbf{1}_N^T G \mathbf{1}_N) = 0 \iff \langle G, E \rangle = 0.$ □

Combining the constraints found by minimizing (2.16) with respect to M and K, we now write the resulting dual problem, where we have eliminated the slack variable w:

$$\begin{array}{ll} \underset{Z,\tilde{R},v}{\text{maximize}} & \mathbf{1}_n^T v \\ \text{subject to} & \mathrm{diag}(E^T(Z - \tilde{R})E) \geq 0 \\ & \mathrm{diag}(\tilde{R} - \kappa Z) = v \\ & \langle \tilde{R}, E \rangle = 0 \\ & Z, \tilde{R} \succeq 0,\ v \geq 0. \end{array} \tag{2.19}$$

The dual problem we have derived explicitly separates semidefinite matrix variables and linear variables as well as limits the growth of the number of equality constraints to scale linearly with the number of nodes and edges in the graph. Solving it using interior point methods is reasonably fast for graphs with up to 1000 edges, meaning that in addition to being substantially faster than the primal formulation, the dual formulation can accommodate significantly larger graphs.

We compare the performance of the SDPT3 algorithm on the primal and dual problems. The goal is to find feasible M and K matrices for (2.15) and (2.19) given κ. We characterize the performance in terms of CPU runtime in seconds on an Intel Quad Core 2 Duo 2.2 GHz system with 8 GB of RAM. In Table 2.1, we consider random graphs with N nodes, m edges, and parameter κ, while in Table 2.2, we consider chain graphs with N nodes with $\kappa = 3$. As compared to the primal formulation, the dual formulation can accommodate graphs with an order of magnitude more nodes.

Table 2.2: Chain Graphs with N Nodes

N	Primal Runtime (s)	Dual Runtime (s)
50	21.076	7.223
100	N/A	18.861
200	N/A	44.928
400	N/A	207.388

2.6 Conclusion

The graph Laplacian is an indispensable tool for assessing the dynamics of a multi-agent system. In this chapter, we have presented a novel approach to impose bounds on the Laplacian spectrum. We have shown how node and edge weights can be adjusted using convex optimization to impose individual constraints on several eigenvalues simultaneously. Finally, we have demonstrated the effectiveness of the approach on multi-agent systems problems arising in formation control and time-scale separated networks.

Chapter 3

Synchronization of Limit Cycle Oscillations

Diffusively coupled models are crucial to understanding the dynamical behavior of a range of engineering and biological systems. In particular, synchronization of diffusively coupled models is an active and rich research area [50]. Conversely, developing conditions that rule out synchrony is also important, as these conditions can facilitate study of spatial pattern formation. One of the major ideas behind pattern formation in cells and organisms is based on diffusion-driven instability [86, 96], which occurs when higher-order spatial modes in a reaction-diffusion partial differential equation (PDE) are destabilized by diffusion [71, 20, 75, 61, 57].

The majority of synchronization studies address phase coupled oscillators [69, 92, 16, 30], which rely on the assumption of weak coupling to be able to represent the subsystems with a single phase variable. Full state models have been studied in [1, 79, 98, 91, 80, 84]; however, these references derive global results that may be conservative when synchronization of trajectories close to a specific attractor, such as a limit cycle, is of interest. The reference [78] gives a method to determine synchronization applicable to a wide class of coupled oscillators; however, it does not allow direct determination of synchronization for intervals of diffusion coefficients and may encounter loss of accuracy due to difficulties in numerically computing the state transition matrix.

In this chapter, we study diffusively coupled nonlinear systems that exhibit limit cycles in the absence of diffusion. We develop analytical and numerical tools to determine whether diffusion stabilizes the spatially homogeneous limit cycle trajectories, thereby synchronizing the oscillations across the spatial domain. Our methods apply to reaction-diffusion PDEs with Neumann boundary conditions as well as compartmental ODEs. In the latter case, each compartment has identical dynamics and represents a well-mixed spatial domain wherein like components in adjacent compartments are coupled by diffusion.

We first linearize the system about an asymptotically stable limit cycle trajectory and then study the resulting periodic linear time varying system. In both the PDE and ODE cases, synchrony amounts to stability of an auxiliary system of the form

$$\dot{x} = (A(t) - \lambda_k D)x, \tag{3.1}$$

where $A(t)$ is periodic, D is a matrix of diffusion coefficients, and λ_k is the kth eigenvalue of the Laplacian operator (for PDEs) or matrix (for ODEs). In the case of sufficiently small or large diffusion, we use Floquet theory to decompose the linearized system into fast and slow time scales, and present results using *two-time scale averaging theory* [83, 94] that guarantee synchrony. In the case of diffusion coefficients of intermediate strength, we turn to a numerical approach, in which we use *harmonic balance* [101, 110] to represent the linearized system as an infinite-dimensional linear time invariant system.

We make use of concepts from robust control, in particular the structured singular value (SSV) [76], to determine stability of the linearized system in the presence of diffusion coefficients spanning a specified finite interval. In particular, our method extends the notion of structured singular value to the infinite-dimensional harmonic transfer operators that may be used to describe the frequency-domain behavior of periodic linear time-varying systems. We apply our tests to a relaxation oscillator system and find that large enough diffusion can indeed lead to loss of synchrony. Unlike standard examples of diffusion-driven instability of a homogeneous steady-state [86, 96, 71], this example demonstrates destabilization of a spatially homogeneous periodic orbit by diffusion.

The stability of (3.1) in which the matrix $A(t)$ is constant has been studied in the literature. In [14], the authors showed that the stability of a homogeneous steady-state in a reaction-diffusion PDE with Neumann boundary conditions is equivalent to the simultaneous stability of a family of matrices of the form (3.1). In this case, the matrix $A(t) = A$ is constant because it represents the Jacobian linearization of the reaction terms at the steady-state. In the typical case where the matrix D of diffusion coefficients is diagonal, a sufficient condition for the desired simultaneous stability property is that A be an additively D-stable matrix [63], which means that $A - D$ is Hurwitz for all diagonal $D \geq 0$. While recent work has sought to characterize additive D-stability for constant matrices [97, 45, 67], the periodic time-varying case addressed here has not been studied.

The remainder of the chapter is organized as follows. In Section 3.1, we formulate the problem, and present an example of a system with an asymptotically stable limit cycle that loses spatial synchrony in the presence of diffusion. In Section 3.2, we outline tests for synchrony in the case of sufficiently small or sufficiently large perturbations. In Section 3.3, we develop a method to verify synchrony for an interval of diffusion coefficients. We present relaxation and ring oscillator examples in Section 3.4, and give the conclusions in Section 3.5. Derivations of our application of structured singular value to periodic linear time-varying systems and harmonic transfer operators are given in the Appendix.

3.1 Problem Formulation

In this section, we formulate the problem of synchronization of limit cycle oscillations in diffusively coupled systems. For both reaction-diffusion systems of PDEs with Neumann boundary conditions and compartmental systems of ODEs, we show that determining synchrony, in the sense of a system exhibiting spatially homogeneous oscillations, amounts to examining stability of a linear system with time-periodic coefficients. To motivate our developments, we also provide an example of a system with an asymptotically stable limit cycle that loses spatial synchrony in the presence of large enough diffusion.

We first discuss systems governed by reaction-diffusion PDEs, and define the spatial domain $\Omega \in \mathbb{R}^r$ with smooth boundary $\partial\Omega$, spatial variable $\chi \in \Omega$, and outward normal vector $\hat{n}(\chi)$ for $\chi \in \partial\Omega$. The PDE model is:

$$\frac{\partial x(t,\chi)}{\partial t} = f(x(t,\chi)) + D\nabla^2 x(t,\chi), \tag{3.2}$$

subject to Neumann boundary conditions $\nabla x_i(t,\chi)\cdot\hat{n}(\chi) = 0$ for all $\chi \in \partial\Omega$, where $x(t,\chi) \in \mathbb{R}^n$, $D \in \mathbb{R}^{n\times n}$, and

$$\nabla^2 x(t,\chi) = [\nabla^2 x_1(t,\chi)\cdots\nabla^2 x_n(t,\chi)]^T \tag{3.3}$$

is a vector of Laplacian operators with respect to the spatial variable χ applied to each entry of x. In a reaction-diffusion system, $x(t,\chi)$ represents a vector of concentrations for the reactants and D is a diagonal matrix of diffusion coefficients. However, for generality of our derivations, we will not assume D to be diagonal unless we state otherwise.

We say that a solution $x(t,\chi)$ of (3.1) synchronizes if $x(t,\chi_j) - x(t,\chi_k) \to 0$ for any two points χ_j and χ_k in Ω. We assume that the lumped system $\dot{x} = f(x)$ has an asymptotically stable limit cycle and that $\bar{x}(t)$ is a solution of $\dot{x} = f(x)$ along the limit cycle. Then $x(t,\chi) = \bar{x}(t)$ for all $\chi \in \Omega$ is a solution of (3.2). In the absence of diffusion ($D = 0$), the system (3.2) admits out-of-phase oscillations, that is, solutions of the form $x(t,\chi) = \bar{x}(t+\varphi(\chi))$, where $\varphi(\chi)$ is a phase that depends on the location χ. To determine whether diffusion eliminates such spatial phase differences, we examine the Jacobian linearization about the limit cycle trajectory $\bar{x}(t,\chi)$:

$$\frac{\partial \tilde{x}(t,\chi)}{\partial t} = (A(t) + D\nabla^2)\tilde{x}(t,\chi) \tag{3.4}$$

where $\tilde{x}(t,\chi) = x(t,\chi) - \bar{x}(t)$ and

$$A(t) = J(\bar{x}(t)) = \left.\frac{\partial f}{\partial x}\right|_{\bar{x}(t)}. \tag{3.5}$$

Let $0 = \lambda_1 \le \lambda_2 \le \ldots$ denote the eigenvalues and $\phi_1(\chi)$, $\phi_2(\chi), \ldots$ denote the corresponding orthogonal eigenfunctions of the operator $L = -\nabla^2$ on Ω with Neumann boundary conditions:

$$L\phi_i(\chi) = \lambda_i\phi_i(\chi),\ \nabla\phi_i(\chi)\cdot\hat{n}(\chi) = 0 \text{ for all } \chi \in \partial\Omega. \tag{3.6}$$

The solution to (3.4) can be expressed as:

$$\tilde{x}(t,\chi) = \sum_{i=1}^{\infty} \sigma_i(t)\phi_i(\chi), \tag{3.7}$$

where $\sigma_i(t) \in \mathbb{R}^n$ satisfy the decoupled system of ODEs:

$$\dot{\sigma}_i = (A(t) - \lambda_i D)\sigma_i,\ i = 1, 2, \ldots. \tag{3.8}$$

Since the eigenfunction $\phi_1(\chi)$ for $\lambda_1 = 0$ is constant, the term corresponding to $i = 1$ represents a spatially homogeneous mode σ_1 governed by $\dot{\sigma}_1 = A(t)\sigma_1$. When the subsystems (3.8) are asymptotically stable for $i = 2, 3, \ldots$, the contributions of the inhomogeneous modes $\phi_2(\chi)$, $\phi_3(\chi), \ldots$ to the solution $\tilde{x}(t,\chi)$ decay to zero in time, which implies that $x(t,\chi)$ synchronizes.

We also study a compartmental ODE model, where each compartment represents a well-mixed spatial domain interconnected with the other compartments over an undirected graph:

$$\dot{x}_i = f(x_i) + D\sum_{j\in N_i}(x_j - x_i),\ \ i = 1, \ldots, N. \tag{3.9}$$

The vector $x_i \in \mathbb{R}^n$ represents each compartment's state, $\mathcal{N}_i$ denotes the neighbors of compartment i, and $D \in \mathbb{R}^{n\times n}$. We say that a solution $(x_1(t), \ldots, x_N(t))$ synchronizes if $x_j(t) - x_k(t) \to 0$ for any pair (j, k). We take the Jacobian linearization about a limit cycle trajectory $\bar{x}(t)$, and aggregate the dynamics of the subsystems using the state variable $\tilde{x} = [\tilde{x}_1^T \cdots \tilde{x}_N^T]^T$, $\tilde{x}_i(t) = x_i(t) - \bar{x}(t)$. We represent the interaction between state variables by a graph Laplacian matrix $L = L^T \in \mathbb{R}^{N\times N}$, defined as

$$L = EE^T, \tag{3.10}$$

where E is an incidence matrix as in (1.1) whose rows represent nodes (compartments) and columns represent edges (couplings between the compartments). The dynamics of the aggregated system may be written as:

$$\dot{\tilde{x}} = (I \otimes A(t) - L \otimes D)\tilde{x}, \tag{3.11}$$

where $A(t)$ is as in (3.5) and $\otimes$ denotes the Kronecker product. Let $U \in \mathbb{R}^{N\times N}$ be a unitary similarity transformation that brings L into the diagonal matrix of its eigenvalues $\Sigma \in \mathbb{R}^{N\times N}$: $L = U\Sigma U^T$. Choosing $\tilde{y} = (U^{-1} \otimes I)\tilde{x}$, we rewrite (3.11) as a block diagonal system, making use of the Kronecker product identity $(M \otimes S)(T \otimes W) = MT \otimes SW$ for matrices M, T and S, W of conformable dimensions, respectively. We then have:

$$\dot{\tilde{y}} = (I \otimes A(t) - \Sigma \otimes D)\tilde{y}, \tag{3.12}$$

which is decoupled into the subsystems:

$$\dot{\tilde{y}}_l = (A(t) - \lambda_l D)\tilde{y}_l,\ l = 1, \ldots, N, \tag{3.13}$$

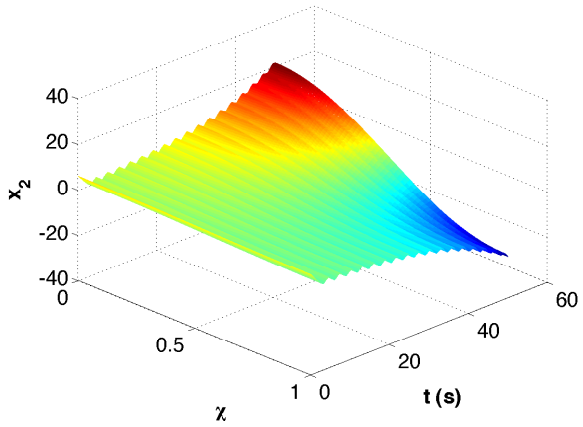

Figure 3.1: Spatio-temporal evolution of x_2 for system (3.2)-(3.14) with $d_1 = 100$, $d_2 = 0$, and $\mu = 0.1$ on the one-dimensional spatial domain $\Omega = [0, 1]$ with initial condition $x_2(0, \chi) = 5 + \cos(\pi\chi)$ and Neumann boundary conditions. The oscillations do not synchronize, and in fact growth of the spatial mode $\phi_2(\chi)$ is observed.

where $\tilde{y}_l \in \mathbb{R}^n$ and λ_l is the lth eigenvalue of the Laplacian matrix, respectively. In particular, $\lambda_1 = 0$ and $\lambda_l > 0, l = 2, 3, \ldots, N$ when the graph is connected. Note that (3.13) is analogous to (3.8) except that it consists of finitely many modes $l = 1, \ldots, N$. If the subsystems (3.13), $l = 2, \ldots, N$, are asymptotically stable, then for any pair $(j, k) \in \{1, \ldots, N\} \times \{1, \ldots, N\}$, we have $x_j(t) - x_k(t) \to 0$ exponentially as $t \to \infty$, which implies that $(x_1(t), \ldots, x_N(t))$ synchronizes.

Motivating Example

To see that a diagonal $D \succeq 0$ does not necessarily guarantee synchronization, consider the system (3.2) with the dynamics:

$$f(x) = \begin{bmatrix} \frac{1}{\mu}(x_1 - \frac{1}{3}x_1^3 - x_2) \\ x_1 + \mu x_2 \end{bmatrix} \text{ and } D = \begin{bmatrix} d_1 & 0 \\ 0 & 0 \end{bmatrix}, \tag{3.14}$$

with $d_1 > 0$. When $\mu > 0$ is sufficiently large, the vector field $f(x)$ has the behavior of a *relaxation oscillator* [64] and admits a stable limit cycle. The Jacobian linearization about the limit cycle trajectory $\bar{x}(t)$ is given by:

$$A(t) = \begin{bmatrix} \frac{1}{\mu}(1 - \bar{x}_1^2(t)) & \frac{1}{\mu} \\ 1 & \mu \end{bmatrix}. \tag{3.15}$$

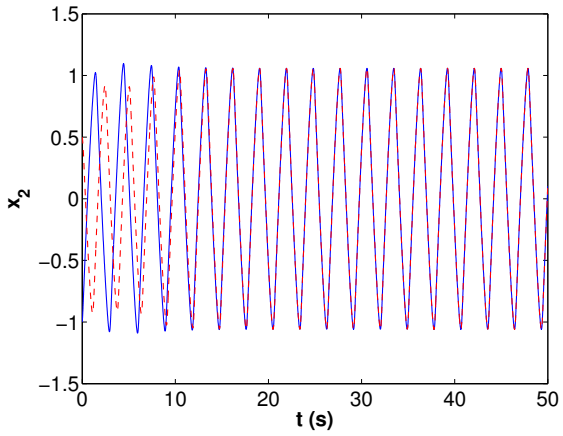

Figure 3.2: Trajectories of x_{12} (blue, solid) and x_{22} (red, dashed) of (3.9) and (3.14) for two compartments synchronize under small diffusion coefficient $d_1 = .5$ and initial conditions $(x_{12}(0), x_{22}(0)) = (-1, .5)$.

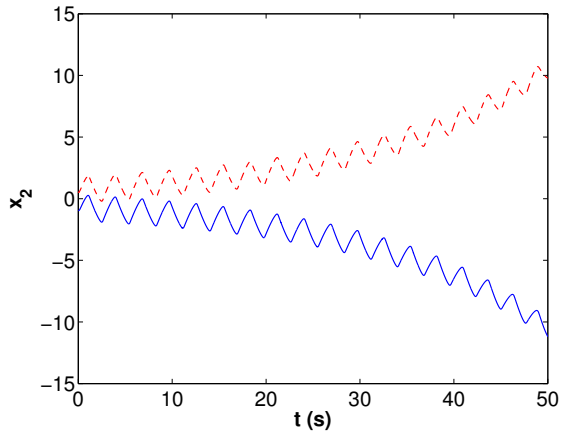

Figure 3.3: Trajectories of x_{12} (blue, solid) and x_{22} (red, dashed) of (3.9) and (3.14) for two compartments do not synchronize under larger diffusion coefficient $d_1 = 100$ and initial conditions $(x_{12}(0), x_{22}(0)) = (-1, .5)$.

When $\lambda_i d_1 \gg 1/\mu$, system (3.8) exhibits two-time scale behavior, with the slow dynamics unstable:

$$\dot{\sigma}_{i2} = \mu\sigma_{i2}. \tag{3.16}$$

Thus, we expect the system (3.2), with $f(x)$ and D as in (3.14), to be unstable when $\lambda_i d_1$ is sufficiently large. Indeed, for $d_1 = 100$ and $\mu = 0.1$, the simulations over the spatial domain $[0, 1]$ demonstrate the growth of the spatial mode $\phi_2(\chi) = \cos(\pi\chi)$; see Figure 3.1. Unlike standard examples of diffusion-driven instability of a homogeneous steady-state [86, 96, 71], this example demonstrates destabilization of a spatially homogeneous periodic orbit by diffusion.

Similar behavior can be observed for the compartmental model (3.9) with two compartments, and $f(x)$ and D given by (3.14). The two-node graph representing the interconnection of the two compartments has Laplacian eigenvalues $\lambda_1 = 0$ and $\lambda_2 = 2$. When d_1 is small, we find that oscillations synchronize spatially, as shown in Figure 3.2. When d_1 is large, the trajectories corresponding to compartments one and two diverge from each other, as shown in Figure 3.3.

3.2 Synchronization under Weak or Strong Coupling

As shown in the previous section, for both the PDE (3.2) and the compartmental ODE (3.9), synchrony is determined by the stability of the time-varying system (3.1). For simplicity of notation we drop λ_k from (3.1) and analyze

$$\dot{x} = (A(t) - D)x, \tag{3.17}$$

since D can be appropriately scaled to account for λ_k.

When D is sufficiently small or large, we use Floquet theory to decompose (3.17) into fast and slow time scales, and develop stability conditions using two-time scale averaging theory.

Recall that $A(t) = \frac{\partial f}{\partial x}\big|_{\bar{x}(t)}$ is the linearization of $f(x)$ about a limit cycle trajectory $\bar{x}(t)$, and let T denote the period of oscillations: $A(t + T) = A(t)$ for all t. We first consider the case with $D = 0$, that is:

$$\dot{x} = A(t)x, \tag{3.18}$$

and note that it admits the periodic solution $x(t) = \dot{\bar{x}}(t)$. To see this, observe the following:

$$\dot{\bar{x}}(t) = f(\bar{x}(t)) \Longrightarrow \ddot{\bar{x}}(t) = \left.\frac{\partial f}{\partial x}\right|_{\bar{x}(t)} \dot{\bar{x}}(t) = A(t)\dot{\bar{x}}(t). \tag{3.19}$$

Floquet's Theorem (Thm. 2.2.5, [35]) implies that the state transition matrix $\Phi(t, t_0)$ of (3.18) is periodic and can be written as

$$\Phi(t, t_0) = U(t) \exp\left(F(t - t_0)\right) V(t_0), \tag{3.20}$$

where $F \in \mathbb{R}^{n\times n}$ is a constant matrix, $U(t+T) = U(t) \in \mathbb{R}^{n\times n}$ and $U(t) = V^{-1}(t) \in \mathbb{R}^{n\times n}$, with the columns of $U(t)$ given by $u_i(t)$ and the rows of $V(t)$ given by $v_j^T(t)$. Since (3.18) results from linearization about a stable limit cycle, F can be written as

$$F = \begin{bmatrix} 0 & 0 \\ 0 & F_2 \end{bmatrix}, \tag{3.21}$$

where F_2 is an $(n-1)\times(n-1)$ Hurwitz matrix and $u_1(t) = \dot{\bar{x}}(t)$. The eigenvalues of F are called *Floquet exponents*, and the evaluation of the state transition matrix over one period with initial condition t_0, $\Phi(t_0+T, t_0) = \exp(FT)$, is called the *monodromy matrix*.

In what follows, we derive a condition that relates the stability of (3.17) with sufficiently small D to $u_1(t)$ and $v_1(t)$. First, we review properties of $u_1(t)$ and $v_1(t)$ that follow from Floquet theory. The definition of $U(t)$ and $V(t)$ implies that $v_j^T(t)u_i(t) = \delta_{ij}$, where δ_{ij} is the Kronecker delta. In particular, $v_1(t)$ is a periodic solution of the adjoint system:

$$\dot{\rho} = -A^T(t)\rho. \tag{3.22}$$

To compute $u_1(t)$ and $v_1(t)$, we follow [27] and numerically integrate

$$\frac{\partial}{\partial t}\Phi(t, t_0) = A(t)\Phi(t, t_0) \tag{3.23}$$

over one period with the initial condition $\Phi(t_0, t_0) = I$. We then compute the eigenvector of the monodromy matrix corresponding to its eigenvalue at one:

$$u_1(t_0) = \Phi(t_0+T, t_0)u_1(t_0). \tag{3.24}$$

Using the numerically-computed state transition matrix $\Phi(t, t_0)$, we then calculate the trajectory $u_1(t) = \Phi(t, t_0)u_1(t_0)$. To obtain $v_1(t)$, we begin by computing the left eigenvector of the monodromy matrix corresponding to its eigenvalue at one:

$$v_1^T(t_0)\Phi(t_0+T, t_0) = v_1^T(t_0). \tag{3.25}$$

We scale $v_1(t_0)$ such that $v_1^T(t_0)u_1(t_0) = 1$. Finally, to obtain $v_1(t)$, we numerically integrate the adjoint system (3.22) backwards in time with the terminal condition $\rho(t_0+T) = v_1(t_0)$.

Having reviewed the case $D = 0$, we now prove a result about the stability of (3.18) with sufficiently small D.

Proposition 6 *Let $v_1^T(t)$ be the first row of $V(t)$ and $u_1(t)$ be the first column of $U(t)$, where $\Phi(t, t_0) = U(t)\exp(F(t-t_0))V(t_0)$ as described above. Given a matrix $D_0 \in \mathbb{R}^{n\times n}$, if the inequality*

$$\int_{t_0}^{t_0+T} v_1^T(t)D_0u_1(t)\,dt > 0 \tag{3.26}$$

holds, then the origin of the system

$$\dot{x} = (A(t) - \epsilon D_0)x \tag{3.27}$$

is exponentially stable for sufficiently small $\epsilon > 0$. □

Proof: Floquet theory implies that the time-varying change of coordinates $y = V(t)x$ transforms (3.18) into a linear time invariant system:

$$\dot{y} = Fy, \tag{3.28}$$

where F is as in (3.21). Introducing the decomposition $y = [w^T \;\; z^T]^T$, we rewrite (3.28) as:

$$\begin{bmatrix} \dot{w} \\ \dot{z} \end{bmatrix} = \begin{bmatrix} 0 & 0 \\ 0 & F_2 \end{bmatrix} \begin{bmatrix} w \\ z \end{bmatrix}. \tag{3.29}$$

When applied to system (3.27), the preceding change of coordinates yields:

$$\begin{bmatrix} \dot{w} \\ \dot{z} \end{bmatrix} = \left(\begin{bmatrix} 0 & 0 \\ 0 & F_2 \end{bmatrix} - \epsilon V(t) D_0 U(t) \right) \begin{bmatrix} w \\ z \end{bmatrix}. \tag{3.30}$$

For small ϵ, this time-varying periodic system exhibits two-time scale behavior, which allows us to exploit the theory of two-time scale averaging [83, 94]. The *averaged slow system* corresponding to (3.30) is given by

$$\begin{aligned} \dot{w}_s &= -\epsilon a w_s, \\ a &= \frac{1}{T} \int_{t_0}^{t_0+T} v_1^T(t) D_0 u_1(t) dt. \end{aligned} \tag{3.31}$$

Since F_2 is Hurwitz, an application of Lemma A1 in Appendix A shows that if $a > 0$, then the equilibrium $y = 0$ is exponentially stable for sufficiently small ϵ. □

Note that Proposition 3.1 does not require D_0 to be diagonal. When D_0 is diagonal, the test (3.26) can be simplified as follows:

Corollary 2 *Let* u_{1i} *and* v_{1j}^T *be the* i*th and* j*th components of* u_1 *and* v_1^T*, respectively. If the inequalities*

$$\int_{t_0}^{t_0+T} v_{1i}^T(t) u_{1i}(t)\, dt > 0,\ i = 1, \ldots, n \tag{3.32}$$

hold, then given any diagonal matrix $D_0 \succeq 0$, $D_0 \neq 0$*, the periodic solution of the linearized system (3.27) is stable for sufficiently small* $\epsilon > 0$. □

We now turn to the case where D is large. Standard results from perturbation theory [64] guarantee stability of (3.17) when D is nonsingular and sufficiently large. When D is singular, we again leverage two-time scale arguments to derive a condition that guarantees stability of (3.17):

Proposition 7 *Given a matrix $D_0 \in \mathbb{R}^{n\times n}$, consider the linear time varying system:*

$$\dot{x} = (A(t) - \epsilon^{-1} D_0)x \tag{3.33}$$

$$A(t) = \begin{bmatrix} A_{11}(t) & A_{12}(t) \\ A_{21}(t) & A_{22}(t) \end{bmatrix}, \; D_0 = \begin{bmatrix} 0 & 0 \\ 0 & D_2 \end{bmatrix}, \tag{3.34}$$

where $x \in \mathbb{R}^n$, $A(t+T) = A(t)$ for all t, $A_{22}(t)$ and D_2 have the same dimension, $-D_2$ is Hurwitz, and $\epsilon > 0$. If

$$\bar{A}_{11} = \frac{1}{T}\int_{t_0}^{t_0+T} A_{11}(t)\, dt \tag{3.35}$$

is Hurwitz, then $x = 0$ is an exponentially stable equilibrium of (3.33) for sufficiently small ϵ. □

The proof follows from Lemma A1. Note that if D_0 is not block diagonal, but is singular with trivial Jordan blocks corresponding to its eigenvalues at zero and all remaining eigenvalues in the closed right half plane, there exists a similarity transformation that will bring (3.33) to the form required by (3.34).

The tests that we have derived, while analytic in nature, may be applied to problems of interest by computing a linearization about a periodic solution, and numerically integrating the resulting differential equation (3.23) in order to obtain u_1 and v_1. We demonstrate the application of these tests in Section 3.4.

3.3 Numerical Verification of Synchronization using SSV

In this section, we develop numerical tools to determine the stability of (3.17) for a family of matrices D parametrized as:

$$D = M + B\Delta C, \tag{3.36}$$

where $M \in \mathbb{R}^{n\times n}$, $B \in \mathbb{R}^{n\times m}$, and $C \in \mathbb{R}^{m\times n}$ are fixed matrices, and $\Delta \in \mathbb{R}^{m\times m}$ is a diagonal matrix whose entries take values in $[-1, 1]$. For example, suppose that the system (3.17) has one diffusible component, with

$$D = \mathrm{diag}([d_1 \;\; 0 \cdots 0]), \tag{3.37}$$

where $d_1 \in [r, R]$. Then D can be written as in (3.36) with $M = \frac{R+r}{2} e_1 e_1^T$ where e_i is a standard basis vector, $B = \left[\frac{R-r}{2} \;\; 0 \cdots 0\right]^T$, $C = [1 \;\; 0 \cdots 0]$, and $\Delta = \delta$ is a scalar. The problem is then to ascertain that the system (3.17) is stable for all values of δ on the interval $[-1, 1]$.

Structured singular value (SSV) analysis provides a useful test for determining the robustness of a stable linear time invariant system to structured modeling uncertainty. However, since (3.38) is time-varying, in order to apply SSV analysis directly we must first bring the system to an equivalent time invariant form. For such analysis, it is useful to rewrite the system (3.17) as:

$$\begin{aligned} \dot{x} &= (A(t) - M)x - Bq \\ y &= Cx \\ q &= \Delta y. \end{aligned} \tag{3.38}$$

Previous efforts to apply SSV analysis to time-varying systems have focused on the time-domain *lifting* idea of [8, 15], outlined in [65, 70, 32], where system (3.38) is discretized and converted to a continuous time invariant system.

Instead, we pursue an SSV analysis that makes use of the *harmonic balance* approach [101] and frequency-domain lifting as in [34], and avoids the numerical difficulties and sensitivity of computing the state transition matrix and discretizing with an adequate number of samples in the lifting approach. Our computational experiments show that the harmonic balance approach frequently leads to less conservative results in establishing the values of diffusion coefficients that lead to instabilities. We give a brief summary of harmonic balance, and then outline its application to the problem of determining the stability of (3.17).

We assume that each entry of the matrix $A(t)$ is a continuous function of t that has an absolutely convergent Fourier series, and so $A(t)$ may be expressed as:

$$A(t) = \sum_{m \in \mathbb{Z}} A_m e^{jm\omega_p t}, \tag{3.39}$$

where ω_p is the fundamental frequency. Define doubly infinite vectors representing the harmonics of the state:

$$X^T = [\cdots x_{-1}^T \;\; x_0^T \;\; x_1^T \cdots], \tag{3.40}$$

and do the same for the input Q and output Y. The doubly infinite block Toeplitz matrix $\mathcal{A}$ is determined by the harmonics of $A(t)$:

$$\mathcal{A} = \begin{bmatrix} \ddots & \vdots & \vdots & \vdots & \\ \cdots & A_0 & A_{-1} & A_{-2} & \cdots \\ \cdots & A_1 & A_0 & A_{-1} & \cdots \\ \cdots & A_2 & A_1 & A_0 & \cdots \\ & \vdots & \vdots & \vdots & \ddots \end{bmatrix}. \tag{3.41}$$

We define the doubly infinite matrices $\mathcal{I} = \text{blkdiag}(I)$, $\mathcal{B} = \text{blkdiag}(B)$, and $\mathcal{C} = \text{blkdiag}(C)$, and define the modulation frequency matrix as:

$$\mathcal{N} = \text{blkdiag}\{jm\omega_p I\},\ \forall m \in \mathbb{Z}. \tag{3.42}$$

We define the matrix $\tilde{\Delta} = \text{blkdiag}(\Delta)$ to be block diagonal with copies of the diagonal matrix Δ in each block, and the matrix $\mathcal{M} = \text{blkdiag}(M)$ to be a block diagonal scaling matrix with copies of the matrix M in each block. We now introduce the harmonic state space model, where $s = j\omega$:

$$\begin{aligned} sX &= (\mathcal{A} - \mathcal{M} - \mathcal{N})X - \mathcal{B}Q \\ Y &= \mathcal{C}X \\ Q &= \tilde{\Delta}Y. \end{aligned} \tag{3.43}$$

We perform SSV analysis to determine if there exist matrices D such that (3.17) is unstable. For the precise definition of the structured singular value in the context of periodic linear-time varying systems represented by a harmonic state space model, we refer the reader to Appendix B. To obtain a computationally tractable test, we truncate the doubly infinite system. As shown in Appendix B, we may approximate (3.43) arbitrarily well. In the examples we consider there exist fewer than ten significant harmonics, and we represent the doubly infinite system by a finite dimensional system. We then perform SSV analysis on the truncated version of (3.43) to determine the range of matrices Δ for which (3.17) remains stable. In particular, we use the MATLAB command *mussv* in the Robust Control Toolbox, which performs SSV analysis to test if there exists a Δ such that (3.43) is unstable. We summarize our procedure in Algorithm 3.

Algorithm 3 Numerical verification of synchrony using harmonic balance

1: Using the parametric decomposition (3.36) for the given family of matrices D under consideration, determine the matrices B and C in order to express (3.17) in the form of (3.38).
2: Determine the Fourier series coefficients of $A(t)$.
3: Define the truncated linear time invariant harmonic state space model as in (3.43).
4: Compute the structured singular value μ of the harmonic state space model.

Following the completion of Algorithm 3, if $\mu > 1$, we compute the corresponding matrix Δ with smallest norm such that the truncated harmonic state space model is unstable. We then use the computed matrix Δ and (3.36) to compute a candidate for a matrix D that makes (3.17) unstable. If $\mu \leq 1$, appealing to the convergence properties in Appendix B provides evidence that system (3.17) is stable. The choice of the number of terms in the truncation resulting from Step 3 involves a tradeoff between numerical accuracy and computation time.

Since the problem of computing the structured singular value of a system is NP complete [76], the Robust Control Toolbox employs linear matrix inequality relaxations as well as a

discretization of the continuous frequency domain, which can lead to numerical inaccuracies and conservatism. This conservatism can pose a problem in certifying stability over large intervals. In many cases, it may be necessary to perform SSV analysis on smaller intervals, and to certify the remaining (possibly infinite) interval using the perturbation arguments of Section 3.2.

3.4 Examples

Example 1 - Relaxation Oscillator
We first discuss numerical results for the *relaxation oscillator* example given by (3.14) in Section 3.1. We set the parameter $\mu = 0.1$, and first study the two compartment ODE model (3.9). When D is small, the techniques of Section 3.2 apply, and we can easily check that the conditions of Corollary 2 are satisfied for nonnegative $\lambda_i d_1 < \epsilon^*$, where ϵ^* is computed from the proof of Lemma A1. In Figure 3.2, we show the oscillations of the solution of x_2 synchronizing spatially under small D, as expected.

We next examine the case of larger D for both (3.9) and (3.2). To apply the harmonic balance method, we compute the harmonic components of $x_1(t)$ and find that eight harmonics are sufficient to represent the signal. We then use the harmonic expansion to generate a corresponding finite dimensional approximation of the matrix $\mathcal{A}$. Because D is diagonal and nonnegative, we set $M = \frac{r+\epsilon^*}{2} e_1 e_1^T$, $B = [\frac{r-\epsilon^*}{2} \;\; 0]^T$, $C = [1 \;\; 0]$, and $\Delta = \delta$, and perform SSV analysis to determine values of d_1 that lead to instabilities. We find that at $\lambda_i d_1 \geq 87.6$, stability is lost.

Indeed, when the product $\lambda_i d_1 \geq 87.6$, the two compartment ODE, with $\lambda_2 = 2$, will exhibit trajectories that diverge, and the reaction-diffusion PDE model, with $\lambda_i = (i-1)^2$, $i = 2, 3, \ldots$, will lose spatial uniformity for initial spatial modes with large enough wavenumber i regardless of d_1. In Figures 3.1 and 3.3, we show that the oscillations of the solution of x_2 do not synchronize spatially for large D, and observe increasing spatial inhomogeneity over time.

Example 2 - Ring Oscillator
We next study a coupled three-stage *ring oscillator* model (Figure 3.4), with the dynamics of each circuit given by:

$$\begin{aligned} \dot{x}_{i1} &= -\eta_1 x_{i1} - \alpha_1 \tanh(\beta_1 x_{i3}) + w_{i1} \\ \dot{x}_{i2} &= -\eta_2 x_{i2} - \alpha_2 \tanh(\beta_2 x_{i1}) \\ \dot{x}_{i3} &= -\eta_3 x_{i3} - \alpha_3 \tanh(\beta_3 x_{i2}), \end{aligned} \tag{3.44}$$

with coupling at node 1 of each circuit. The parameters $\eta_i = \frac{1}{R_i C_i}$, α_1, and β_1 correspond to

the gain of each inverter. The coupling is defined by:

$$w_{i1} = -d_1 \left(\sum_{j \in \mathcal{N}_i} (x_{i1} - x_{j1}) \right), \tag{3.45}$$

where $d_1 = 1/(RC_1)$ and $\mathcal{N}_i$ denotes the set of circuits to which circuit i is connected. The Laplacian matrix describing the interaction between three coupled circuits as in Figure 3.4 is given by:

$$L = \begin{bmatrix} 2 & -1 & -1 \\ -1 & 2 & -1 \\ -1 & -1 & 2 \end{bmatrix}. \tag{3.46}$$

Following (3.9), the vector field $f(x)$ is given by (3.44) with $D = \mathrm{diag}([d_1 \;\; 0 \;\; 0])$.

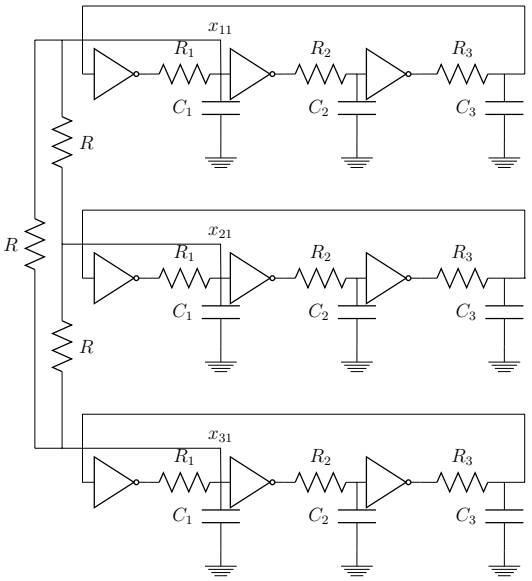

Figure 3.4: Three-stage ring oscillators as in (3.44) coupled through node 1.

In order for (3.44) with w_{i1} to admit a limit cycle, it must have $\alpha_i \beta_i > 2$ [44]. We set $\eta_i = 1$, $\alpha_i = 2$, and $\beta_i = 1.2$ for all i. When d_1 is small, we use the techniques of Section 3.2 to study the effects of small D on (3.9). Upon computing $u_1(t)$ and $v_1(t)$, it is readily seen that the conditions of Corollary 2 are satisfied. Thus, the equilibrium at $x = 0$ is exponentially stable for nonnegative $\lambda_i d_1 < \epsilon^*$, where ϵ^* is computed from the proof of Lemma A1.

We next apply Proposition 7 to study the effects of large D on (3.9). Linearization about a limit cycle trajectory $\bar{x}(t)$ brings (3.44) to the form:

$$\begin{bmatrix} \dot{x}_1 \\ \dot{x}_2 \\ \dot{x}_3 \end{bmatrix} = - \left(\begin{bmatrix} \lambda_i d_1 & 0 & 0 \\ 0 & 0 & 0 \\ 0 & 0 & 0 \end{bmatrix} - \begin{bmatrix} 1 & 0 & \gamma_1(\bar{x}_1) \\ \gamma_2(\bar{x}_2) & 1 & 0 \\ 0 & \gamma_3(\bar{x}_3) & 1 \end{bmatrix} \right) \begin{bmatrix} x_1 \\ x_2 \\ x_3 \end{bmatrix}, \tag{3.47}$$

with $\gamma_1(\bar{x}_1) = \alpha_1\beta_1\text{sech}\,(\beta_1\bar{x}_3)^2$, $\gamma_2(\bar{x}_2) = \alpha_2\beta_2\text{sech}\,(\beta_2\bar{x}_1)^2$, and $\gamma_3(\bar{x}_3) = \alpha_3\beta_3\text{sech}\,(\beta_3\bar{x}_2)^2$. When d_1 is large, the system exhibits two-time scale behavior. Since $D \succeq 0$ is diagonal and the averaged slow system corresponding to $[x_2 \;\; x_3]^T$, given by:

$$\begin{bmatrix} \dot{x}_2 \\ \dot{x}_3 \end{bmatrix} = -\left(\int_{t_0}^{t_0+T} \begin{bmatrix} 1 & 0 \\ \gamma_3(\bar{x}_3) & 1 \end{bmatrix} dt\right) \begin{bmatrix} x_2 \\ x_3 \end{bmatrix}, \tag{3.48}$$

has an exponentially stable equilibrium at zero, we conclude from Proposition 7 that the equilibrium at $x = 0$ is exponentially stable for $\lambda_i d_1 > m^*$, where m^* is computed from the proof of Lemma A1.

We use SSV analysis to certify synchrony for the remaining interval $[\epsilon^*, m^*]$. Following Section 3.3, we set $M = \frac{m^*+\epsilon^*}{2} e_1 e_1^T$, $B = \left[\frac{m^*-\epsilon^*}{2} \;\; 0 \ldots 0\right]^T$, $C = [1 \;\; 0 \ldots 0]$, and $\Delta = \delta$. A discrete Fourier transform of a periodic trajectory $\bar{x}(t)$ suggests that eight harmonics are sufficient to represent the truncated harmonic state space model for the time-varying system. SSV analysis indicates that coefficients $\lambda_i d_1 \in [\epsilon^*, m^*]$ will result in (3.9) being stable. In Figure 3.5 we show an example of a coefficient $d_1 \in [\epsilon^*, m^*]$ with synchronized oscillations.

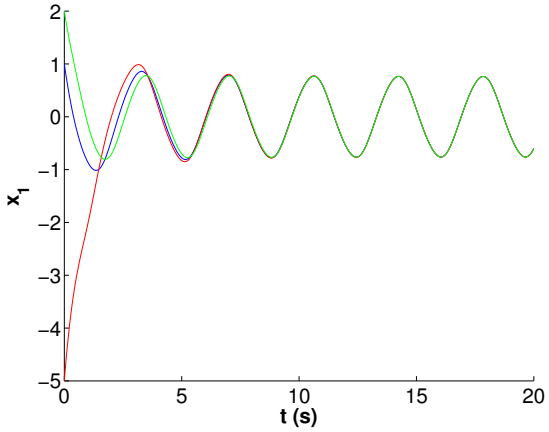

Figure 3.5: Coupled identical three-staged ring oscillators as in (3.44) with $\eta_i = 1$, $\alpha_i = 2$, and $\beta_i = 1.2$ for all i. Oscillations synchronize with initial conditions $x_{11} = 1$ (blue), $x_{21} = -5$ (red), and $x_{31} = 2$ (green). For brevity we show only the first component.

3.5 Conclusion

We have studied diffusively coupled compartmental ODEs as well as reaction-diffusion PDEs that admit stable limit cycles. We have established analytic tests using two-time scale averaging theory to study the case of weak or strong coupling. We then presented a numerical method applying the harmonic balance and structured singular value analysis on intervals

of intermediate coupling strength to determine whether limit cycle oscillations synchronize. Finally, we applied our tests to examples, where we identified cases in which diffusion leads to loss of spatial synchrony. Our results could also be used to decide on coupling strengths to guarantee synchrony in diffusively coupled systems such as voltage controlled oscillators and multiagent systems in which agent dynamics can be destabilized by high gain feedback.

Chapter 4

Synchronization under Space-Dependent Diffusive Coupling

We present a condition that guarantees synchronization in diffusively coupled compartmental systems of ODEs and reaction-diffusion PDEs. The majority of the literature makes use of global Lipschitz conditions on the vector field of the uncoupled dynamics to guarantee synchronization [4, 19, 60, 74]. In [1], the author derived a significantly relaxed condition that restricts the Jacobian of the vector field describing the uncoupled dynamics in order to guarantee synchronization. Using the results in [1] as a starting point, we derive a condition that allows each set of like components to have its own weighted coupling structure describing the topology of the interconnection between compartments. The condition we derive furthermore allows the diffusive coupling to vary spatially.

We begin our discussion in Section 4.1 by studying compartmental ODE models, where each compartment represents a well-mixed spatial domain wherein like components in different compartments are diffusively coupled. In Section 4.2, we apply the LMI tests to study the behavior of a coupled ring oscillator circuit. We emphasize that each node in a component may have its own set of neighboring nodes to which it is diffusively coupled independent of the set of neighbors of other nodes in the same compartment. We next turn to reaction-diffusion PDEs with Neumann boundary condition in Section 4.3, and establish a condition guaranteeing spatial homogeneity analogous to the result for compartmental ODEs. We summarize our contribution in Section 4.4.

4.1 Compartmental Systems of ODEs

We begin by considering a compartmental ODE model where each compartment represents a spatial domain interconnected with the other compartments over an undirected graph:

$$\dot{x}_{i,k} = f(x_i)_k + \sum_{j \in N_{i,k}} w_{ij}^{(k)}(x_{j,k} - x_{i,k}), \;\; i = 1, \ldots, N. \tag{4.1}$$

The vector $x_i \in \mathbb{R}^n$ is the state of the i-th compartment, the vector field $f(x_i)_k$ is the k-th component of the vector field $f(x_i)$ acting on x_i, the set $\mathcal{N}_{i,k}$ consists of the neighbors of the k-th component of compartment i, and the scalar $w_{ij}^{(k)} = w_{ji}^{(k)} \in \mathbb{R}$ is a weighting factor. We aggregate the dynamics of each compartment using the stacked vector $X = [x_1^T \ldots x_N^T]^T$ and represent the interconnections between like components in different compartments by a generalized symmetric positive semidefinite graph Laplacian matrix $L_k \in \mathbb{R}^{N \times N}$:

$$\dot{X} = F(X) - \left(\sum_{k=1}^{n} L_k \otimes E_k \right) X, \tag{4.2}$$

where $E_k = e_k e_k^T \in \mathbb{R}^{n \times n}$ is the product of the k-th standard basis vector e_k multiplied by its transpose, and $F(X) = [f(x_1)^T \ldots f(x_N)^T]^T$. In the event that the k-th set of like components are not interconnected with one another, we set $L_k = 0$. Define $\lambda_2^{(k)}$ as the second smallest eigenvalue of L_k, and note that since $L_k 1_N = 0$,

$$z^T L_k z \geq \lambda_2^{(k)} z^T z \tag{4.3}$$

for all $z \in \mathbb{R}^n$ with $z \perp 1_N$. Let $J(x) = \frac{\partial f}{\partial x}\,|_x$ denote the Jacobian of $f(x)$ at x.

Theorem 8 *Consider the system (4.2). Suppose there exists a convex set $\mathcal{X} \in \mathbb{R}^n$, a positive definite matrix P, and a constant $\epsilon > 0$ such that the following conditions hold:*

$$P\left(J(x) - \sum_{k=1}^{n} \lambda_2^{(k)} E_k \right) + \left(J(x) - \sum_{k=1}^{n} \lambda_2^{(k)} E_k \right)^T P \preceq -\epsilon I \;\; \forall x \in \mathcal{X} \tag{4.4}$$

$$PE_k + E_k P \succeq 0 \text{ for each } k \in \{1, \ldots, n\} \text{ with } L_k \neq 0. \tag{4.5}$$

If solutions are bounded, then for any pair $(i, j) \in \{1, \ldots, N\} \times \{1, \ldots, N\}$ and any index $k \in \{1, \ldots, n\}$, we have: $x_{i,k}(t) - x_{j,k}(t) \to 0$ exponentially as $t \to \infty$. $\square$

Proof: First recall that $z^T L_k z \geq \lambda_2^{(k)} z^T z$ for all $z \perp 1_N$, and that $z^T (L_k \otimes I_n) z \geq \lambda_2^{(k)} z^T z$ for all $z \perp 1_N \otimes I_n$. Define the following terms:

$$\begin{aligned} \bar{x} = \frac{1}{N} \sum_{i=1}^{N} x_i = \frac{1}{N} (1_N^T \otimes I_n) X \\ \bar{X} = 1_N \otimes \bar{x} \\ \tilde{x}_i = x_i - \bar{x} \\ \tilde{X} = X - \bar{X}. \end{aligned} \tag{4.6}$$

Since $\sum_{i=1}^{N} \tilde{x}_i = 0$, it holds that $\tilde{X}^T (1_N \otimes M) = 0$ for all matrices M with n rows. The dynamics of $\tilde{X}$ are given by:

$$\begin{aligned} \dot{\tilde{X}} &= F(X) - \dot{\bar{X}} - LX \\ &= F(X) - \dot{\bar{X}} - L\tilde{X}, \end{aligned} \tag{4.7}$$

where $L = \sum_{k=1}^{n} L_k \otimes E_k$. We differentiate the candidate Lyapunov function $V = \frac{1}{2} \tilde{X}^T (I_N \otimes P) \tilde{X}$:

$$\begin{aligned} \dot{V} &= \tilde{X}^T (I_N \otimes P)(F(X) - \dot{\bar{X}}) - \tilde{X}^T (I_N \otimes P) L \tilde{X} \\ &= \tilde{X}^T (I_N \otimes P)(F(X) - \dot{\bar{X}}) - \tilde{X}^T \sum_{k=1}^{n} (L_k \otimes P E_k) \tilde{X}. \end{aligned} \tag{4.8}$$

We observe that

$$(L_k \otimes P E_k) + (L_k \otimes P E_k)^T = L_k \otimes (P E_k + E_k P), \tag{4.9}$$

and that because condition (4.5) holds, there exists a matrix Q_k such that $Q_k^T Q_k = \frac{1}{2}(P E_k + E_k P)$. Then

$$\begin{aligned} \tilde{X}^T (L_k \otimes P E_k) \tilde{X} &= \tilde{X}^T (I_N \otimes Q_k^T)(L_k \otimes I_n)(I_N \otimes Q_k) \tilde{X} \\ &= y_k^T (L_k \otimes I_n) y_k, \end{aligned} \tag{4.10}$$

where $y_k = (I_N \otimes Q_k) \tilde{X}$. Because of the orthogonality relation $y_k \perp 1_N \otimes I_n$ and condition (4.3), it follows that

$$\begin{aligned} \tilde{X}^T (I_N \otimes P) L \tilde{X} &= \sum_{k=1}^{n} y_k^T (L_k \otimes I_n) y_k \\ &\geq \sum_{k=1}^{n} \lambda_2^{(k)} y_k^T y_k \\ &= \sum_{k=1}^{n} \lambda_2^{(k)} \tilde{X}^T (I_N \otimes P E_k) \tilde{X} \\ &= \sum_{k=1}^{n} \lambda_2^{(k)} \sum_{i=1}^{N} \tilde{x}_i^T P E_k \tilde{x}_i. \end{aligned} \tag{4.11}$$

Defining $F(\bar{X}) = 1_N \otimes f(\bar{x})$ and adding and subtracting $\tilde{X}(I_N \otimes P)F(\bar{X})$, we have:

$$\begin{aligned}
\dot{V} &\leq \tilde{X}^T(I_N \otimes P)(F(X) - \dot{\bar{X}}) - \sum_{k=1}^{n} \lambda_2^{(k)} \sum_{i=1}^{N} \tilde{x}_i^T P E_k \tilde{x}_i \\
&= \tilde{X}^T(I_N \otimes P)(F(X) - F(\bar{X})) + \tilde{X}^T(I_N \otimes P)(1_N \otimes (f(\bar{x}) - \dot{\bar{x}})) \\
&\quad - \sum_{k=1}^{n} \lambda_2^{(k)} \sum_{i=1}^{N} \tilde{x}_i^T P E_k \tilde{x}_i \\
&= \tilde{X}^T(I_N \otimes P)(F(X) - F(\bar{X})) + \tilde{X}^T(1_N \otimes P(f(\bar{x}) - \dot{\bar{x}})) \\
&\quad - \sum_{k=1}^{n} \lambda_2^{(k)} \sum_{i=1}^{N} \tilde{x}_i^T P E_k \tilde{x}_i.
\end{aligned} \tag{4.12}$$

Recalling that $\bar{X}^T(1_N \otimes M) = 0$, we take $M = P(f(\bar{x}) - \dot{\bar{x}})$ and apply the mean value theorem:

$$\begin{aligned}
\dot{V} &\leq \left(\sum_{i=1}^{N} \tilde{x}_i^T P \left(f(x_i) - f(\bar{x}) \right) \right) - \left(\sum_{k=1}^{n} \lambda_2^{(k)} \sum_{i=1}^{N} \tilde{x}_i^T P E_k \tilde{x}_i \right) \\
&= \sum_{i=1}^{N} \tilde{x}_i^T \left(P(f(x_i) - f(\bar{x})) - P \sum_{k=1}^{n} \lambda_2^{(k)} E_k \right) \tilde{x}_i \\
&= \sum_{i=1}^{N} \int_0^1 \tilde{x}_i^T P \left(J(\bar{x} + s\tilde{x}_i) - \sum_{k=1}^{n} \lambda_2^{(k)} E_k \right) \tilde{x}_i \, ds.
\end{aligned} \tag{4.13}$$

Because condition (4.4) holds, we have:

$$\dot{V} \leq -\frac{\epsilon}{2} \tilde{X}^T \tilde{X} \leq -\frac{\epsilon}{\lambda_{\max}(P)} V, \tag{4.14}$$

which concludes the proof. □

The additional condition that the product PE_k be symmetric for each $k \in \{1, \ldots, n\}$ with $L_k \neq 0$ allows us to generalize Proposition 8, as in [1], to handle non-symmetric generalized graph Laplacians (e.g., where $w_{ij}^{(k)} \neq w_{ji}^{(k)}$). In place of (4.9), take

$$(L_k \otimes PE_k) + (L_k \otimes PE_k)^T = (L_k + L_k^T) \otimes (PE_k), \tag{4.15}$$

which holds when PE_k is symmetric, and define $\lambda_2^{(k)}$ as the smallest positive number such that (4.3) holds.

In order to check the conditions of Theorem 8, we note two results that follow from ([1], Theorems 2 and 3), where the Jacobian matrix over the convex set $\mathcal{X}$ is itself parametrized by a convex set.

Theorem 9 *If there exist constant matrices $Z_1, \ldots, Z_q$ and $S_l, \ldots, S_m$ such that*

$$J(x) \in conv\{Z_1, \ldots, Z_q\} + cone\{S_l, \ldots, S_m\} \;\; \forall\, x \in \mathcal{X}, \tag{4.16}$$

then the existence of a symmetric matrix P satisfying

$$\begin{aligned} P\left(Z_k - \sum_{k=1}^{n} \lambda_2^{(k)} E_k\right) + \left(Z_k - \sum_{k=1}^{n} \lambda_2^{(k)} E_k\right)^T P \prec 0, \;\; k = 1, \ldots, q \\ PS_k + S_k^T P \preceq 0, \;\; k = 1, \ldots, m \end{aligned} \tag{4.17}$$

implies condition (4.4) for some $\epsilon > 0$. If $J(x)$ is surjective onto $conv\{Z_1, \ldots, Z_q\} + cone\{S_l, \ldots, S_m\}$, then the converse is true. □

Next, we define a *convex box* as:

$$\text{box}\{M_0, M_1, \ldots, M_p\} = \{M_0 + \omega_1 M_1 + \ldots + \omega_p M_p \,|\, \omega_k \in [0,1] \text{ for each } k = 1, \ldots, p\}. \tag{4.18}$$

Theorem 10 *Suppose that $J(x)$ is contained in a convex box:*

$$J(x) \in box\{A_0, A_1, \ldots, A_l\} \;\; \forall\, x \in \mathcal{X}, \tag{4.19}$$

where $A_1, \ldots, A_l$ are rank-one matrices that can be written as $A_i = B_i C_i^T$, with B_i, $C_i \in \mathbb{R}^n$. If there exists a positive definite matrix $\mathcal{P}$ with:

$$\mathcal{P} = \begin{bmatrix} P & 0 & \ldots & 0 \\ 0 & q_l & 0 & 0 \\ \vdots & \ddots & \ddots & \vdots \\ 0 & \ldots & 0 & q_l \end{bmatrix}, \;\; P \in \mathbb{R}^{n \times n}, \; q_i \in \mathbb{R}, \; i = 1, \ldots, l, \tag{4.20}$$

satisfying:

$$\mathcal{P} \begin{bmatrix} A_0 - \sum_{k=1}^{n} \lambda_2^{(k)} E_k & B \\ C^T & -I_n \end{bmatrix} + \begin{bmatrix} A_0 - \sum_{k=1}^{n} \lambda_2^{(k)} E_k & B \\ C^T & -I_n \end{bmatrix}^T \mathcal{P} \prec 0, \tag{4.21}$$

with $B = [B_1 \ldots B_l]$ and $C = [C_1 \ldots C_l]$, then the upper left (positive definite) principal submatrix P satisfies condition (4.4) for some $\epsilon > 0$. If $l = 1$ and the image of $\mathcal{X}$ is surjective onto $box\{A_0, A_1\}$, then the converse is true. □

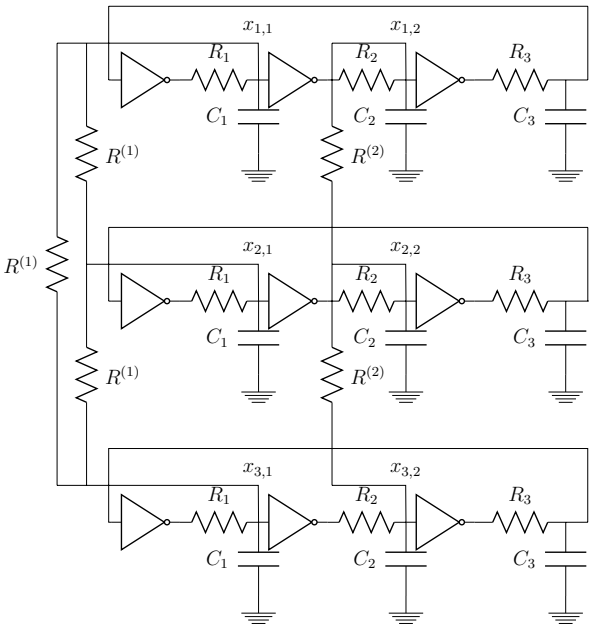

Figure 4.1: Example of a three-stage ring oscillator circuit as in (4.22) coupled through nodes 1 and 2.

4.2 Ring Oscillator Circuit Example

Consider the n-stage ring oscillator whose dynamics are given by:

$$\begin{aligned}
\dot{x}_{i,1} &= -\eta_1 x_{i,1} - \alpha_1 \tanh(\beta_1 x_{i,n}) + w_{i,1} \\
\dot{x}_{i,2} &= -\eta_2 x_{i,2} + \alpha_2 \tanh(\beta_2 x_{i,1}) + w_{i,2} \\
&\vdots \\
\dot{x}_{i,n} &= -\eta_n x_{i,n} + \alpha_n \tanh(\beta_n x_{i,n-1}) + w_{i,n},
\end{aligned} \tag{4.22}$$

with coupling between corresponding nodes of each circuit. The parameters $\eta_k = \frac{1}{R_k C_k}$, α_k, and β_k correspond to the gain of each inverter. The input is given by:

$$w_{i,k} = d_k \sum_{j \in \mathcal{N}_{i,k}} (x_{j,k} - x_{i,k}), \tag{4.23}$$

where $d_k = \frac{1}{R^{(k)} C_k}$ and $\mathcal{N}_{i,k}$ denotes the nodes to which node k of circuit i is connected. We wish to determine if the solution trajectories of each set of like nodes of the coupled ring oscillator circuit given by (4.22)-(4.23) synchronize, that is:

$$x_{i,k} - x_{j,k} \to 0 \text{ exponentially as } t \to \infty \tag{4.24}$$

for any pair $(i, j) \in \{1, \ldots, N\} \times \{1, \ldots, N\}$ and any index $k \in \{1, \ldots, n\}$.

For clarity in our discussion, we take $n = 3$ as in Figure 4.1, noting that the derivation is identical for any choice of n. We first write the Jacobian of the system (4.22), where we have omitted the subscripts indicating circuit membership:

$$J(x) = \begin{bmatrix} -\eta_1 & 0 & -\alpha_1\beta_1\text{sech}^2(\beta_1 x_3) \\ \alpha_2\beta_2\text{sech}^2(\beta_2 x_1) & -\eta_2 & 0 \\ 0 & \alpha_3\beta_3\text{sech}^2(\beta_3 x_2) & -\eta_3 \end{bmatrix}. \tag{4.25}$$

Define the matrices

$$\begin{aligned} A_0 &= \begin{bmatrix} -\eta_1 & 0 & 0 \\ 0 & -\eta_2 & 0 \\ 0 & 0 & -\eta_3 \end{bmatrix} \quad A_1 = \begin{bmatrix} 0 & 0 & -\alpha_1\beta_1 \\ 0 & 0 & 0 \\ 0 & 0 & 0 \end{bmatrix} \\ A_2 &= \begin{bmatrix} 0 & 0 & 0 \\ \alpha_2\beta_2 & 0 & 0 \\ 0 & 0 & 0 \end{bmatrix} \quad A_3 = \begin{bmatrix} 0 & 0 & 0 \\ 0 & 0 & 0 \\ 0 & \alpha_3\beta_3 & 0 \end{bmatrix}. \end{aligned} \tag{4.26}$$

Then it follows that $J(x)$ is contained in a convex box:

$$J(x) \in \text{box}\{A_0, A_1, A_2, A_3\}. \tag{4.27}$$

While the method of Theorem 9 involves parametrizing a convex box as a convex hull with 2^p vertices, and potentially a prohibitively large linear matrix inequality computation, the problem structure can be exploited using Theorem 10 to obtain a simple analytical condition for synchronization of trajectories. In particular, the Jacobian of the ring oscillator exhibits a *cyclic* structure. The matrix for which we seek a $\mathcal{P}$ satisfying (4.21) is given by:

$$\begin{aligned} M &= \begin{bmatrix} A_0 - \sum_{k=1}^{n} \lambda_2^{(k)} E_k & B \\ C^T & -I \end{bmatrix} \\ &= \begin{bmatrix} -\eta_1 - \lambda_2^{(1)} & 0 & 0 & 0 & 0 & -\alpha_1\beta_1 \\ 0 & -\eta_2 - \lambda_2^{(2)} & 0 & \alpha_2\beta_2 & 0 & 0 \\ 0 & 0 & -\eta_3 - \lambda_2^{(3)} & 0 & \alpha_3\beta_3 & 0 \\ 1 & 0 & 0 & -1 & 0 & 0 \\ 0 & 1 & 0 & 0 & -1 & 0 \\ 0 & 0 & 1 & 0 & 0 & -1 \end{bmatrix}. \end{aligned} \tag{4.28}$$

Note that the matrix M exhibits a cyclic structure, and by a suitable permutation G of its rows and columns, it can be brought into a cyclic form $\tilde{M} = GMG^T$. Since $\tilde{M}$ is cyclic, it is amenable to an application of the *secant criterion* [3], which implies that the condition

$$\frac{\Pi_{k=1}^{3} \alpha_k\beta_k}{\Pi_{l=1}^{3}(\eta_l + \lambda_l)} < \sec^3\left(\frac{\pi}{3}\right) \tag{4.29}$$

holds if and only if $\tilde{M}$ satisfies

$$\tilde{\mathcal{P}}\tilde{M} + \tilde{M}^T\tilde{\mathcal{P}} \prec 0 \tag{4.30}$$

for some diagonal $\tilde{\mathcal{P}} \succ 0$. Pre- and post-multiplying (4.30) by G^T and G, respectively, we have

$$G^T\tilde{\mathcal{P}}GM + M^TG^T\tilde{\mathcal{P}}G \prec 0. \tag{4.31}$$

Note that $G^T\tilde{\mathcal{P}}G$ is diagonal, and so if $\tilde{M}$ is diagonally stable, then M is diagonally stable as well. We conclude that if the secant criterion in (4.29) is satisfied, then Theorem 10 holds, and so Theorem 8 holds, with:

$$x_{i,k} - x_{j,k} \to 0 \text{ exponentially as } t \to \infty \tag{4.32}$$

for any pair $(i, j) \in \{1, \ldots, N\} \times \{1, \ldots, N\}$ and any index $k \in \{1, 2, 3\}$.

We note that the condition for synchrony that we have found recovers Theorem 2 in [44], which makes use of an input-output approach to synchronization [84]. We have derived the condition using Lyapunov functions in an entirely different manner from the input-output approach.

4.3 Reaction-Diffusion PDEs

Consider the connected, bounded domain $\Omega \subseteq \mathbb{R}^r$ with smooth boundary $\partial\Omega$, spatial variable $\chi \in \Omega$, and outward normal vector $\hat{n}(\chi)$ for $\chi \in \partial\Omega$. We consider elliptic operators L_k given by:

$$L_k u(t,\chi) = -\nabla \cdot (A_k(\chi)\nabla u(t,\chi)), \;\; A_k : \Omega \to \mathbb{R}^{r\times r}, \;\; k \in \{1, \ldots, n\}, \tag{4.33}$$

where the function $A_k(\chi)$ is symmetric and bounded and $\exists \alpha > 0$ such that for all $\chi \in \Omega$ and for all $\zeta = (\zeta_1, \zeta_2, \ldots, \zeta_r) \in \mathbb{R}^r$, $\sum_{i,j}^r a_{ij}(\chi)\zeta_i\zeta_j \geq \alpha|\zeta|^2$. We will study the reaction-diffusion equation:

$$\frac{\partial x(t,\chi)}{\partial t} = f(x(t,\chi)) + \mathcal{L}x(t,\chi), \tag{4.34}$$

subject to Neumann boundary conditions

$$\nabla x_i(t,\chi) \cdot \hat{n}(\chi) = 0 \;\; \forall \chi \in \partial\Omega, \tag{4.35}$$

where "$\cdot$" is the inner product in $\mathbb{R}^r$, $\hat{n}(\chi)$ is a vector normal to $\partial\Omega$, $x(t,\chi) \in \mathbb{R}^n$, and

$$\mathcal{L}x(t,\chi) = -[\nabla \cdot (A_1(\chi)\nabla x_1(t,\chi)) \ldots \nabla \cdot (A_n(\chi)\nabla x_n(t,\chi))]^T \tag{4.36}$$

is a vector of elliptic operators with respect to the spatial variable χ applied to each entry of $x(t,\chi)$. In a reaction-diffusion system, x represents a vector of concentrations for the reactants.

Define:

$$\bar{x}(t) := \frac{1}{|\Omega|}\int_\Omega x(t,\chi)d\chi, \quad \tilde{x}(t,\chi) := x(t,\chi) - \bar{x}(t) \tag{4.37}$$

In Theorem 11 below, we show that the solutions of (4.34) achieve spatial uniformity under the conditions (4.4)-(4.5):

Theorem 11 *Consider the system (4.34). Suppose there exists a convex set $\mathcal{X} \subseteq \mathbb{R}^n$, positive definite matrix P, and constant $\epsilon > 0$ such that the conditions (4.4)-(4.5) hold. Then for every bounded classical solution $x(t,\chi) : [0,\infty) \times \Omega \to \mathcal{X}$, $||\pi\{x(t,\chi)\}||_{L^2(\Omega)} \to 0$ exponentially as $t \to \infty$.* □

Theorem 11 applies to classical solutions that exist for all $t \geq 0$. Results on the existence of classical solutions to reaction-diffusion PDEs can be found in [89, 90, 42].

Proof of Theorem 11: First define $\tilde{x} = \pi\{x\}$. Note that

$$\frac{\partial \tilde{x}(t,\chi)}{\partial t} = \pi\{f(x(t,\chi))\} + \mathcal{L}x(t,\chi). \tag{4.38}$$

Consider the candidate Lyapunov function

$$V = \frac{1}{2}\int_\Omega \tilde{x}(t,\chi) \cdot P\tilde{x}(t,\chi)d\chi. \tag{4.39}$$

Differentiating, we have:

$$\dot{V} \leq \int_\Omega \tilde{x}(t,\chi) \cdot P\pi\{f(x(t,\chi))\}d\chi + \int_\Omega \tilde{x}(t,\chi) \cdot P\mathcal{L}x(t,\chi)d\chi. \tag{4.40}$$

We consider the expansion:

$$\int_\Omega \tilde{x}(t,\chi) \cdot P\mathcal{L}x(t,\chi)d\chi = \sum_{k=1}^{n} \int_\Omega \tilde{x}(t,\chi) \cdot PE_k\mathcal{L}x(t,\chi)d\chi, \tag{4.41}$$

and note that

$$\int_\Omega \tilde{x}(t,\chi) \cdot PE_k\mathcal{L}x(t,\chi)d\chi = \int_\Omega \tilde{x}(t,\chi) \cdot PE_k\mathcal{L}_k x(t,\chi)d\chi, \tag{4.42}$$

where the linear operator $\mathcal{L}_k$ is defined:

$$\mathcal{L}_k x(t,\chi) = [L_k x_k(t,\chi) \ \ \ldots \ \ L_k x_k(t,\chi) \ \ \ldots \ \ L_k x_k(t,\chi)]^T. \tag{4.43}$$

From the condition (4.5), we know there exists a matrix Q_k such that $Q_k^T Q_k = \frac{1}{2}(PE_k + E_k P)$. Substituting, we have:

$$\int_\Omega \tilde{x}(t,\chi) \cdot PE_k\mathcal{L}_k x(t,\chi)d\chi = \int_\Omega Q_k\tilde{x}(t,\chi) \cdot Q_k\mathcal{L}_k\tilde{x}(t,\chi)d\chi = \int_\Omega y_k(t,\chi) \cdot \mathcal{L}_k y_k(t,\chi)d\chi, \tag{4.44}$$

where $y_k(t,\chi) = Q_k\tilde{x}(t,\chi)$. Consider the following identity:

$$\nabla \cdot (gG) = g\nabla \cdot G + G \cdot \nabla g. \tag{4.45}$$

Taking $G = A_k(\chi)\nabla y_{k,i}(t,\chi)$ and $g = y_{k,i}(t,\chi)$, we next integrate both sides of the identity, noting the Neumann boundary conditions, and apply the divergence theorem, finding that the left hand side of the integrated identity is zero. We then have:

$$\int_\Omega y_{k,i}(t,\chi)\nabla\cdot(A_k(\chi)\nabla y_{k,i}(t,\chi))\,d\chi = -\int_\Omega \nabla y_{k,i}(t,\chi)\cdot(A_k(\chi)\nabla y_{k,i}(t,\chi))\,d\chi. \tag{4.46}$$

Noting that $\int_\Omega y_k(t,\chi)\,d\chi = Q_k\int_\Omega \tilde{x}(t,\chi)\,d\chi = 0$, we apply Lemma 1:

$$\int_\Omega \nabla y_{k,i}(t,\chi)\cdot(A_k(\chi)\nabla y_{k,i}(t,\chi))\,d\chi \geq \lambda_2^{(k)}\int_\Omega y_{k,i}(t,\chi)^2\,d\chi, \tag{4.47}$$

where $\lambda_2^{(k)}$ is the second Neumann eigenvalue of L_k. Substituting, we have:

$$\begin{aligned}\int_\Omega \tilde{x}(t,\chi)\cdot P\mathcal{L}x(t,\chi)d\chi &= \sum_{k=1}^n\int_\Omega y_k(t,\chi)\cdot\mathcal{L}_k y_k(t,\chi)d\chi\\ &\leq -\sum_{k=1}^n\lambda_2^{(k)}\int_\Omega y_k(t,\chi)\cdot y_k(t,\chi)d\chi\\ &= -\sum_{k=1}^n\lambda_2^{(k)}\int_\Omega \tilde{x}(t,\chi)\cdot PE_k\tilde{x}(t,\chi)d\chi.\end{aligned} \tag{4.48}$$

After adding to and subtracting $\int_\Omega \tilde{x}(t,\chi)\cdot f(\bar{x}(t))d\chi$ from the right hand side of (4.40), we arrive at:

$$\begin{aligned}\dot{V} &\leq \int_\Omega \tilde{x}(t,\chi)\cdot Pf(x(t,\chi)) - f(\bar{x}(t))d\chi - \sum_{k=1}^n\lambda_2^{(k)}\int_\Omega \tilde{x}(t,\chi)\cdot PE_k\tilde{x}(t,\chi)d\chi\\ &= \int_\Omega \tilde{x}(t,\chi)\cdot P\left(f(x(t,\chi)) - f(\bar{x}(t)) - \sum_{k=1}^n\lambda_2^{(k)}E_k\tilde{x}(t,\chi)\right)d\chi.\end{aligned} \tag{4.49}$$

An application of the mean value theorem to $f(x(t,\chi)) - f(\bar{x}(t,\chi))$ taken together with condition (4.4) gives:

$$\begin{aligned}\dot{V} &\leq \int_0^1\int_\Omega \tilde{x}(t,\chi)^T P\left(J(\bar{x}(t)+s\tilde{x}(t,\chi)) - \sum_{k=1}^n\lambda_2^{(k)}E_k\right)\tilde{x}(t,\chi)\,d\chi\,ds\\ &\leq \int_0^1\int_\Omega -\frac{\epsilon}{2}\tilde{x}(t,\chi)\cdot\tilde{x}(t,\chi)\,d\chi\,ds \leq -\frac{\epsilon}{\lambda_{\max}(P)}V,\end{aligned} \tag{4.50}$$

which concludes the proof. □

4.4 Conclusion

We have derived Lyapunov conditions that guarantee synchronization in compartmental ODEs and reaction-diffusion PDEs when the diffusion terms vary between species. We have used convex optimization to develop tests using linear matrix inequalities that imply the inequality conditions, and have applied the tests to coupled ring oscillator circuits.

Chapter 5

Adaptive Synchronization of Diffusively Coupled Systems

The majority of the literature assumes a static interconnection between the nodes in full state models [1, 79, 98, 91, 80, 84, 78] or phase variables in phase coupled oscillator models [69, 92, 16, 30]. However, recently, the situation where the interconnection strengths are adapted according to local synchronization errors has started to attract interest. In [5], the authors proposed a phase-coupled oscillator model in which local interactions were reinforced between agents with similar behavior and weakened between agents with divergent behavior, leading to enhanced local synchronization. In [24], the authors presented an adaptive law to establish synchrony across agents in a coupled compartmental system of ODEs. In [107], the authors relaxed the full-state coupling assumption.

In this chapter, we present an adaptive algorithm that guarantees synchrony in diffusively coupled nonlinear systems using an incremental output-feedback passivity property [104, 85, 87] of the agents. A similar property was employed in [84] for static networks without adaptation. A related condition that restricts the Jacobian of the vector field describing the uncoupled dynamics was used in [1] to guarantee spatial homogeneity in reaction-diffusion PDEs, and generalized to heterogeneous diffusion in Chapter 4. Using these results as a starting point, here we first consider compartmental models and derive adaptive laws that update interconnection strengths locally to achieve sufficient connectivity for synchronization. We next consider reaction-diffusion PDEs, and show that a similar control law that adapts the strength of diffusion coefficients guarantees spatial homogeneity. We present numerical examples that demonstrate the effectiveness of adaptation in enhancing synchrony and that lend insight to understanding the structure and bottleneck edges of the network.

Our results make several key contributions differing from the existing literature on adaptive networks. A fundamental achievement of our approach is that it applies to systems that satisfy an incremental output-feedback passivity property, which encompasses a broad and

numerically-verifiable class of systems, including those studied in [24, 107] but extending them significantly [38, 39]. Another feature of our method is the ability to handle multiple input-output channels interconnected according to different graphs. In this case, the edge weights for each graph are adjusted with separate update rules. In addition, we present a novel PDE analogue of the proposed adaptation, in which we consider systems defined on a spatial continuum rather than discrete compartments connected according to graph topologies. In [26], the author considered synchronization and consensus in linear parabolic distributed systems, and in [25] presented an adaptive algorithm for identical linear spatially-distributed systems coupled by a graph to guarantee state regulation and to improve convergence of coupled agents to common transient trajectories. However, nonlinear models and nonequilibrium dynamics were not considered. We study nonlinear models and do not make any assumptions on the attractors of the models. This allows us to achieve synchronization for limit cycle oscillators, multi-stable systems, etc. Furthermore, to our knowledge the literature does not address the question of spatial homogenization in reaction-diffusion PDEs in which the coefficients of the elliptic operator vary in time.

The chapter is organized as follows. In Section 5.1, we present the adaptive algorithm for compartmental systems of ODEs. We then present examples of the result applied to nonlinear oscillators and multiagent systems in Section 5.2. In Section 5.3, we present the adaptive algorithm for reaction-diffusion PDEs, and give an example of a system whose nominal dynamics are bistable with diffusive coupling on a domain with a bottleneck. We conclude and offer directions for future research in Section 5.4.

5.1 Compartmental Systems of ODEs

A. Main Result

Consider a collection of N dynamical systems H_i, $i = 1, \ldots, N$, defined by:

$$H_i: \quad \dot{x}_i = f(x_i) + g(x_i)u_i \quad i = 1, \ldots, N \tag{5.1}$$

$$y_i = h(x_i), \tag{5.2}$$

in which $x_i \in \mathbb{R}^n$, $u_i \in \mathbb{R}^p$, $y_i \in \mathbb{R}^p$, and $f(\cdot) : \mathbb{R}^n \to \mathbb{R}^n$, $g(\cdot) : \mathbb{R}^n \to \mathbb{R}^{n\times p}$, and $h(\cdot) : \mathbb{R}^n \to \mathbb{R}^p$ are continuously differentiable maps. Recall from Section 1.2 that H_i is said to satisfy an incremental output-feedback passivity property [91, 84] if there exist a positive definite storage function $S : \mathbb{R}^n \to \mathbb{R}$ and a scalar $\theta \in \mathbb{R}$ such that:

$$\frac{d}{dt}S(\delta x) =: \dot{S}(\delta x) \leq \theta \delta y^T \delta y + \delta u^T \delta y. \tag{5.3}$$

Let $\mathcal{G}$ be an undirected, connected graph with N nodes and M edges, where the nodes $i = 1, \ldots, N$ represent the dynamical systems given by H_i, and the edges represent the

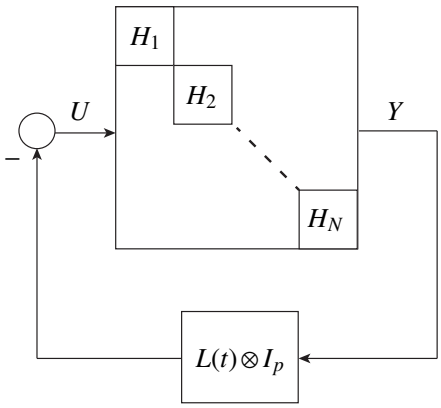

Figure 5.1: Dynamical systems H_i, $i = 1, \ldots, N$, coupled according to the weighted Laplacian matrix $L(t) \otimes I_p$. The vectors U and Y denote $U = [u_1^T \cdots u_N^T]^T$ and $Y = [y_1^T \cdots y_N^T]^T$.

couplings between systems. To represent the coupling terms, define the inputs:

$$u_i = \sum_{j=1}^{N} k_{ij} (y_j - y_i) \quad i = 1, \ldots, N, \tag{5.4}$$

in which the scalars $k_{ij} = k_{ji}$ for each pair (i, j). Nodes i and j are called neighbors in $\mathcal{G}$ if there is a edge in $\mathcal{G}$ connecting i with j. We take $k_{ij} = 0$ when nodes i and j are not neighbors in $\mathcal{G}$ so that the dynamical systems defined by (5.1)-(5.2), $i = 1, \ldots, N$, are coupled according to the graph structure. When i and j are neighbors, $k_{ij} = k_{ji}$ is updated according to:

$$\dot{k}_{ij} = \gamma_{ij} (y_i - y_j)^T (y_i - y_j) \tag{5.5}$$

where $\gamma_{ij} = \gamma_{ji} > 0$ is an adaptation gain to be selected by the designer. This update law increases $k_{ij}(t)$ according to the synchronization error between nodes i and j and can be implemented at each node. To maintain the symmetry $k_{ij}(t) = k_{ji}(t)$, nodes i and j would employ the same adaptation gain $\gamma_{ij} = \gamma_{ji}$ and start their updates with equal initial conditions $k_{ij}(0) = k_{ji}(0)$. To avoid numerical drift, occasional resets can be incorporated with a minimal additional communication requirement.

Next, we assign an arbitrary orientation to the edges of the graph $\mathcal{G}$, label the edges $\ell = 1, \ldots, M$, and introduce the $N \times M$ incidence matrix E as in (1.1). We define $U = [u_1^T \cdots u_N^T]^T$, $Y = [y_1^T \cdots y_N^T]^T$, and

$$L(t) = EK(t)E^T \tag{5.6}$$

where E is the graph incidence matrix defined in (1.1) and $K(t)$ is a diagonal matrix of the edge weights. Thus, $L(t)$ is a weighted Laplacian matrix where the weights are updated according to (5.5), and (5.4) becomes:

$$U = -(L(t) \otimes I_p)Y. \tag{5.7}$$

We show the networked dynamical systems H_i with the feedback (5.7) in Figure 5.1. Next, define

$$\bar{x} := \frac{1}{N}(x_1 + \cdots + x_N), \quad \tilde{x}_i := x_i - \bar{x}, \quad \text{and} \quad \tilde{y}_i := y_i - \bar{y}. \tag{5.8}$$

Theorem 12 *Consider the interconnected system (5.1)-(5.2)-(5.4), $i = 1, \ldots, N$, where $k_{ij} = k_{j\,i}$ is updated according to (5.5) when nodes i and j are neighbors in $\mathcal{G}$ and is interpreted as zero otherwise, and suppose that there exists a storage function for (5.1)-(5.2) that satisfies (5.3). If the solutions are bounded, then $\tilde{y}_i(t) \to 0$ as $t \to \infty$.* □

Proof: We first consider the function:

$$V = \frac{1}{2N} \sum_{i=1}^{N} \sum_{j=1}^{N} S(x_i - x_j). \tag{5.9}$$

Differentiating with respect to time, we have:

$$\dot{V} \leq \frac{1}{2N} \sum_{i=1}^{N} \sum_{j=1}^{N} \theta(y_i - y_j)^T (y_i - y_j) + (u_i - u_j)^T (y_i - y_j). \tag{5.10}$$

Defining $\bar{u} := \frac{1}{N}\sum_{i=1}^{N} u_i$ and $\bar{y} := \frac{1}{N}\sum_{i=1}^{N} y_i$, we have:

$$\sum_{i=1}^{N} \sum_{j=1}^{N} (u_i - u_j)^T (y_i - y_j) = N \sum_{i=1}^{N} 2u_i^T y_i - \bar{u}^T y_i - u_i^T \bar{y} \tag{5.11}$$

$$= N \sum_{i=1}^{N} (u_i - \bar{u})^T y_i + u_i^T (y_i - \bar{y}) \tag{5.12}$$

$$= 2N \sum_{i=1}^{N} \tilde{u}_i^T \tilde{y}_i, \tag{5.13}$$

where we have made use of the fact that $\sum_{i=1}^{N} (u_i - \bar{u})^T v = 0$ for constant v. Substituting (5.13) in the second product of the right hand side of (5.10) and expanding its first product similarly, we have:

$$\dot{V} \leq \theta \tilde{Y}^T \tilde{Y} + \tilde{Y}^T \tilde{U}, \tag{5.14}$$

where $\tilde{Y} := (\Pi \otimes I_p) Y$, $\tilde{U} := (\Pi \otimes I_p) U$, and $\Pi := I - \frac{1}{N} \mathbf{1_N} \mathbf{1_N}^T$. We next define $\tilde{k}_{ij} = k_{ij} - k_{ij}^*$ where

$$k_{ij}^* = \begin{cases} k^* & \text{if } i \text{ and } j \text{ are neighbors in } \mathcal{G} \\ 0 & \text{otherwise} \end{cases} \tag{5.15}$$

and k^* is a constant to be selected. Consider the function:

$$W = \frac{1}{4} \sum_{i=1}^{N} \sum_{j=1}^{N} \frac{1}{\gamma_{ij}} \tilde{k}_{ij}^2. \tag{5.16}$$

Differentiating with respect to time, we have:

$$\begin{aligned}\dot{W} &= \frac{1}{2}\sum_{i=1}^{N}\sum_{j=1}^{N}\tilde{k}_{ij}(y_i - y_j)^T(y_i - y_j) \\ &= \frac{1}{2}\sum_{i=1}^{N}\sum_{j=1}^{N}\tilde{k}_{ij}(\tilde{y}_i - \tilde{y}_j)^T(\tilde{y}_i - \tilde{y}_j).\end{aligned} \tag{5.17}$$

We note that $(E\otimes I_p)^T\tilde{Y}$, with E defined as in (1.1), is a column vector that is a concatenation of p-dimensional components, and the ℓth such component is $\tilde{y}_i - \tilde{y}_j$, where i is the head and j is the tail of edge ℓ. It then follows from (5.15) that:

$$\begin{aligned}\sum_{i=1}^{N}\sum_{j=1}^{N}k_{ij}^*(\tilde{y}_i - \tilde{y}_j)^T(\tilde{y}_i - \tilde{y}_j) &= 2k^*\tilde{Y}^T(E\otimes I_p)(E\otimes I_p)^T\tilde{Y} \\ &= 2k^*\tilde{Y}^T(EE^T\otimes I_p)\tilde{Y}.\end{aligned} \tag{5.18}$$

Since EE^T is the Laplacian matrix for the graph $\mathcal{G}$, its smallest eigenvalue is $\lambda_1 = 0$ and the vector of ones $\mathbf{1}_N$ is a corresponding eigenvector. Likewise, for $EE^T \otimes I_p$, $\lambda_1 = 0$ has multiplicity p and the corresponding eigenspace is the range of $\mathbf{1}_N \otimes I_p$. Because $\mathcal{G}$ is connected, the second smallest eigenvalue λ_2 is strictly positive and, since $\tilde{Y}^T(\mathbf{1}_N \otimes I_p) = 0$ from (5.8), the following inequality holds:

$$\tilde{Y}^T(EE^T\otimes I_p)\tilde{Y} \geq \lambda_2\tilde{Y}^T\tilde{Y}. \tag{5.19}$$

Substituting, we then have

$$\begin{aligned}\dot{W} &= \tilde{Y}^T(L(t)\otimes I_p)\tilde{Y} - k^*\tilde{Y}^T(EE^T\otimes I_p)\tilde{Y} \\ &\leq -\tilde{U}^T\tilde{Y} - k^*\lambda_2\tilde{Y}^T\tilde{Y}.\end{aligned} \tag{5.20}$$

The candidate Lyapunov function $Z = V + W$ then satisfies:

$$\dot{Z} \leq -(k^*\lambda_2 - \theta)\tilde{Y}^T\tilde{Y}, \tag{5.21}$$

and choosing k^* large enough that $\epsilon := k^*\lambda_2 - \theta > 0$ guarantees:

$$\dot{Z} \leq -\epsilon\tilde{Y}^T\tilde{Y}. \tag{5.22}$$

By integrating both sides of the inequality (5.22), we conclude that $\tilde{y}_i(t)$ is in $\mathcal{L}_2$, $i = 1, \ldots, N$. Furthermore, the boundedness of solutions implies that $\dot{x}_i(t)$ and, thus $\dot{\tilde{y}}_i(t)$ is bounded. Barbalat's Lemma [64] then guarantees $\tilde{y}_i(t) \to 0$ as $t \to \infty$. □

Remark 1 *An extension of Theorem 12 to the case of multiple input-output channels, connected according to different graphs, is straightforward. The system now takes the form:*

$$\dot{x}_i = f(x_i) + \sum_{q=1}^{m} g^{(q)}(x_i) u_i^{(q)} \tag{5.23}$$

$$y_i^{(q)} = h^{(q)}(x_i), \tag{5.24}$$

where $g^{(q)}$ and $h^{(q)}$ are continuously-differentiable vector fields and $y_i^{(q)} \in \mathbb{R}^{p_q}$, $q = 1, \ldots, m$. A graph $\mathcal{G}^{(q)}$ is defined for each channel q and $k_{ij}^{(q)} = k_{ji}^{(q)} \neq 0$ only when nodes i and j are adjacent in $\mathcal{G}^{(q)}$. The update rule (5.5) then becomes:

$$\dot{k}_{ij}^{(q)} = \gamma_{ij}^{(q)} \, (y_i^{(q)} - y_j^{(q)})^T (y_i^{(q)} - y_j^{(q)}), \quad \gamma_{ij}^{(q)} > 0, \quad q = 1, \ldots, m, \tag{5.25}$$

and the inputs in (5.4) are now:

$$u_i^{(q)} = \sum_{j=1}^{N} k_{ij}^{(q)} \left(y_j^{(q)} - y_i^{(q)} \right).$$

The assumption (5.3) is modified as:

$$\dot{S}(\delta x) \leq \sum_{q=1}^{m} \theta \delta y^{(q)T} \delta y^{(q)} + \omega^{(q)} \delta u^{(q)T} \delta y^{(q)}, \tag{5.26}$$

and the storage function W in the proof of Theorem 12 is modified as:

$$W = \sum_{q=1}^{m} \sum_{i=1}^{N} \sum_{j=1}^{N} \frac{\omega^{(q)}}{2\gamma_{ij}^{(q)}} \left(\tilde{k}_{ij}^{(q)} \right)^2, \tag{5.27}$$

where $\omega^{(q)} > 0$. The steps of the proof are otherwise identical and are not repeated to avoid excessive notation. □

Remark 2 *Since the proof of Theorem 1 analyzes the evolution of x_i relative to the average $\bar{x}$, it cannot reach any conclusions about the absolute behavior of the variables x_i. Thus, boundedness of the solutions does not follow from the proof and was assumed in the theorem. However, it is possible to conclude boundedness with an additional restriction on the vector field $f(x)$ when $g(x)$ is constant. Since $k_{ij} = k_{ji}$, the coupling terms in (5.4) do not affect the evolution of the average $\bar{x}$, which is governed by:*

$$\dot{\bar{x}} = \frac{1}{N} \sum_{i=1}^{N} f(x_i) = \frac{1}{N} \sum_{i=1}^{N} f(\bar{x} + \tilde{x}_i). \tag{5.28}$$

If this system has a bounded-input-bounded-state (BIBS) property when $\tilde{x}_i$ are interpreted as inputs, then we conclude boundedness of all solutions. This follows because the Lyapunov arguments in the proof show that $\tilde{x}_i(t)$ are bounded on the maximal interval of existence $[0, t_f)$ with bounds that do not depend on t_f and, thus, a similar conclusion holds for $\bar{x}(t)$ implying that $t_f = \infty$. □

B. Rapprochement with Classical Adaptive Control

To give further insight into the proof of Theorem 1 and to make a connection to classical model reference adaptive control (MRAC), we draw a detailed block diagram of $L(t) \otimes I_p$ in Figure 5.2 that encompasses the adaptation of edge weights. Adding and subtracting k^* from each edge weight and defining $\tilde{k}_{ij}(t) = k_{ij}(t) - k^*$, we rewrite (5.6) as:

$$L(t) = k^* L_0 + E\tilde{K}(t)E^T \tag{5.29}$$

where $L_0 := EE^T$ is the unweighted Laplacian and $\tilde{K}(t)$ is a diagonal matrix with entries $\tilde{k}_{ij}(t)$. The upper branch in Figure 5.2 represents the first term $k^* L_0$ and the lower branch represents the second term $E\tilde{K}(t)E^T$, further depicting the evolution of $\tilde{k}_{ij}(t)$ according to (5.5).

The symmetry of the multiplication blocks before and after the integrator ensures passivity of the lower branch, and is analogous to pre- and post-multiplication with the *regressor* and its transpose in MRAC [58]. The upper branch is a feedthrough term that provides the excess of passivity needed to compensate for the shortage of passivity in the feedforward path in Figure 5.1. Note that the passivity properties discussed above are with respect to $\tilde{U}$ and $\tilde{Y}$ which are obtained from U and Y by subtracting their orthogonal projections onto the range space of $\mathbf{1}_N \otimes I_p$. Since this corresponds to the eigenspace for the smallest eigenvalue $\lambda_1 = 0$ of $L_0 \otimes I_p$, the excess of passivity, $k^*\lambda_2$, provided by $k^* L_0 \otimes I_p$ is due to the second smallest eigenvalue $\lambda_2 > 0$.

As in MRAC, the passivity properties demonstrated here are instrumental for a systematic construction of a Lyapunov function from the associated storage functions. Indeed, the Lyapunov function $Z = V + W$ in the proof of Theorem 1 comprises of V, which certifies a shortage of passivity in the feedforward system in Figure 5.1, and W, which certifies an excess of passivity in the feedback path. The excess compensates for the shortage in (5.21)-(5.22) and $Z = V + W$ serves as a Lyapunov function.

C. A Class of Systems Satisfying the Incremental Passivity Assumption

We now highlight a class of systems for which the incremental output feedback passivity assumption (5.3) and its generalization (5.26) are easily verifiable. Consider a system of the

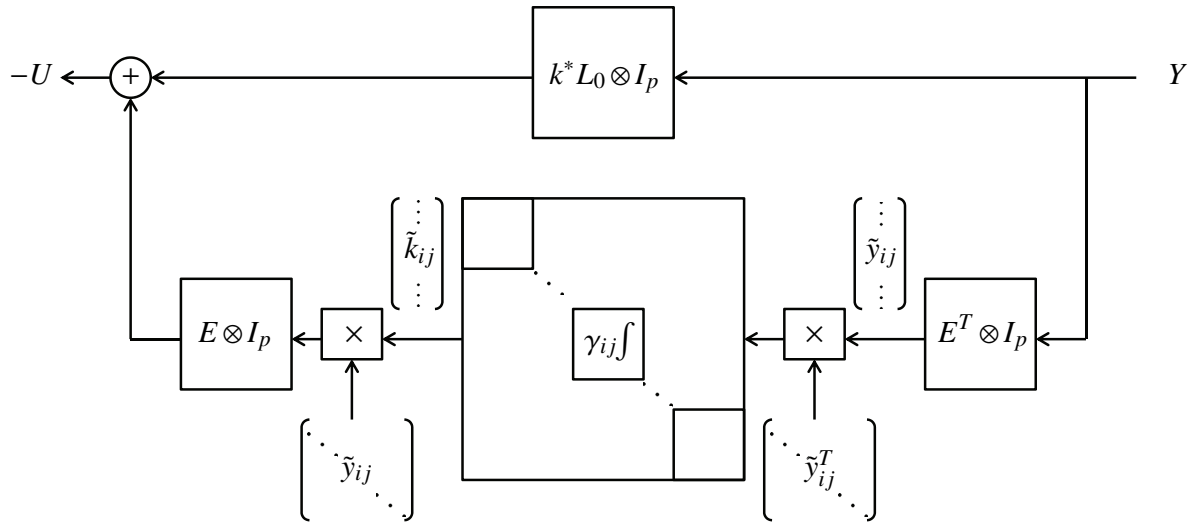

Figure 5.2: The feedback path in Figure 5.1 redrawn to include the edge weight adaptation (5.5). The Laplacian is rewritten as $L(t) = EK(t)E^T = k^*L_0 + E\tilde{K}(t)E^T$ where $L_0 = EE^T$ and $\tilde{K}(t)$ is a diagonal matrix of entries $\tilde{k}_{ij}(t) = k_{ij}(t) - k^*$. The evolution of $\tilde{k}_{ij}(t)$ is represented with the lower branch of the block diagram. In particular, $(E^T \otimes I_p)Y$ is a vector that is a concatenation of p-dimensional components of the form $\tilde{y}_{ij}(t) := y_i(t) - y_j(t)$ for each edge (i, j).

form:

$$\dot{x} = f(x) + \sum_{q=1}^{m} B^{(q)} u^{(q)} \tag{5.30}$$

$$y^{(q)} = C^{(q)} x, \tag{5.31}$$

where $B^{(q)} \in \mathbb{R}^{n \times p_q}$, $B = [B^{(1)} \cdots B^{(m)}] \in \mathbb{R}^{n \times p}$, $C^{(q)} \in \mathbb{R}^{p_q \times n}$, and $C = [{C^{(1)}}^T \cdots {C^{(m)}}^T]^T \in \mathbb{R}^{p \times n}$. We define the Jacobian

$$J(x) = \frac{\partial f(x)}{\partial x} \tag{5.32}$$

and give a condition that guarantees the existence of a quadratic storage function satisfying (5.26).

Lemma 9 *Suppose there exist a constant $\theta > 0$, scalars $\omega^{(i)} > 0$ for $i = 1, \ldots, m$, and a matrix $P = P^T > 0$ such that:*

$$PJ(x) + J(x)^T P \leq \theta C^T C \tag{5.33}$$

$$PB = [\omega^{(1)} {C^{(1)}}^T \cdots \omega^{(m)} {C^{(m)}}^T]. \tag{5.34}$$

Then the storage function $S = \frac{1}{2}(x_i - x_j)^T P (x_i - x_j)$ satisfies (5.26). □

Proof: Differentiating with respect to time, we have:

$$\begin{aligned}
\dot{S} =&(x_i - x_j)^T P(f(x_i) - f(x_j) + Bu_i - Bu_j) && (5.35)\\
=&(x_i - x_j)^T P \int_0^1 J(x_j + s(x_i - x_j))\, ds\, (x_i - x_j) && (5.36)\\
&+ \sum_{q=1}^{m} \omega^{(q)} (y_i^{(q)} - y_j^{(q)})^T (u_i^{(q)} - u_j^{(q)})\\
\leq&\frac{\theta}{2}(x_i - x_j)^T C^T C (x_i - x_j) + \sum_{q=1}^{m} \omega^{(q)} (y_i^{(q)} - y_j^{(q)})^T (u_i^{(q)} - u_j^{(q)}) && (5.37)\\
\leq&\sum_{q=1}^{m} \theta (y_i^{(q)} - y_j^{(q)})^T (y_i^{(q)} - y_j^{(q)}) + \omega^{(q)} (y_i^{(q)} - y_j^{(q)})^T (u_i^{(q)} - u_j^{(q)}), && (5.38)
\end{aligned}$$

where (5.36) follows from the Mean Value Theorem. □

A subset of these systems where the product BC is diagonal and the assumptions (5.33)-(5.34) of Lemma 9 hold with $P = I$ is considered in [24, 23, 107]. In contrast, Lemma 9 allows $P \neq I$, does not restrict BC to be diagonal, and furthermore allows multiple input-output channels connected according to different graphs. Note that the general class of systems studied in Section 5.1-A is even less restrictive, as we do not insist on a quadratic storage function. Fully characterizing this general class is a current research topic and significant advances are reported in [38, 39].

The next result, a modification of Theorem 3 in [1], leads to a sufficient condition for (5.33) that may be numerically verified using linear matrix inequalities.

Theorem 13 *Suppose that:*

$$J(x) \in \{A_0 + \kappa_1 A_1 + \ldots + \kappa_p A_l \,|\, \kappa_i \in [0,1],\, i = 1, \ldots, p\}, \tag{5.39}$$

where $A_1, \ldots, A_l$ are rank-one matrices that can be written as $A_i = G_i H_i^T$, with G_i, $H_i \in \mathbb{R}^n$. If there exists a matrix $\mathcal{P} = \mathcal{P}^T > 0$ with:

$$\begin{gathered}
\mathcal{P} = \begin{bmatrix} P & 0 & \ldots & 0 \\ 0 & q_1 & 0 & 0 \\ \vdots & \ddots & \ddots & \vdots \\ 0 & \ldots & 0 & q_l \end{bmatrix} \\
P \in \mathbb{R}^{n \times n},\, q_i \in \mathbb{R},\, i = 1, \ldots, l,
\end{gathered} \tag{5.40}$$

satisfying:

$$\mathcal{P} \begin{bmatrix} A_0 & G \\ H^T & -I_n \end{bmatrix} + \begin{bmatrix} A_0 & G \\ H^T & -I_n \end{bmatrix}^T \mathcal{P} \leq \begin{bmatrix} \theta C^T C & 0 \\ 0 & 0 \end{bmatrix}, \tag{5.41}$$

with $G = [G_1 \ldots G_l]$ and $H = [H_1 \ldots H_l]$, then the upper left principal submatrix $P = P^T > 0$ satisfies (5.33). □

5.2 Numerical Examples

In this section, we first consider ring oscillator circuits coupled according to differing graphs. Subsequently, we turn to the problem of mitigating time scale separation in clustered networks. Both examples demonstrate the benefits of adaptive coupling in improving synchronization.

A. Nonlinear oscillator synchronization

We illustrate the adaptive approach on a nonlinear oscillator. In Chapter 3, we presented a method to check for synchrony of limit cycle oscillations in diffusively coupled systems. In an example, we considered a ring oscillator model in which three interconnected three-stage ring oscillators (Figure 5.3) were coupled through the first node. Ring oscillators constitute a class of voltage-controlled oscillators frequently found in clock recovery circuits and disk-drive read channels [28, 72], and are also encountered in synthetic gene circuits [53]. We showed that trajectories sufficiently close to a limit cycle trajectory of the nominal system synchronized under small diffusive coupling.

We now demonstrate that the adaptive algorithm described in this chapter allows additional flexibility in assigning differing coupling structures to each component. The dynamics of each oscillator is given by:

$$f(x) = \begin{bmatrix} -\eta_1 x_1 - \alpha_1 \tanh(x_3) \\ -\eta_2 x_2 - \alpha_2 \tanh(x_1) \\ -\eta_3 x_3 - \alpha_3 \tanh(x_2) \end{bmatrix}. \tag{5.42}$$

If $\Pi_{i=1}^{3} \alpha_i > 8$ and $\eta_i = 1$ for all i, (5.42) admits a limit cycle [44]. We set $\eta_i = 1$ and $\alpha_i = 2.2$ for all i.

We set each adaptation gain $\gamma_{ij} = 1$. In our first simulation, the second node in each circuit is coupled to corresponding nodes by a path graph (blue in Figure 5.3) with $B = C^T = [0\ \ 1\ \ 0]^T$ as in Section 5.1-C. An application of Theorem 13 shows that the assumptions in Lemma 9 hold, e.g., with $\theta = 12.425$, $P = \mathrm{Diag}([1.000\ \ 2.593\ \ 0.663])$. We show the evolution of the trajectories corresponding to the third node in Figure 5.4, which synchronized as expected.

In our next simulation, we allow coupling through two nodes (Remark 1) and connect the first node by a cycle graph (green in Figure 5.3) with $B_1 = C_1^T = [1\ \ 0\ \ 0]^T$ and the second node as before with $B_2 = C_2^T = [0\ \ 1\ \ 0]^T$. An application of Theorem 13 shows that the assumptions in Lemma 9, with:

$$PB = [\omega^{(1)} {C^{(2)}}^T \omega^{(2)} {C^{(2)}}^T], \tag{5.43}$$

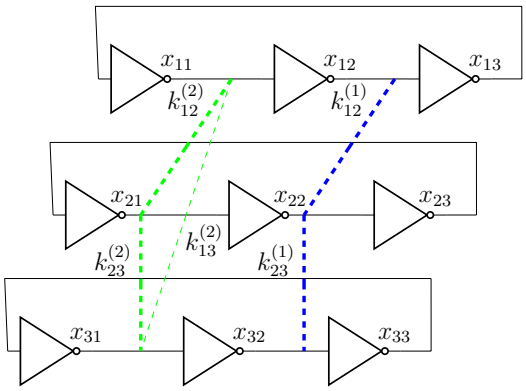

Figure 5.3: Example of three-stage ring oscillators as in (5.42) coupled through nodes 1 and 2.

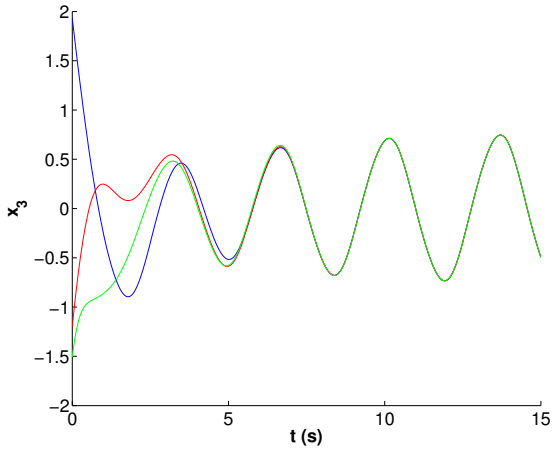

Figure 5.4: Evolution of trajectories corresponding to third node x_{3i} in each circuit $i = 1, 2, 3$, coupled through second node with adaptation. Trajectories synchronize.

hold, e.g., with $\theta = 7.704$, $P = \text{Diag}([1.000 \;\; 1.622 \;\; 1.656])$, and $\omega^{(1)} = 1$ and $\omega^{(2)} = P_{22}$. The corresponding trajectories and weight updates in Figures 5.5 and 5.6 show that synchronization is accelerated.

B. Mitigating time scale separation in clustered networks

In [9], it was shown that a network consisting of several densely-connected clusters of nodes interconnected to other clusters by sparse edges exhibited a time scale separation, in which agents within each cluster quickly synchronized, while the clusters themselves subsequently synchronized in a slower time scale. In our simulations, we consider a 48 node network with

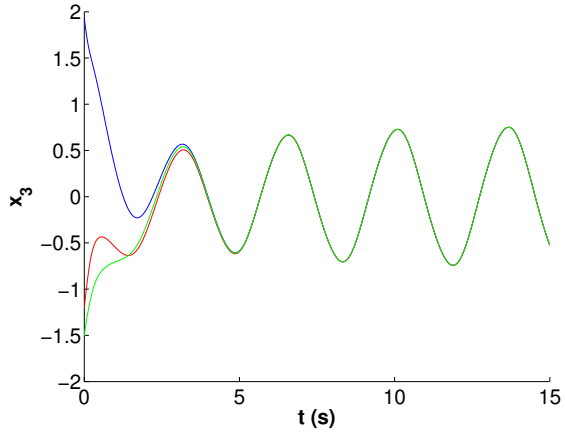

Figure 5.5: Evolution of trajectories corresponding to third node x_{i3} in each circuit $i = 1, 2, 3$, coupled through first and second nodes with adaptation. Trajectory synchronization is improved.

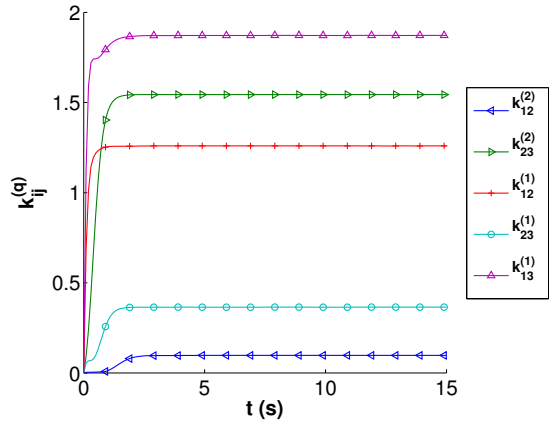

Figure 5.6: Evolution of weights of graphs corresponding to coupling of first and second nodes with adaptation.

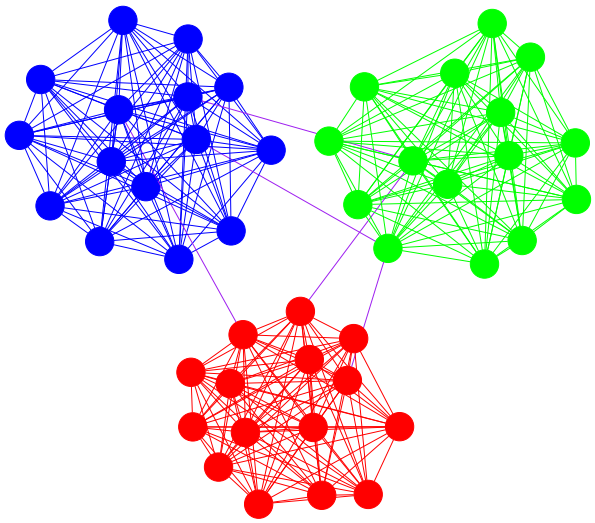

Figure 5.7: Example of 48 node clustered graph with sparse interconnection edges between clusters.

three completely connected components with randomly generated external edges between each cluster pair, shown in Figure 5.7. Each node obeys the following dynamics:

$$\dot{x}_i = \sum_{j \in \mathcal{N}_i} k_{ij}(x_j - x_i), \tag{5.44}$$

and the assumptions in Lemma 9 are trivially satisfied.

In the first case, we turn adaptation off, and set the weights $k_{ij} = 1$ for all i, j. As expected, the agents cluster into groups (denoted by blue, green, and red in Figure 5.8). In the second case, we turn adaptation on. We set the gains γ_{ij} corresponding to within-cluster edges to unity, and those corresponding to external edges to 10^3. For example, cluster head nodes in sensor networks, which may be the endpoints of edges between clusters, typically have greater computational and power resources in order to adapt quickly to changes in other parts of the network and relay the information to the rest of the cluster. We set the initial weights to $k_{ij}(0) = 1$, which are the constant values in the nonadaptive simulation. With adaptation, the time scale separation is mitigated and the agents' trajectories converge more quickly (Figure 5.9), with external edge weights evolving (Figure 5.10) as global synchrony is achieved. As one may expect from the structure of the network, the curves corresponding to the edges between clusters reach the largest values.

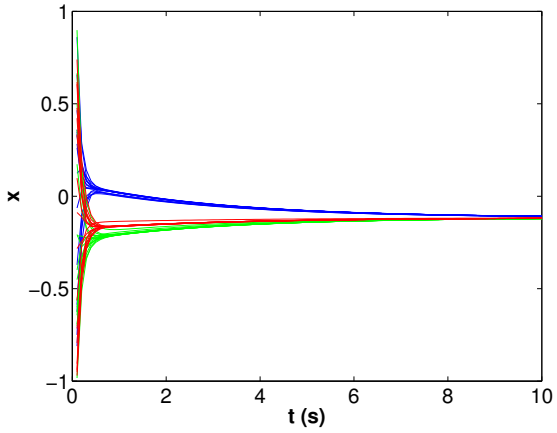

Figure 5.8: Evolution of agents with adaptation turned off. The agents first synchronize within their clusters (denoted by blue, green, and red as in Figure 5.7), and then synchronize globally.

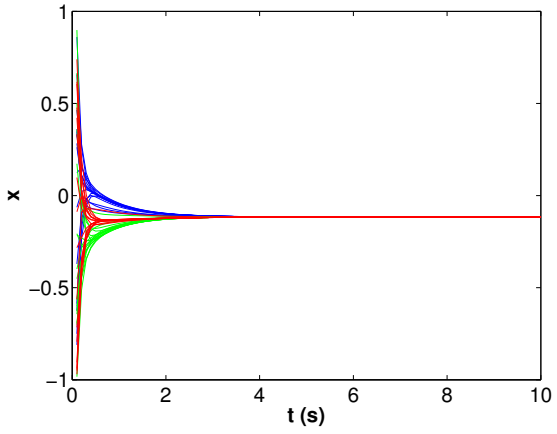

Figure 5.9: Evolution of agents with adaptation turned on. The agents of each cluster (denoted by blue, green, and red as in Figure 5.7) quickly synchronize to a common value.

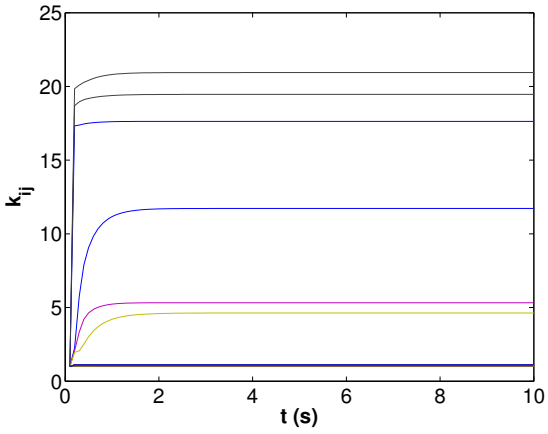

Figure 5.10: Evolution of weights of coupling graph as in Figure 5.7 with adaptation turned on. Weights continue to evolve until synchrony is attained, with the greatest stress on the sparse edges between clusters.

5.3 Reaction-Diffusion PDEs

In this section, we formulate the problem of spatial homogenization for systems of reaction-diffusion PDEs, which is analogous to the problem of synchronization of like components in compartmental systems of ODEs.

A. Main Result

Let Ω be a bounded and connected domain in $\mathbb{R}^r$ with smooth boundary $\partial\Omega$, and consider the PDE:

$$\frac{\partial x(t,\chi)}{\partial t} = f(x(t,\chi)) + \sum_{\ell=1}^{p} g_\ell(x(t,\chi))u_\ell \tag{5.45}$$

$$y_\ell(t,\chi) = h_\ell(x(t,\chi)), \quad \ell = 1,\dots,p \tag{5.46}$$

$$u_\ell = \nabla\cdot(k(t,\chi)\nabla y_\ell(t,\chi)), \quad \ell = 1,\dots,p, \tag{5.47}$$

where $\chi \in \Omega$ is the spatial variable, $x(t,\chi) \in \mathbb{R}^n$ is the state variable with initial condition $x(0,\chi) = x_0(\chi)$, $k(t,\chi) \in \mathbb{R}$, $f(\cdot) : \mathbb{R}^n \to \mathbb{R}^n$, $g(\cdot) = [g_1 \cdots g_p] : \mathbb{R}^n \to \mathbb{R}^{n\times p}$, and $h(\cdot) = [h_1^T \cdots h_p^T]^T : \mathbb{R}^n \to \mathbb{R}^p$ are continuously differentiable maps, $\nabla\cdot$ is the divergence operator and ∇ represents the gradient with respect to the spatial variable χ. We assume Neumann boundary conditions:

$$\nabla x_i(t,\chi)\cdot\hat{n}(\chi) = 0 \quad \forall\chi\in\partial\Omega,\ \forall t\geq 0, \quad i = 1,\dots,n \tag{5.48}$$

where "$\cdot$" is the inner product in $\mathbb{R}^r$, $x_i(t,\chi)$ denotes the ith entry of the vector $x(t,\chi)$ and $\hat{n}(\chi)$ is a vector normal to the boundary $\partial\Omega$.

In relation to synchronization of each like state $x_{i,k}$ across compartments $i = 1, \ldots, N$, we now derive an adaptive law that guarantees synchronization of each concentration $x_i(t,\chi)$ across the spatial domain Ω. The topology of Ω is the spatial continuum analogue to the topology of the interconnection graph $\mathcal{G}$, which represents the network of compartments. In analogy with (5.5), we introduce the update law:

$$\frac{\partial k(t,\chi)}{\partial t} = \gamma(\chi) \sum_{\ell=1}^{p} \nabla y_\ell(t,\chi) \cdot \nabla y_\ell(t,\chi), \tag{5.49}$$

where $\gamma(\chi) > 0$ is a design choice, with the initial condition $k(0,\chi) = k_0(\chi)$. Define:

$$\begin{aligned} \bar{x}(t) := \frac{1}{|\Omega|} \int_\Omega x(t,\chi) d\chi, \quad \tilde{x}(t,\chi) := x(t,\chi) - \bar{x}(t) \\ \tilde{y}_\ell(t,\chi) := y_\ell(t,\chi) - \bar{y}_\ell(t). \end{aligned} \tag{5.50}$$

In Theorem 14 below, we give conditions that guarantee the following output synchronization property:

$$\lim_{t\to\infty} \int_\Omega |\tilde{y}(t,\chi)|^2 d\chi = 0, \tag{5.51}$$

where $|\cdot|$ denotes the Euclidean norm.

Theorem 14 *Consider the system (5.45)-(5.47) with boundary condition (5.48), and suppose that there exists a storage function for (5.45)-(5.46) that satisfies (5.3). Then, the update law (5.49) guarantees (5.51) for every bounded classical solution*[1]. □

Theorem 14 applies to classical solutions that exist for all $t \geq 0$. Results on the existence of classical solutions to reaction-diffusion PDEs can be found in [89, 90, 42]; well-posedness in the context of adaptive control of distributed parameter systems is considered in [55, 10].

Proof of Theorem 14: We first consider the function:

$$V = \frac{1}{2|\Omega|} \int_\Omega \int_\Omega S(x(t,\chi_a) - x(t,\chi_b))\, d\chi_a\, d\chi_b. \tag{5.52}$$

Note that (5.45)-(5.46), without the coupling term (5.47), is identical to (5.1)-(5.2). Therefore, using (5.3), we have:

$$\begin{aligned} \dot{V} \leq & \frac{1}{2|\Omega|} \int_\Omega \int_\Omega \theta(y(t,\chi_a) - y(t,\chi_b)) \cdot (y(t,\chi_a) - y(t,\chi_b)) \\ & + (u(t,\chi_a) - u(t,\chi_b)) \cdot (y(t,\chi_a) - y(t,\chi_b))\, d\chi_a\, d\chi_b. \end{aligned} \tag{5.53}$$

[1] A solution of a PDE of order k is said to be *classical* it it is at least k times continuously differentiable so that all derivatives that appear in the PDE exist and are continuous [33].

Defining $\bar{u}(t) := \int_\Omega u(t,\chi)\,d\chi$ and $\bar{y}(t) := \int_\Omega y(t,\chi)\,d\chi$, we have:

$$\int_\Omega \int_\Omega (u(t,\chi_a) - u(t,\chi_b)) \cdot (y(t,\chi_a) - y(t,\chi_b))\,d\chi_a\,d\chi_b \tag{5.54}$$

$$= \int_\Omega \int_\Omega u(t,\chi_a)\cdot y(t,\chi_a) - u(t,\chi_a)\cdot y(t,\chi_b) \tag{5.55}$$
$$- u(t,\chi_b)\cdot y(t,\chi_a) + u(t,\chi_b)\cdot y(t,\chi_b)\,d\chi_a\,d\chi_b$$

$$= |\Omega| \int_\Omega u(t,\chi_a)\cdot y(t,\chi_a)\,d\chi_a - |\Omega| \int_\Omega u(t,\chi_a)\cdot \bar{y}(t)\,d\chi_a \tag{5.56}$$
$$- |\Omega| \int_\Omega \bar{u}(t)\cdot y(t,\chi_a)\,d\chi_a + |\Omega| \int_\Omega u(t,\chi_b)\cdot y(t,\chi_b)\,d\chi_b.$$

Rewriting (5.56) with a substitution of variables, we have:

$$|\Omega| \int_\Omega 2u(t,\chi)\cdot y(t,\chi) - u(t,\chi)\cdot \bar{y}(t) - \bar{u}(t)\cdot y(t,\chi)\,d\chi \tag{5.57}$$

$$= |\Omega| \int_\Omega u(t,\chi)\cdot (y(t,\chi) - \bar{y}(t)) + (u(t,\chi) - \bar{u}(t))\cdot y(t,\chi)\,d\chi \tag{5.58}$$

$$= 2|\Omega| \int_\Omega (u(t,\chi) - \bar{u}(t))\cdot (y(t,\chi) - \bar{y}(t))\,d\chi, \tag{5.59}$$

where we have made use of the fact that $\int_\Omega (u(t,\chi) - \bar{u}(t))\cdot v(t)\,d\chi = 0$ for $v(t)$ not dependent on χ. Substituting (5.59) in the second product of the right hand side of (5.53) and expanding its first product similarly, we have:

$$\dot{V} \le \int_\Omega \theta\tilde{y}(t,\chi)\cdot\tilde{y}(t,\chi) + \tilde{y}(t,\chi)\cdot\tilde{u}(t,\chi)\,d\chi. \tag{5.60}$$

We next define:

$$W = \int_\Omega \frac{1}{2\gamma(\chi)} |\tilde{k}(t,\chi)|^2 d\chi \tag{5.61}$$

where $\tilde{k}(t,\chi) = k(t,\chi) - k^*$, and k^* is to be selected. Taking derivatives with respect to time, applying (5.49), and substituting $\nabla y_\ell(t,\chi) = \nabla\tilde{y}_\ell(t,\chi)$, we get:

$$\dot{W} = \sum_{\ell=1}^{p} \int_\Omega \tilde{k}(t,\chi)\nabla\tilde{y}_\ell(t,\chi)\cdot\nabla\tilde{y}_\ell(t,\chi) d\chi. \tag{5.62}$$

We now claim that:

$$\int_\Omega \tilde{y}_\ell(t,\chi)\nabla\cdot(k(t,\chi)\nabla\tilde{y}_\ell(t,\chi)) d\chi = -\int_\Omega k(t,\chi)\nabla\tilde{y}_\ell(t,\chi)\cdot\nabla\tilde{y}_\ell(t,\chi) d\chi. \tag{5.63}$$

This follows by first applying the identity $\nabla \cdot (fF) = f\nabla \cdot F + F \cdot \nabla f$, which holds when f is scalar valued, with $F = k(t,\chi)\nabla\tilde{y}_\ell(t,\chi)$ and $f = \tilde{y}_\ell(t,\chi)$, next integrating both sides of the identity over Ω, and finally noting that the left-hand side is zero, since:

$$\int_\Omega \nabla \cdot (\tilde{y}_\ell(t,\chi)k(t,\chi)\nabla\tilde{y}_\ell(t,\chi))d\chi = \int_{\partial\Omega} \tilde{y}_\ell(t,\chi)k(t,\chi)\nabla\tilde{y}_\ell(t,\chi)\cdot\hat{n}(\chi)dS \tag{5.64}$$

from the Divergence Theorem and $\nabla\tilde{y}_\ell(t,\chi)\cdot\hat{n}(\chi) = 0$ for $\chi \in \partial\Omega$ from the boundary condition (5.48). Moreover, because $\int_\Omega \tilde{y}_\ell(t,\chi)d\chi = 0$, it follows from Lemma 1 that:

$$\int_\Omega |\nabla\tilde{y}_\ell(t,\chi)|^2 d\chi \geq \lambda_2 \int_\Omega \tilde{y}_\ell(t,\chi)^2 d\chi \tag{5.65}$$

where λ_2 denotes the second smallest of the eigenvalues $0 = \lambda_1 \leq \lambda_2 \leq \cdots$ of the operator $L = -\nabla^2$ on Ω with Neumann boundary condition, and $\lambda_2 > 0$ since Ω is connected. Substituting in (5.62), we have:

$$\begin{aligned} \dot{W} &= \sum_{\ell=1}^{p} \int_\Omega -\tilde{y}_\ell(t,\chi)\cdot\tilde{u}(t,\chi) - k^*\lambda_2\tilde{y}_\ell(t,\chi)^2\, d\chi \\ &= -\int_\Omega \tilde{y}(t,\chi)\cdot\tilde{u}(t,\chi) + k^*\lambda_2\tilde{y}(t,\chi)\cdot\tilde{y}(t,\chi)\, d\chi \end{aligned} \tag{5.66}$$

The candidate Lyapunov function $Z = V + W$ then satisfies:

$$\dot{Z} \leq -(k^*\lambda_2 - \theta)\int_\Omega |\tilde{y}(t,\chi)|^2\, d\chi, \tag{5.67}$$

and choosing k^* large enough that $\epsilon := k^*\lambda_2 - \theta > 0$ guarantees:

$$\dot{Z} \leq -\epsilon \int_\Omega |\tilde{y}(t,\chi)|^2\, d\chi =: -\epsilon Q(t). \tag{5.68}$$

This implies that $\lim_{T\to\infty}\int_0^T Q(t)dt$ exists and is bounded. Since $\dot{Q}(t)$ is also bounded, it follows from Barbalat's Lemma [64] that $Q(t) \to 0$ as $t \to \infty$ which proves (5.51). □

B. Bistable Reaction-Diffusion PDE

Consider a continuous domain consisting of two rectangular subdomains joined by their intersection as in Figure 5.11. Suppose the system is governed by (5.45)-(5.46) where $B = C = 1$ and

$$f(x) = x - x^3. \tag{5.69}$$

Thus, the assumptions of Lemma 9 hold with $P = 1$ and $\theta = 2$.

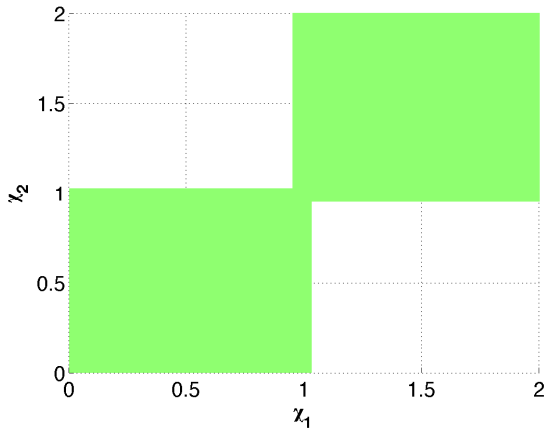

Figure 5.11: Two rectangular subdomains joined by their intersection.

Note from (5.69) that each point in the space is a bistable system with stable equilibria at ± 1 and a saddle point at 0. To simulate the reaction-diffusion system, we employ a second-order finite-difference scheme to discretize the diffusion operator, and solve the resulting system of ODEs in MATLAB. Indeed, when we set the edge weights to zero and turn off the adaptation, $x(t, \chi)$ evolves independently at each point in space and converges to $+1$ or -1 (Figure 5.13). Next, we turn on the adaptation with gain $\gamma(\chi) = 1$ and initial condition $k(0, \chi) = 1$ for all χ. Figures 5.14 and 5.15 confirm that the solution becomes spatially uniform, converging to a consensus value of $+1$ or -1, depending on the initial conditions. The final distribution of weights for the solution in Figure 5.14 is shown in Figure 5.16. Note from (5.49) that $k(t, \chi)$ converges to the squared L_2 norm of the gradient $\nabla x(t, \chi)$ at each point χ. As one may expect from the weakly connected structure of the domain, the portion of k corresponding to the bottleneck between rectangular subdomains reaches the largest value, indicating a high "stress" on the bottleneck.

5.4 Conclusion

We have developed adaptive synchronization laws that allow the interconnection strength to evolve according to local synchronization errors. We studied both compartmental ODE and reaction-diffusion PDE models, and demonstrated the benefits of the adaptive approach in eliminating the slow time scales due to bottlenecks in the interconnection graph for ODEs and the spatial domain for PDEs. Indeed, the interconnection strengths reach larger values around bottlenecks, which means that the proposed algorithms establish stronger connections where needed in a decentralized way.

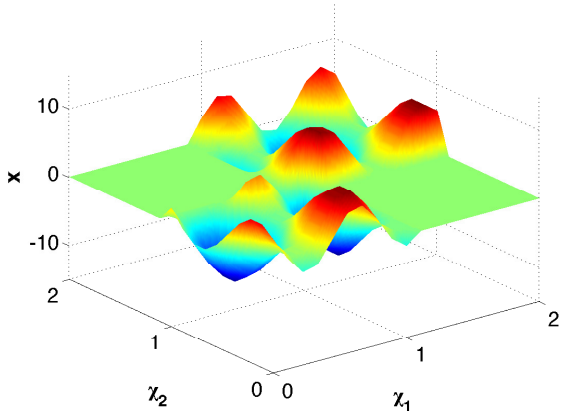

Figure 5.12: Solution $x(t, \chi)$ at initial time $t = 0$ s.

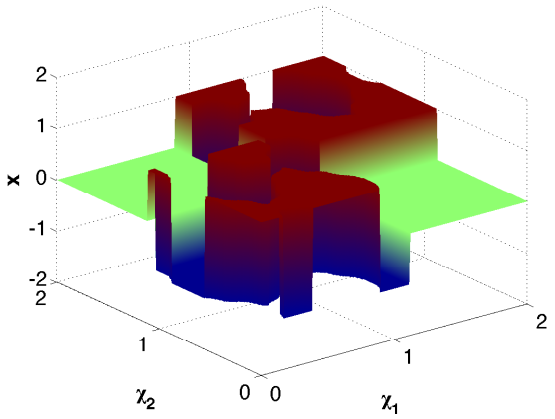

Figure 5.13: Solution $x(t, \chi)$ with no adaptation and initial condition in Figure 5.12 at time $t = 10$ s. Solution converges to patches at 0, $+1$, and -1.

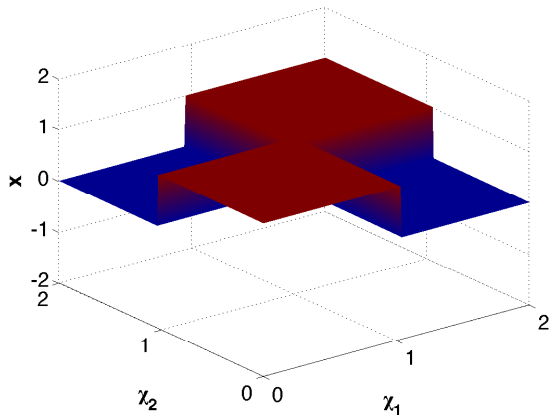

Figure 5.14: Solution $x(t, \chi)$ with adaptation and initial condition in Figure 5.12 at time $t = 10$ s that converges to $+1$.

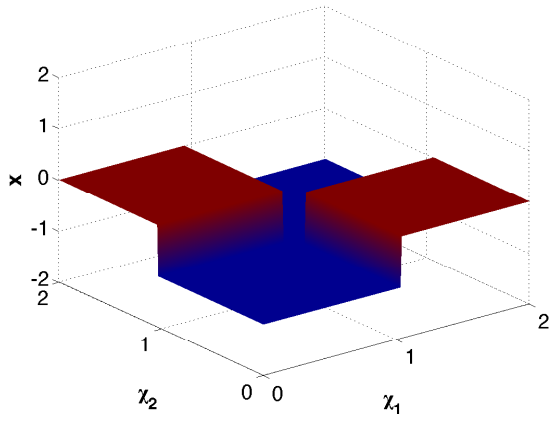

Figure 5.15: Solution $x(t, \chi)$ from a different initial condition with adaptation at time $t = 10$ s that converges to -1.

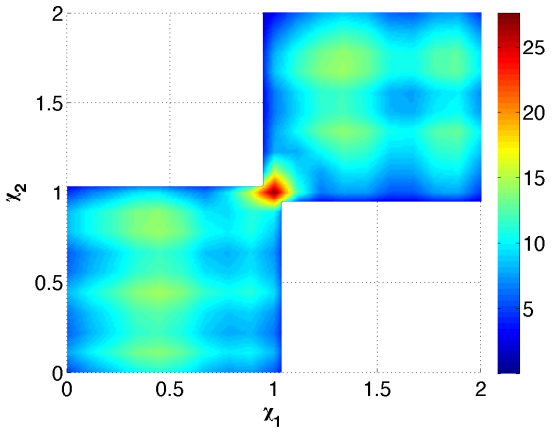

Figure 5.16: Weights $k(t, \chi)$ at time $t = 10$ s for the solution with initial condition in Figure 5.12. The red at the center of the domain indicates increased stress in the portion of the domain corresponding to the bottleneck between regions.

Chapter 6

Synchronization under space and time-dependent heterogeneities

Common to much of the literature is the assumption that the agents to be synchronized are homogeneous with identical dynamics, and are furthermore not subject to disturbances. However, recent work has considered synchronization and consensus in the presence of exogenous inputs. In [7], the authors addressed the problem of robust dynamic average consensus (DAC), in which the use of partial model information about a broad class of time-varying inputs enabled exact tracking of the average of the inputs through the use of the internal model principle [40] and the structure of the proportional-integral average consensus estimator formulated in [41]. The internal model principle has been useful in establishing necessary and sufficient conditions for output regulation [77] and synchronization [103, 102, 22]. Reference [13] proposed internal model control strategies in which controllers were placed on the edges of the interconnection graph to achieve output synchronization under time-varying disturbances. Recent work has also addressed robust synchronization in cyclic feedback systems [52] and in the presence of structured uncertainties [29].

Spatial homogenization of reaction-diffusion PDEs has also been studied in the literature. In [1], the author gave a Lyapunov inequality for the Jacobian of the reaction term, significantly reducing conservatism of dominant approaches making use of global Lipschitz bounds [19]. However, the problem of spatial homogenization of reaction-diffusion PDEs subject to heterogeneities has not yet been addressed.

In this chapter, we consider synchronization of nonlinear systems satisfying an incremental passivity property and subject to a class of disturbance inputs including constants and sinusoids. Building on the robust DAC estimator in [7], we propose a distributed control law that achieves output synchronization in the presence of disturbances by defining an internal model subsystem at each node corresponding to the disturbance inputs. Our controller applies to systems with multiple input and output channels and allows non-identical heterogeneities to

enter each channel.

A key property of our approach is that local communication, computation and memory requirements are independent of the number of the systems in the network and the network connectivity, which is of interest in dense networks under processing and communication constraints. In contrast to the edge-based approach [13], which defines an internal model subsystem for each edge in the graph, our approach introduces such a subsystem only to each node, offering the advantage of a reduced number of internal states.

We next address the PDE case and present a distributed control law that achieves spatial homogenization in reaction-diffusion PDEs in the presence of spatially and temporally-varying heterogeneities.

The rest of the chapter is organized as follows. Section 6.1 reviews output synchronization of diffusively coupled networks with incrementally passive systems under input disturbances. Our main result on spatial homogenization under heterogeneities is presented Section 6.2. In Section 6.3, we illustrate the effectiveness of our control law on models with ring oscillator dynamics and bistable dynamics. Conclusions and future work are discussed in Section 6.4.

Notation: Let 1_N be the $N \times 1$ vector with all entries 1. Let 0_N be the $N \times 1$ vector with all entries 0. Let the transpose of a real matrix A be denoted by A^T. Let I_N denote the $N \times N$ identity matrix.

6.1 Compartmental Systems of ODEs

Consider a collection of N dynamical systems H_i, $i = 1, \ldots, N$, defined by:

$$H_i: \quad \dot{x}_i = f(x_i) + g(x_i)u_i \quad i = 1, \ldots, N \tag{6.1}$$

$$y_i = h(x_i), \tag{6.2}$$

in which $x_i \in \mathbb{R}^n$, $u_i \in \mathbb{R}^p$, $y_i \in \mathbb{R}^p$, and $f(\cdot) : \mathbb{R}^n \to \mathbb{R}^n$, $g(\cdot) : \mathbb{R}^n \to \mathbb{R}^{n \times p}$, and $h(\cdot) : \mathbb{R}^n \to \mathbb{R}^p$ are continuously differentiable maps. Recall from Section 1.2 that H_i is said to satisfy an incremental output-feedback passivity property [91, 84] if there exist a positive definite storage function $S : \mathbb{R}^n \to \mathbb{R}$ and a scalar $\theta \in \mathbb{R}$ such that:

$$\frac{d}{dt} S(\delta x) =: \dot{S}(\delta x) \leq \theta \delta y^T \delta y + \delta u^T \delta y. \tag{6.3}$$

Consider the case where the input u_i for each H_i is subject to a class of unknown disturbances $\phi_i(t) \in \mathbb{R}^p$, i.e.,

$$u_i = u_i^* + \phi_i, \tag{6.4}$$

in which each disturbance ϕ_i can be characterized by

$$\dot{\xi}_i = A\xi_i, \quad \xi_i(0) \in \mathbb{R}^d \tag{6.5}$$

$$\phi_i = C\xi_i, \tag{6.6}$$

with $A = -A^T \in \mathbb{R}^{d\times d}$, $C \in \mathbb{R}^{p\times d}$, and the pair (A, C) observable. This class includes constant as well as sinusoidal disturbances.

Main Result

We seek to design the control u^* such that the outputs y_i, $i = 1, \ldots, N$ synchronize. First, corresponding to each subsystem H_i, we define an internal model subsystem G_i. Let $\mathcal{G}_I$ be an undirected, connected graph with N nodes and M_I edges corresponding to the information flow between the G_i subsystems. Each G_i is given by:

$$G_i: \quad \dot{\zeta}_i = A\zeta_i + B_i \sum_{j=1}^{N} n_{ij}(y_i - y_j) \tag{6.7}$$

$$\eta_i = B_i^T \zeta_i, \tag{6.8}$$

where $B_i \in \mathbb{R}^{d\times p}$, (A, B_i^T) is designed to be observable, and the initial condition $\zeta_i(0)$ may be arbitrarily chosen. The coupling term $\sum_{j=1}^{N} n_{ij}(y_i - y_j)$ is such that $n_{ij} = n_{ji} > 0$ if there is an edge in $\mathcal{G}_I$ connecting nodes i and j, and $n_{ij} = 0$ otherwise. Note that since $A = -A^T$ and G_i is a linear system, it is straightforward to show that G_i is passive and thus incrementally passive with respect to input $\sum_{j=1}^{N} n_{ij}(y_i - y_j)$ and output η_i.

Next, let $\mathcal{G}_P$ be an undirected graph with N nodes and M_P edges corresponding to the coupling of the H_i subsystems. We propose the controller

$$u_i^* = -\sum_{j=1}^{N} p_{ij}(y_i - y_j) - \sum_{j=1}^{N} n_{ij}(\eta_i - \eta_j), \tag{6.9}$$

in which $p_{ij} = p_{ji} > 0$ if there is an edge connecting nodes i and j in $\mathcal{G}_P$, and $p_{ij} = 0$ otherwise, and n_{ij} as in (6.7). The left and right sums represent the coupling between outputs of the H_i and G_i subsystems, respectively.

Next, we assign an arbitrary orientation to the edges of the graph $\mathcal{G}_P$, label the edges $\ell = 1, \ldots, M_P$, and introduce the $N \times M_P$ incidence matrix E as in (1.1). We define $U = [u_1^T \cdots u_N^T]^T$, $Y = [y_1^T \cdots y_N^T]^T$, and

$$L_P = E_P K_P E_P^T, \tag{6.10}$$

where E_P is the graph incidence matrix defined in (1.1) and K_P is a diagonal matrix of the edge weights p_{ij}. We denote by λ_2 the second smallest eigenvalue of L_P.

Similarly, we define a weighted graph Laplacian L_I for $\mathcal{G}_I$ by introducing the $N\times M_I$ incidence matrix E_I and diagonal matrix K_I of edge weights n_{ij}:

$$L_I = E_I K_I E_I^T. \tag{6.11}$$

We define $U = [u_1^T \cdots u_N^T]^T$, $Y = [y_1^T \cdots y_N^T]^T$, $U^* = [u_1^{*T} \ldots \bar{u}_N^{*T}]^T$ and $H = [\eta_1^T \ldots \eta_N^T]^T$. Then the control in (6.9) can be rewritten as

$$U^* = -(L_P \otimes I_p)Y - (L_I \otimes I_p)H. \tag{6.12}$$

The diagram in Fig. 6.1 shows the closed-loop system given by (6.1), (6.2), (6.4), (6.9), (6.7) and (6.8).

Next, define

$$\bar{x} := \frac{1}{N}(x_1 + \cdots + x_N), \quad \tilde{x}_i := x_i - \bar{x}, \quad \text{and} \quad \tilde{y}_i := y_i - \bar{y}. \tag{6.13}$$

We first address the case where $B_i^T = C$ for all $i = 1, \ldots, N$, and using the control in (6.9), we prove the following theorem to guarantee output synchronization for the subsystems H_i:

Theorem 15 *Consider the nonlinear systems H_i in* (6.1)-(6.2) *satisfying* (6.3) *with the input given in* (6.4), (6.7)-(6.8), *and* (6.9), *with $B_i^T = C$ for all $i = 1, \ldots, N$. Suppose that $\lambda_2 - \theta > 0$ and that $\mathcal{G}_I$ is connected. If the solutions are bounded, then $\tilde{y}_i(t) \to 0$ as $t \to \infty$.* □

If $\theta < 0$, i.e., H_i possesses an excess of incremental passivity, Theorem 15 allows λ_2 to be zero, which means that the graph $\mathcal{G}_P$ need not be connected. However, if $\theta \geq 0$, it follows that $\lambda_2 > \theta \geq 0$, which means that $\mathcal{G}_P$ must be connected.

We next employ the incremental passivity property of both H_i and G_i and the symmetry of both L_I and L_P to prove Theorem 15.

Proof of Theorem 15: First, consider the storage function

$$V = \frac{1}{2N} \sum_{i=1}^{N} \sum_{j=1}^{N} S(x_i - x_j), \tag{6.14}$$

and define $\Pi := I - \frac{1}{N}\mathbf{1}_N\mathbf{1}_N^T$. The time derivative of (6.14) along (6.1)-(6.2) is given by

$$\begin{aligned} \dot{V} &\leq \frac{1}{2N} \sum_{i=1}^{N} \sum_{j=1}^{N} \left[\theta(y_i - y_j)^T(y_i - y_j) + (y_i - y_j)^T(u_i - u_j)\right] && (6.15) \\ &= \theta \tilde{Y}^T \tilde{Y} + \tilde{Y}^T \tilde{U}, && (6.16) \end{aligned}$$

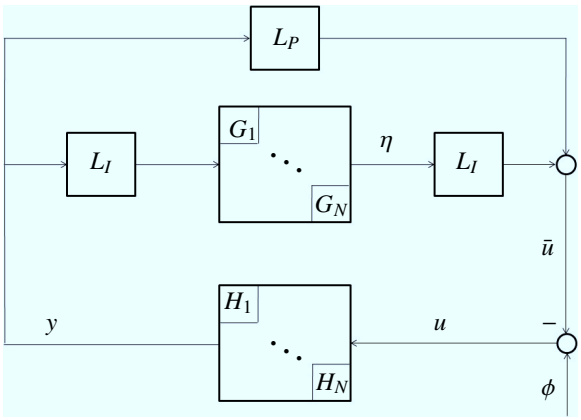

Figure 6.1: The block diagram of the closed-loop system given by (6.1)-(6.2), (6.4), (6.7)-(6.8), and (6.9).

where $\tilde{Y} := (\Pi \otimes I_p)Y$ and $\tilde{U} := (\Pi \otimes I_p)U$. The equality in (6.16) follows because

$$\sum_{i=1}^{N}\sum_{j=1}^{N}(y_i - y_j)^T(u_i - u_j) = N\sum_{i=1}^{N} 2y_i^T u_i - \bar{y}^T u_i - y_i^T \bar{u} \tag{6.17}$$

$$= N\sum_{i=1}^{N}(y_i - \bar{y})^T u_i + y_i^T(u_i - \bar{u}) \tag{6.18}$$

$$= 2N\sum_{i=1}^{N}\tilde{y}_i^T\tilde{u}_i, \tag{6.19}$$

where we have made use of the fact that $\sum_{i=1}^{N}(u_i - \bar{u})^T v = 0$ for constant v. We define $\Phi = [\phi_1^T \dots \phi_N^T]^T$ and $\tilde{\Phi} = (\Pi \otimes I_p)\Phi$ and substitute (6.4) into (6.16), obtaining

$$\dot{V} \leq \theta\tilde{Y}^T\tilde{Y} + \tilde{Y}(\tilde{\Phi} + U^*). \tag{6.20}$$

Substituting (6.12) into (6.20), we have

$$\begin{aligned}\dot{V} &\leq \theta\tilde{Y}^T\tilde{Y} + \tilde{Y}^T(\tilde{\Phi} - (L_I \otimes I_p)H - (L_P \otimes I_p)Y) \\ &= \theta\tilde{Y}^T\tilde{Y} - \tilde{Y}^T(L_P \otimes I_p)\tilde{Y} + \tilde{Y}^T(\tilde{\Phi} - (L_I \otimes I_p)H).\end{aligned} \tag{6.21}$$

Since $\tilde{Y}^T(\mathbf{1}_N \otimes I_p) = 0$ and $\lambda_1 = 0$ is an eigenvalue of $L_P \otimes I_p$ with eigenspace equal to the range of $\mathbf{1}_N \otimes I_p$, from (6.21) we have:

$$\dot{V} \leq -(\lambda_2 - \theta)\tilde{Y}^T\tilde{Y} + \tilde{Y}^T(\tilde{\Phi} - (L_I \otimes I_p)H). \tag{6.22}$$

We next consider the auxiliary systems

$$\dot{\hat{\xi}}_i = A\hat{\xi}_i, \quad \hat{\xi}_i(0) \in \mathbb{R}^d, \quad i = 1, \ldots, N \tag{6.23}$$
$$\hat{\phi}_i = C\hat{\xi}_i. \tag{6.24}$$

Defining $\Xi = [\xi_1^T \ldots \xi_N^T]^T$ and $\hat{\Phi} = [\hat{\phi}_1^T \ldots \hat{\phi}_N^T]^T$, we show that an appropriate choice of $\hat{\xi}_(0)$, $i = 1, \ldots, N$ guarantees

$$\tilde{\Phi} = (L_I \otimes I_p)\hat{\Phi}. \tag{6.25}$$

We define a matrix $Q \in \mathbb{R}^{N\times(N-1)}$ that satisfies $Q^T\mathbf{1}_N = 0$, $QQ^T = \Pi$ and $Q^TQ = I_{N-1}$. We let

$$\Gamma = Q(Q^TL_IQ)^{-1}Q^T \tag{6.26}$$

and denote by Γ_{ij} the element at the ith row and jth column of Γ. The inverse of Q^TL_IQ exists because $\mathbf{1}_N$ spans the null spaces of L_I and Q^T. Note that Γ is the Moore-Penrose pseudoinverse of L_I.

To verify (6.25), we note that $\hat{\Xi}(0) = (\Gamma \otimes I_d)\Xi(0)$ results in $\hat{\Phi} = (\Gamma \otimes I_p)\Phi$. Using (6.26), we obtain

$$(Q^TL_I \otimes I_p)\hat{\Phi} = (Q^T \otimes I_p)\Phi. \tag{6.27}$$

Pre-multiplying (6.27) by $(Q\otimes I_p)$ and noting $QQ^TL_I = \Pi L_I = L_I$ together guarantee (6.25).

Having proved that (6.25) can be achieved by appropriately selecting $z_i(0)$ in (6.34) and $\xi_i(0)$ in (6.23), we define

$$\delta_i := \zeta_i - \hat{\xi}_i, \quad i = 1, \ldots, N, \tag{6.28}$$

and consider the following storage function:

$$W = \frac{1}{2}\sum_{i=1}^{N}\delta_i^T\delta_i. \tag{6.29}$$

Using (6.7), (6.8), (6.34) and (6.35), we obtain:

$$\dot{W} = \sum_{i=1}^{N}\delta_i^TC\sum_{j=1}^{N}n_{ij}(y_i - y_j) \tag{6.30}$$
$$= (H - \hat{\Phi})^T(L_I \otimes I_p)Y. \tag{6.31}$$

The sum $Z = V + W$ yields

$$\begin{aligned}\dot{Z} &= \dot{V} + \dot{W}\\ &\leq -(\lambda_2 - \theta)\tilde{Y}^T\tilde{Y} + \tilde{Y}^T(\tilde{\Phi} - (L_I \otimes I_p)H) + (H - \hat{\Phi})^T(L_I \otimes I_p)\tilde{Y}\\ &= -(\lambda_2 - \theta)\tilde{Y}^T\tilde{Y} + \tilde{Y}^T(\tilde{\Phi} - (L_I \otimes I_p)\hat{\Phi}).\end{aligned} \tag{6.32}$$

By choosing $z_i(0)$ in (6.34) such that (6.36) is guaranteed, we have

$$\dot{Z} \leq -(\lambda_2 - \theta)\tilde{Y}^T\tilde{Y} \leq 0. \tag{6.33}$$

By integrating both sides of (6.33), we see that $\tilde{y}_i(t)$ is in $\mathcal{L}_2$, $i = 1, \ldots, N$. Furthermore, the boundedness of solutions implies that $\dot{x}_i$ and thus $\dot{y}_i$ are bounded for all i. An application of Barbalat's Lemma [64] guarantees that $\tilde{y}_i(t) \to 0$ as $t \to \infty$. □

Remark 3 *In the event that A and C in (6.5)-(6.6) have a specific block diagonal structure, we may choose $B_i \neq C$ in (6.7)-(6.8). Suppose that $A = blkdiag\{A_1, \ldots, A_p\}$ with $A_k \in \mathbb{R}^{d_k \times d_k}$ and $\sum_{k=1}^{p} d_k = d$, $C \in \mathbb{R}^{p \times d}$ with $C = blkdiag\{C_1, \ldots, C_p\}$ with $C_k \in \mathbb{R}^{1 \times d_k}$, and the pairs (A_k, C_k) observable. Suppose also that $B_i = blkdiag\{B_i^{(1)}, \ldots, B_i^{(p)}\}$ with $B_i^{(k)} \in \mathbb{R}^{d_k \times 1}$ where the pairs $(A_k, B_i^{(k)T})$ are designed to be observable.*

To address the fact that each B_i differs from C, we introduce the auxiliary systems

$$\dot{z}_i = Az_i, \quad z_i(0) \in \mathbb{R}^d, \quad i = 1, \ldots, N \tag{6.34}$$

$$\psi_i = B_i^T z_i, \tag{6.35}$$

and define $\Psi = [\psi_1^T \ldots \psi_N^T]^T$. We show that an appropriate choice of $z_i(0)$, $i = 1, \ldots, N$ implies $\Psi = \hat{\Phi}$, and thus guarantees

$$\tilde{\Phi} = (L_I \otimes I_p)\Psi. \tag{6.36}$$

In particular, we choose $z_i(0) = \mathcal{O}_{B_i}^{-1}\mathcal{O}_C\hat{\xi}_i(0)$, where $\mathcal{O}_{B_i}$ is the block diagonal matrix of observability matrices corresponding to the pairs $(A_k, B_i^{(k)T})$ of (6.7)-(6.8) and $\mathcal{O}_C$ is the block diagonal matrix of observability matrices corresponding to the pairs (A_k, C_k) of (6.23)-(6.24). Since $z_i(0) = \mathcal{O}_{B_i}^{-1}\mathcal{O}_C\hat{\xi}_i(0)$, $z_i(t) = \mathcal{O}_{B_i}^{-1}\mathcal{O}_C\hat{\xi}_i(t)$, which means $\mathcal{O}_{B_i}z_i(t) = \mathcal{O}_C\hat{\xi}_i(t)$. Noting that the first rows of each block of $\mathcal{O}_{B_i}$ and $\mathcal{O}_C$ are $B_i^{(k)T}$ and $C^{(k)}$, respectively, we have $\psi_i = blkdiag\{B_i^{(1)T}, \ldots, B_i^{(p)T}\}z_i = blkdiag\{C_1, \ldots, C_p\}\hat{\xi}_i = \hat{\phi}_i$, $i = 1, \ldots, N$. We modify the difference δ_i in (6.28) and (6.29) as $\delta_i := \zeta_i - z_i$. The rest of the proof is identical and is omitted to avoid repetition. □

6.2 Reaction-Diffusion PDEs

In this section, we formulate the problem of spatial homogenization for systems of reaction-diffusion PDEs, which is analogous to the problem of synchronization of like components in compartmental systems of ODEs.

Let Ω be a bounded and connected domain in $\mathbb{R}^r$ with smooth boundary $\partial\Omega$, and consider the PDE:

$$\begin{aligned} \frac{\partial x(t,\chi)}{\partial t} &= f(x(t,\chi)) + \sum_{\ell=1}^{p} g_\ell(x(t,\chi))u_\ell(t,\chi) && (6.37)\\ y_\ell(t,\chi) &= h_\ell(x(t,\chi)), \quad \ell = 1,\dots,p, && (6.38) \end{aligned}$$

where $\chi \in \Omega$ is the spatial variable, $x(t,\chi) \in \mathbb{R}^n$ is the state variable with initial condition $x(0,\chi) = x_0(\chi)$, $f(\cdot) : \mathbb{R}^n \to \mathbb{R}^n$, $g(\cdot) = [g_1 \cdots g_p] : \mathbb{R}^n \to \mathbb{R}^{n\times p}$, and $h(\cdot) = [h_1^T \cdots h_p^T]^T : \mathbb{R}^n \to \mathbb{R}^p$ are continuously differentiable maps, and the inputs $u_\ell(t,\chi)$ consist of linear differential operators to be specified below. In what follows, we will assume Neumann boundary conditions:

$$\nabla x_i(t,\chi)\cdot\hat{n}(\chi) = 0 \quad \forall\chi\in\partial\Omega,\ \forall t \geq 0, \quad i = 1,\dots,n \tag{6.39}$$

where ∇ represents the gradient with respect to the spatial variable χ, "$\cdot$" is the inner product in $\mathbb{R}^r$, $x_i(t,\chi)$ denotes the ith entry of the vector $x(t,\chi)$ and $\hat{n}(\chi)$ is a vector normal to the boundary $\partial\Omega$.

We consider the scenario where the input $u(t,\chi) = [u_1(t,\chi)\dots u_p(t,\chi)]^T$ is subject to a class of unknown heterogeneities $\phi(t,\chi) = [\phi_1(t,\chi)\ \dots\ \phi_p(t,\chi)]^T$, i.e.,

$$u(t,\chi) = u^*(t,\chi) + \phi(t,\chi). \tag{6.40}$$

We assume that the heterogeneity $\phi(t,\chi)$ can be characterized by

$$\begin{aligned} \dot{\xi}(t,\chi) &= A\xi(t,\chi)\\ \phi(t,\chi) &= C\xi(t,\chi), \end{aligned} \tag{6.41}$$

in which $A \in \mathbb{R}^{d\times d}$ satisfies $A = -A^T$, $C \in \mathbb{R}^{p\times d}$, the pair (A,C) is observable, and the initial condition $\xi(0,\chi)$ may be arbitrarily chosen in $L_2(\Omega)$. We assume that the matrix A is available.

In relation to synchronization of each like output $y_{i,k}$ across compartments $i = 1,\dots,N$, we now derive a control law that guarantees homogenization of each output $y_\ell(t,\chi)$ across the spatial domain Ω. The topology of Ω is the spatial continuum analogue to the topology of the interconnection graph, which represents the network of compartments.

Main Result

We seek to design the control $u^*(t,\chi)$ such that the outputs $y(t,\chi) = [y_1(t,\chi)\dots y_p(t,\chi)]^T$ are homogenized spatially. As in Section 6.1, we consider the following design of $u^*(t,\chi)$:

$$u^*(t,\chi) = \nabla\cdot(p(\chi)\nabla y(t,\chi)) - \nabla\cdot(n(\chi)\nabla\eta(t,\chi)), \tag{6.42}$$

in which $\nabla\cdot$ is the divergence operator, $\nabla\cdot(n(\chi)\nabla(v(t,\chi)))$ with slight abuse of notation is the vector representation of the diffusion operator $\nabla\cdot(n(\chi)\nabla(\cdot))$ applied to each component $v_\ell(t,\chi)$ of $v(t,\chi)$:

$$\nabla\cdot(n(\chi)\nabla(v(t,\chi))) = [\nabla\cdot(n(\chi)\nabla(v_1(t,\chi)))\ldots\nabla\cdot(n(\chi)\nabla(v_p(t,\chi)))]^T, \tag{6.43}$$

$p(\chi), n(\chi)\in\mathbb{R}$ are diffusion coefficients with $p(\chi)>0$, $n(\chi)>0$, and η is to be defined below. The first term in (6.42) serves an analogous role to that of (6.9). For the second term, we design η to be the output of the internal model system G given by

$$G:\ \frac{\partial\zeta(t,\chi)}{\partial t} = A\zeta(t,\chi)+B\nabla\cdot(n(\chi)\nabla y(t,\chi)) \tag{6.44}$$

$$\eta(t,\chi) = B^T\zeta(t,\chi), \tag{6.45}$$

where (A,B^T) is designed to be observable with $B\in\mathbb{R}^{d\times p}$, and the initial condition $\zeta(0,\chi)$ may be arbitrarily chosen in $L_2(\Omega)$.

Define:

$$\bar{x}(t) := \frac{1}{|\Omega|}\int_\Omega x(t,\chi)d\chi,\quad \tilde{x}(t,\chi) := x(t,\chi)-\bar{x}(t)$$
$$\tilde{y}_\ell(t,\chi) := y_\ell(t,\chi)-\bar{y}_\ell(t). \tag{6.46}$$

In Theorem 16 below, we give conditions that guarantee the following output synchronization property:

$$\lim_{t\to\infty}\int_\Omega|\tilde{y}(t,\chi)|^2d\chi = 0, \tag{6.47}$$

where $|\cdot|$ denotes the Euclidean norm. As in Theorem 15, we consider the case where $B^T=C$.

Theorem 16 *Consider the system (6.37)-(6.38) with the boundary condition in (6.39) on a connected, bounded domain Ω, with the input given in* (6.40), (6.42), (6.44)-(6.45) *and $B^T=C$. Suppose there exists a storage function for (6.37)-(6.38) satisfying (6.3) with $\lambda_2-\theta>0$. Then for every bounded classical solution*[1]*, the outputs synchronize in the sense of (6.47).* □

Theorem 16 applies to classical solutions that exist for all $t\geq 0$. Results on the existence of classical solutions to reaction-diffusion PDEs can be found in [89, 90, 42].

Proof of Theorem 16: We first consider the function:

$$V = \frac{1}{2|\Omega|}\int_\Omega\int_\Omega S(x(t,\chi_a)-x(t,\chi_b))\,d\chi_a\,d\chi_b. \tag{6.48}$$

[1]A solution of a PDE of order k is said to be *classical* it it is at least k times continuously differentiable so that all derivatives that appear in the PDE exist and are continuous [33].

Note that (6.37)-(6.38), without the coupling term (6.40), is identical to (6.1)-(6.2). Therefore, using (6.3), we have:

$$\begin{aligned}\dot{V} \leq & \frac{1}{2|\Omega|}\int_\Omega\int_\Omega \theta(y(t,\chi_a)-y(t,\chi_b))\cdot(y(t,\chi_a)-y(t,\chi_b)) \\ & + (u(t,\chi_a)-u(t,\chi_b))\cdot(y(t,\chi_a)-y(t,\chi_b))\,d\chi_a\,d\chi_b.\end{aligned} \tag{6.49}$$

Defining $\bar{u}(t) := \frac{1}{|\Omega|}\int_\Omega u(t,\chi)\,d\chi$ and $\bar{y}(t) := \frac{1}{|\Omega|}\int_\Omega y(t,\chi)\,d\chi$, we have:

$$\int_\Omega\int_\Omega (u(t,\chi_a)-u(t,\chi_b))\cdot(y(t,\chi_a)-y(t,\chi_b))\,d\chi_a\,d\chi_b \tag{6.50}$$

$$\begin{aligned}= & \int_\Omega\int_\Omega u(t,\chi_a)\cdot y(t,\chi_a) - u(t,\chi_a)\cdot y(t,\chi_b) \\ & - u(t,\chi_b)\cdot y(t,\chi_a) + u(t,\chi_b)\cdot y(t,\chi_b)\,d\chi_a\,d\chi_b\end{aligned} \tag{6.51}$$

$$\begin{aligned}= & |\Omega|\int_\Omega u(t,\chi_a)\cdot y(t,\chi_a)\,d\chi_a - |\Omega|\int_\Omega u(t,\chi_a)\cdot\bar{y}(t)\,d\chi_a \\ & - |\Omega|\int_\Omega \bar{u}(t)\cdot y(t,\chi_a)\,d\chi_a + |\Omega|\int_\Omega u(t,\chi_b)\cdot y(t,\chi_b)\,d\chi_b.\end{aligned} \tag{6.52}$$

Rewriting (6.52) with a substitution of variables, we have:

$$|\Omega|\int_\Omega 2u(t,\chi)\cdot y(t,\chi) - u(t,\chi)\cdot\bar{y}(t) - \bar{u}(t)\cdot y(t,\chi)\,d\chi \tag{6.53}$$

$$= |\Omega|\int_\Omega u(t,\chi)\cdot(y(t,\chi)-\bar{y}(t)) + (u(t,\chi)-\bar{u}(t))\cdot y(t,\chi)\,d\chi \tag{6.54}$$

$$= 2|\Omega|\int_\Omega (u(t,\chi)-\bar{u}(t))\cdot(y(t,\chi)-\bar{y}(t))\,d\chi, \tag{6.55}$$

where we have made use of the fact that $\int_\Omega (u(t,\chi)-\bar{u}(t))\cdot v(t)\,d\chi = 0$ for $v(t)$ not dependent on χ. Substituting (6.55) in the second product of the right hand side of (6.49) and expanding its first product similarly, we have:

$$\dot{V} \leq \int_\Omega \theta\tilde{y}(t,\chi)\cdot\tilde{y}(t,\chi) + \tilde{y}(t,\chi)\cdot\tilde{u}(t,\chi)\,d\chi. \tag{6.56}$$

Substituting (6.40) into (6.56), we have:

$$\begin{aligned}\dot{V} \leq & \int_\Omega \theta\tilde{y}(t,\chi)\cdot\tilde{y}(t,\chi) + \sum_{\ell=1}^{p}\tilde{y}_\ell(t,\chi)\Big(\phi_\ell(t,\chi) \\ & + \nabla\cdot(p(\chi)\nabla y_\ell(t,\chi)) - \nabla\cdot(n(\chi)\nabla\eta_\ell(t,\chi))\Big)\,d\chi\end{aligned} \tag{6.57}$$

$$\begin{aligned}= & \int_\Omega \theta\tilde{y}(t,\chi)\cdot\tilde{y}(t,\chi) + \sum_{\ell=1}^{p}\Big[\tilde{y}_\ell(t,\chi)\nabla\cdot(p(\chi)\nabla\tilde{y}_\ell(t,\chi)) \\ & + \tilde{y}_\ell(t,\chi)\Big(\phi_\ell(t,\chi) - \nabla\cdot(n(\chi)\nabla\eta_\ell(t,\chi))\Big)\Big]\,d\chi.\end{aligned} \tag{6.58}$$

We now claim that:

$$\int_\Omega \tilde{y}_\ell(t,\chi)\nabla\cdot(p(\chi)\nabla\tilde{y}_\ell(t,\chi))d\chi = -\int_\Omega p(\chi)\nabla\tilde{y}_\ell(t,\chi)\cdot\nabla\tilde{y}_\ell(t,\chi)d\chi. \tag{6.59}$$

To see this, consider the identity

$$\nabla\cdot(fF) = f\nabla\cdot F + F\cdot\nabla f, \tag{6.60}$$

which holds when f is scalar-valued. Defining $F = p(\chi)\nabla\tilde{y}_\ell(t,\chi)$ and $f = \tilde{y}_\ell(t,\chi)$ and integrating both sides of the identity over Ω, we have

$$\begin{aligned}\int_\Omega \nabla\cdot(\tilde{y}_\ell(t,\chi)p(\chi)\nabla\tilde{y}_\ell(t,\chi))d\chi = &\int_\Omega \tilde{y}_\ell(t,\chi)\nabla\cdot(p(\chi)\nabla\tilde{y}_\ell(t,\chi))d\chi \\ &+ \int_\Omega p(\chi)\nabla\tilde{y}_\ell(t,\chi)\cdot\nabla\tilde{y}_\ell(t,\chi)d\chi.\end{aligned} \tag{6.61}$$

Applying the Divergence Theorem and noting that $\nabla\tilde{y}_\ell(t,\chi)\cdot\hat{n}(\chi) = 0$ for $\chi\in\partial\Omega$ from the boundary condition (6.39), we have:

$$\int_\Omega \nabla\cdot(\tilde{y}_\ell(t,\chi)p(\chi)\nabla\tilde{y}_\ell(t,\chi))d\chi = \int_{\partial\Omega}\tilde{y}_\ell(t,\chi)p(\chi)\nabla\tilde{y}_\ell(t,\chi)\cdot\hat{n}(\chi)dS = 0, \tag{6.62}$$

verifying (6.59). Moreover, because $\int_\Omega \tilde{y}_\ell(t,\chi)d\chi = 0$, it follows from Lemma 1 that:

$$\int_\Omega p(\chi)\nabla\tilde{y}_\ell(t,\chi)\cdot\nabla\tilde{y}_\ell(t,\chi)d\chi \geq \lambda_2\int_\Omega \tilde{y}_\ell(t,\chi)^2 d\chi. \tag{6.63}$$

Substituting in (6.58) and using the fact that $\int_\Omega \tilde{y}_\ell(t,\chi)\bar{\phi}_\ell(t)\,d\chi = 0$, we have:

$$\dot{V} \leq \int_\Omega -(\lambda_2-\theta)\tilde{y}(t,\chi)\cdot\tilde{y}(t,\chi) + \sum_{\ell=1}^{p}\tilde{y}_\ell(t,\chi)\big(\tilde{\phi}_\ell - \nabla\cdot(n(\chi)\nabla\eta_\ell(t,\chi))\big)\,d\chi, \tag{6.64}$$

where $\tilde{\phi}_\ell(t,\chi) = \phi_\ell(t,\chi) - \bar{\phi}_\ell(t,\chi)$.

We next consider the auxiliary system:

$$\dot{\hat{\xi}}(t,\chi) = A\hat{\xi}(t,\chi) \tag{6.65}$$

$$\hat{\phi}(t,\chi) = C\hat{\xi}(t,\chi). \tag{6.66}$$

Noting that the eigenfunctions of the elliptic operator $\nabla\cdot(n(\chi)\nabla(\cdot))$ form a complete orthogonal basis for $L_2(\Omega)$, and that $\int_\Omega \tilde{\phi}_\ell(t,\chi)\,d\chi = 0$, $\ell = 1,\ldots,p$, the initial conditions of $\hat{\xi}(t,\chi)$ may be chosen such that

$$\nabla\cdot(n(\chi)\nabla\hat{\phi}_\ell(0,\chi)) = \tilde{\phi}_\ell(0,\chi), \quad \ell = 1,\ldots,p \tag{6.67}$$

and thus $\nabla \cdot (n(\chi)\nabla\hat{\phi}_\ell(t,\chi)) = \tilde{\phi}_\ell(t,\chi)$ for all $\ell = 1, \ldots, p$.

We define

$$\delta(t,\chi) := \zeta(t,\chi) - \hat{\xi}(t,\chi), \tag{6.68}$$

and consider the following storage function:

$$W = \frac{1}{2}\int_\Omega \delta(t,\chi)\cdot\delta(t,\chi)\,d\chi. \tag{6.69}$$

Differentiating W with respect to time, we obtain:

$$\dot{W} = \int_\Omega \delta(t,\chi)\cdot C\left(\nabla\cdot(n(\chi)\nabla\tilde{y}(t,\chi))\right)\,d\chi \tag{6.70}$$

$$= \int_\Omega (\eta(t,\chi) - \hat{\phi}(t,\chi))\cdot(\nabla\cdot(n(\chi)\nabla\tilde{y}(t,\chi)))\,d\chi. \tag{6.71}$$

The sum $Z = V + W$ yields

$$\dot{Z} = \dot{V} + \dot{W} \tag{6.72}$$

$$\leq \int_\Omega -(\lambda_2-\theta)\tilde{y}(t,\chi)\cdot\tilde{y}(t,\chi) + \sum_{\ell=1}^{p}\Big[\tilde{y}_\ell(t,\chi)\Big(\tilde{\phi}_\ell(t,\chi) - \nabla\cdot(n(\chi)\nabla\eta_\ell(t,\chi))\Big) \tag{6.73}$$

$$+ \Big(\eta_\ell(t,\chi) - \hat{\phi}_\ell(t,\chi)\Big)\Big(\nabla\cdot(n(\chi)\nabla\tilde{y}_\ell(t,\chi))\Big)\Big]\,d\chi.$$

We now make use of the self-adjointness property of the diffusion operator, apply the identity in (6.60) with $f = \tilde{y}_\ell(t,\chi)$ and $F = n(\chi)\nabla\eta_\ell(t,\chi)$, and get

$$\int_\Omega \tilde{y}_\ell(t,\chi)\nabla\cdot(n(\chi)\nabla\eta_\ell(t,\chi))d\chi = -\int_\Omega n(\chi)\nabla\tilde{\eta}_\ell(t,\chi)\cdot\nabla\tilde{y}_\ell(t,\chi)d\chi \tag{6.74}$$

$$= \int_\Omega \eta_\ell(t,\chi)\nabla\cdot(n(\chi)\nabla y_\ell(t,\chi))d\chi, \tag{6.75}$$

where the second equality follows with a subsequent application of the identity with $f = \eta_\ell(t,\chi)$ and $F = n(\chi)\nabla\tilde{y}_\ell(t,\chi)$. Similarly, we have:

$$\int_\Omega \hat{\phi}_\ell(t,\chi)\nabla\cdot(n(\chi)\nabla y_\ell(t,\chi))d\chi = \int_\Omega \tilde{y}_\ell(t,\chi)\nabla\cdot(n(\chi)\nabla\hat{\phi}_\ell(t,\chi))d\chi. \tag{6.76}$$

Substituting (6.75) and (6.76) into (6.73), we then have:

$$\dot{Z} \leq \int_\Omega -(\lambda_2-\theta)\tilde{y}(t,\chi)\cdot\tilde{y}(t,\chi) + \sum_{\ell=1}^{p}\tilde{y}_\ell(t,\chi)\Big(\tilde{\phi}_\ell(t,\chi) - \nabla\cdot(n(\chi)\nabla\hat{\phi}_\ell(t,\chi))\Big)\,d\chi. \tag{6.77}$$

By choosing $\hat{\xi}_\ell(0,\chi)$ such that (6.67) is satisfied, we have:

$$\dot{Z} \leq \int_\Omega -(\lambda_2 - \theta)\tilde{y}(t,\chi)\cdot\tilde{y}(t,\chi)\,d\chi = -\epsilon\int_\Omega |\tilde{y}(t,\chi)|^2\,d\chi =: -\epsilon Q(t). \tag{6.78}$$

This implies that $\lim_{T\to\infty}\int_0^T Q(t)\,dt$ exists and is bounded. Since $\dot{Q}(t)$ is also bounded, it follows from Barbalat's Lemma [64] that $Q(t)\to 0$ as $t\to\infty$, which proves (6.47). □

Remark 4 *When A and C have block diagonal structure as in Remark 3, we may choose $B \neq C$. In particular, suppose $A = blkdiag\{A_1,\ldots,A_p\}$ with $A_k \in \mathbb{R}^{d_k\times d_k}$ and $\sum_{k=1}^p d_k = d$, $C\in\mathbb{R}^{p\times d}$ with $C = blkdiag\{C_1,\ldots,C_p\}$ with $C_k\in\mathbb{R}^{1\times d_k}$, and the pairs (A_k,C_k) observable. Then B in (6.44)-(6.45) may be chosen such that $B = blockdiag\{B_1,\ldots,B_p\}$ and $B_k\in\mathbb{R}^{d_k\times 1}$ with the pairs (A_k,B_k^T) observable. The proof is modified as in Remark 3, and is omitted to avoid excessive notation.* □

6.3 Numerical Examples

In this section, we consider several numerical examples. We first consider a compartmental system with nominal bistable dynamic. We then turn to the spatially continuous case, and first consider a ring oscillator model subject to a constant, spatially-varying heterogeneity. We subsequently consider a system with nominal bistable dynamics subject to a spatially and temporally-varying heterogeneity. The examples demonstrate the effectiveness of the internal model approach in guaranteeing spatial homogenization in the presence of heterogeneities.

A. Bistable Compartmental System

We consider a 48 node network with three completely connected components with randomly generated external links between each cluster pair, as in Figure 5.7. We assume that the coupling graphs $\mathcal{G}_P$ and $\mathcal{G}_I$ are identical. Each node obeys the following dynamics:

$$\dot{x}_i = f(x_i) + \phi_i(t) - \sum_{j\in\mathcal{N}_i} p_{ij}(x_i - x_j) - \sum_{j\in\mathcal{N}_i} n_{ij}(\eta_i - \eta_j), \tag{6.79}$$

where $f(x_i) = x_i - x_i^3$ and $\phi_i(t)$ is given by:

$$\phi_i(t) = \sin(2\pi t + \frac{\pi}{N}i) \tag{6.80}$$

with initial conditions $x_i(0)$ drawn uniformly at random from $[-1,1]$. We set $p_{ij}=1$ for each pair (i,j) that is an edge in the coupling graph and specify n_{ij} for each simulation below.

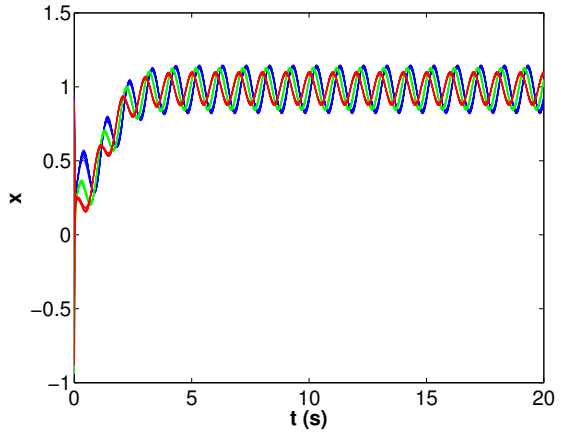

Figure 6.2: Evolution of trajectories as in (6.79) with disturbances (6.80) with $n_{ij} = 0$ for all i, j. Trajectories do not synchronize.

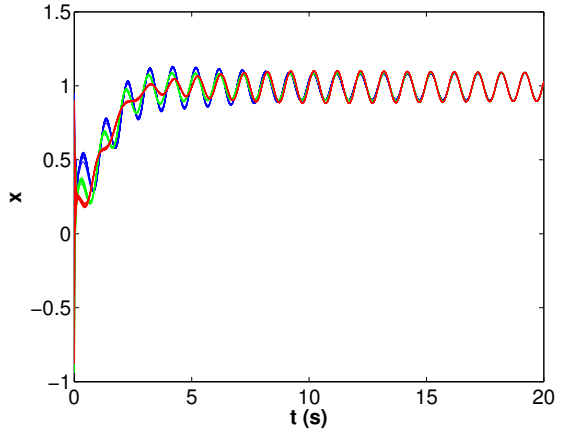

Figure 6.3: Evolution of trajectories as in (6.79) with disturbances (6.80) with internal model controllers, where $n_{ij} = 1$ for each pair (i, j) that is an edge in the coupling graph. Trajectories synchronize.

Figure 6.2 shows the trajectories x_i in the presence of the input disturbances (6.80) with $n_{ij} = 0$ for all i, j. Trajectories synchronize somewhat within clusters, but do not synchronize across all agents. We then set $n_{ij} = 1$ for each pair (i, j) that is an edge in the coupling graph. Under the internal model controllers, the trajectories synchronize, as shown in Figure 6.3.

B. Nonlinear oscillator synchronization

We illustrate the adaptive approach on a nonlinear oscillator. In Chapter 3, we presented a method to check for synchrony of limit cycle oscillations in compartmental diffusively coupled systems. In an example, we considered a ring oscillator model in which three interconnected three-stage ring oscillators were coupled through the first node. Ring oscillators constitute a class of voltage-controlled oscillators frequently found in clock recovery circuits and disk-drive read channels [28, 72], and are also encountered in synthetic gene circuits [53]. We showed that trajectories sufficiently close to a limit cycle trajectory of the nominal system synchronized under small diffusive coupling.

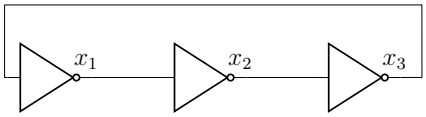

Figure 6.4: Three-stage ring oscillator schematic with dynamics given in (6.81).

The dynamics of the three-stage ring oscillator depicted in Figure 6.4 is given by:

$$f(x) = \begin{bmatrix} -\kappa_1 x_1 - \alpha_1 \tanh(x_3) \\ -\kappa_2 x_2 - \alpha_2 \tanh(x_1) \\ -\kappa_3 x_3 - \alpha_3 \tanh(x_2) \end{bmatrix}. \tag{6.81}$$

If $\Pi_{i=1}^{3} \alpha_i > 8$ and $\kappa_i = 1$ for all i, (6.81) admits a limit cycle [44]. We set $\kappa_i = 1$ and $\alpha_i = 2.2$ for all i. We set $y_\ell = x_\ell$, and define $g_\ell(x(t,\chi)) = e_\ell$, where e_ℓ, $\ell = 1, 2, 3$, are the standard basis vectors of $\mathbb{R}^3$. It can be shown that there exists a quadratic storage function such that the ring oscillator model with the given parameters satisfies the inequality (6.3) with $\theta = 7.704$ (see the example in Section 5.2-A), and so the assumption of Theorem 2 is satisfied whenever $\lambda_2 > 7.704$.

We subject the model to constant, spatially-varying heterogeneities:

$$\phi_\ell(\chi) = 5\sin(10\chi), \quad \ell = 1, 2, 3. \tag{6.82}$$

We consider the initial conditions:

$$x_1(0,\chi) = 1 + 1.1\cos(2\pi\chi) + 1 \tag{6.83}$$
$$x_2(0,\chi) = -1 + 3.4\cos(\pi\chi) - 1 \tag{6.84}$$
$$x_3(0,\chi) = 0.5 + 2.6\sin(2\pi\chi + \pi/2). \tag{6.85}$$

We simulate the system on the one dimensional spatial domain $\Omega = [0, 1]$. Figure 6.5 shows the evolution of $x_1(t,\chi)$ in the absence of heterogeneities. In Figure 6.6, we show the trajectory of $x_1(t,\chi)$ in the absence of the internal model subsystems and demonstrate

lack of spatial homogenization. We next apply the output of the internal model subsystems with $n(\chi) = 1$ and initial condition $\zeta_\ell(0, \chi) = 1$, $\ell = 1, 2, 3$. The trajectories $x(t, \chi)$ become spatially homogeneous as shown in Figure 6.7 for $x_1(t, \chi)$. In Figure 6.8, we show the output $\eta_1(t, \chi)$ of the internal model subsystem G_1.

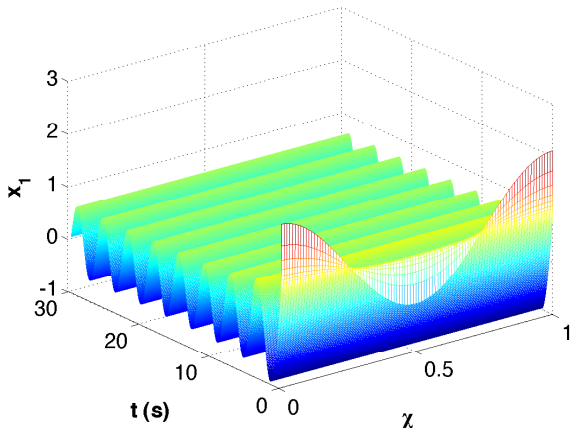

Figure 6.5: Evolution of $x_1(t, \chi)$ as in (6.81) with initial condition $x_1(0, \chi) = 1 + 1.1 \cos(2\pi\chi)$ in the absence of heterogeneity.

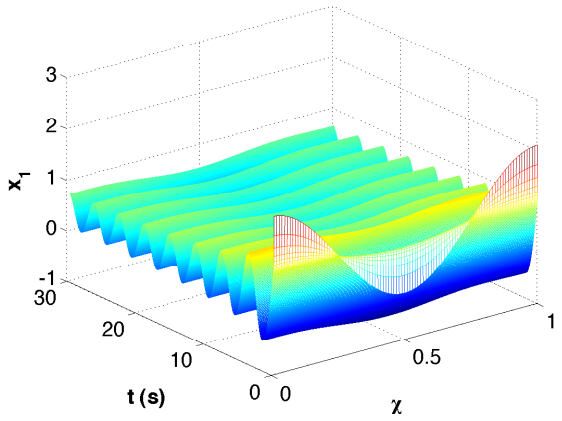

Figure 6.6: Evolution of $x_1(t, \chi)$ as in (6.81) with initial condition $x_1(0, \chi) = 1 + 1.1 \cos(2\pi\chi)$ with heterogeneity as in (6.82) without internal model controller. Spatial heterogeneity persists.

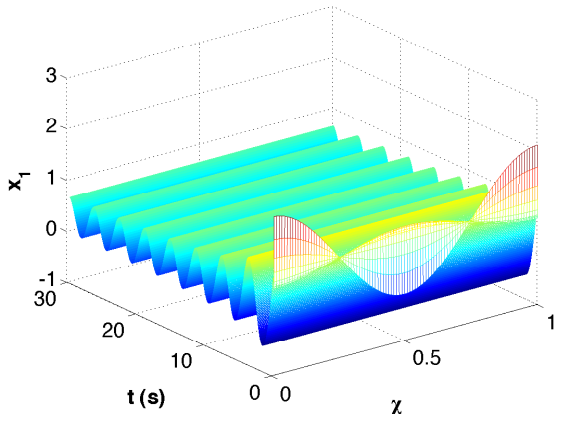

Figure 6.7: Evolution of $x_1(t, \chi)$ as in (6.81) with initial condition $x_1(0, \chi) = 1 + 1.1\cos(2\pi\chi)$ with heterogeneity as in (6.82) with internal model controller. Spatial homogenization occurs.

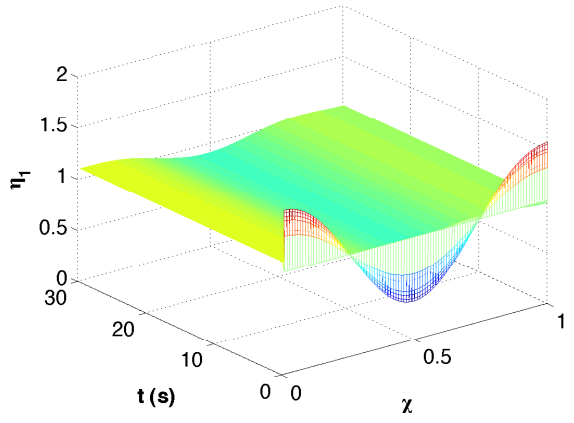

Figure 6.8: Evolution of internal model controller $\eta_1(t, \chi)$ with initial condition $\eta_1(0, \chi) = 1$ and heterogeneity as in (6.82).

C. Bistable Reaction-Diffusion System

Consider a bistable system defined with the dynamics

$$f(x) = x - x^3 \tag{6.86}$$

with $y = x$ and $g(x(t,\chi)) = 1$. Note from (6.86) that each point in the space is a bistable system with stable equilibria at ± 1 and a saddle point at 0. It can be shown that there exists a quadratic storage function such that the system satisfies the inequality (6.3) with $\theta = 2$ (see the example in Section 5.3-B), and so the assumption of Theorem 2 is satisfied whenver $\lambda_2 > 2$.

We subject the model to a spatially and temporally-varying heterogeneity:

$$\phi(t,\chi) = 10\sin(\pi t + 2\pi\chi). \tag{6.87}$$

We consider the initial condition

$$x(0,\chi) = 0.1 + 3.5\cos(2\pi\chi). \tag{6.88}$$

We simulate the system on the one dimensional spatial domain $\Omega = [0,1]$. Figure 6.9 shows the evolution of $x(t,\chi)$ in the absence of heterogeneities. In Figure 6.10, we show the trajectory of $x(t,\chi)$ in the presence of heterogeneities without internal model control and demonstrate lack of spatial homogenization. We next apply the output of the internal model controllers with $n(\chi) = 1$ and initial condition $\zeta(0,\chi) = 1$. The trajectory of $x(t,\chi)$ becomes spatially homogeneous as shown in Figure 6.11. Note that the internal model control compensates for effects due to the differences $\phi(t,\chi) - \bar{\phi}(t)$. The remaining (spatially homogeneous) effect is due to $\bar{\phi}(t)$, which is zero for (6.87), and so the spatial heterogeneity is completely attenuated and the trajectory tends to an equilibrium value across the spatial and temporal dimensions. In Figure 6.12, we show the output $\eta(t,\chi)$ of the internal model subsystem G in the case of the heterogeneity in (6.87).

We next modify $\phi(t,\chi)$:

$$\phi(t,\chi) = 10\sin(\pi t + 1.7\pi\chi), \quad \ell = 1,\ldots,3, \tag{6.89}$$

and simulate the system again. Note that since the average $\bar{\phi}(t)$ is no longer zero, the trajectory in Figure 6.13 exhibits spatially uniform oscillations.

6.4 Conclusion

We have studied spatial homogenization of nonlinear systems that are incrementally passive, and designed a distributed control law that guarantees spatial homogeneity in the presence of

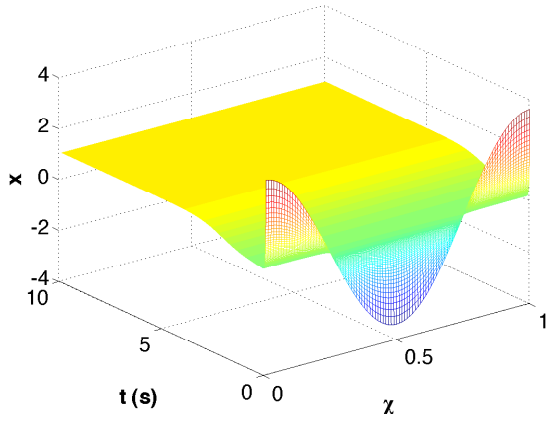

Figure 6.9: Evolution of $x(t, \chi)$ as in (6.86) with initial condition $x(0, \chi) = 0.1 + 3.5\cos(2\pi\chi)$ in the absence of heterogeneities.

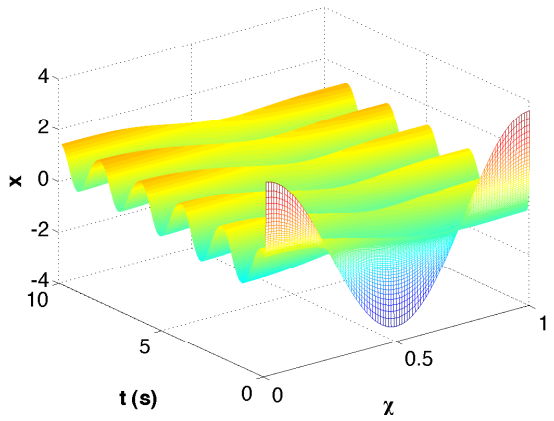

Figure 6.10: Evolution of $x(t, \chi)$ as in (6.86) with initial condition $x(0, \chi) = 0.1 + 3.5\cos(2\pi\chi)$ with heterogeneity as in (6.87) without internal model controller. Spatial heterogeneity persists.

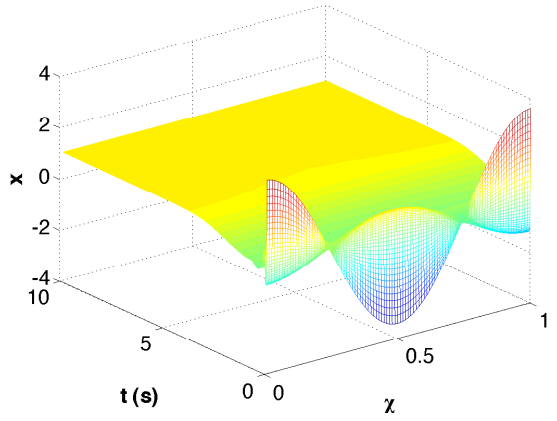

Figure 6.11: Evolution of $x(t, \chi)$ as in (6.86) with initial condition $x(0, \chi) = 0.1+3.5\cos(2\pi\chi)$ with heterogeneity as in (6.87) with internal model controller. Spatial homogenization occurs with equilibrium across spatial and temporal dimensions recovered.

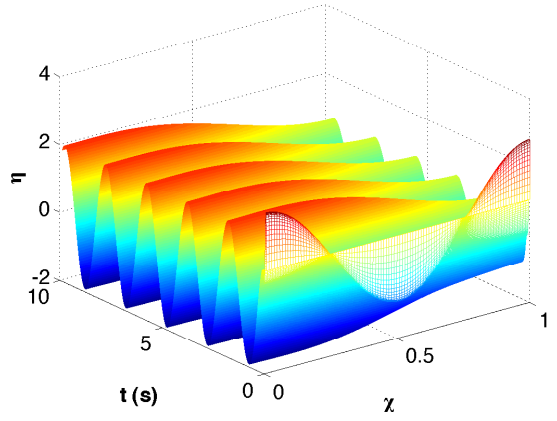

Figure 6.12: Evolution of internal model controller $\eta(t, \chi)$ with initial condition $\eta(0, \chi) = 1$ and heterogeneity as in (6.87).

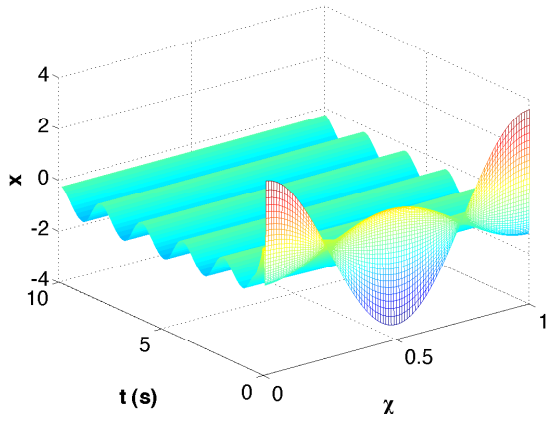

Figure 6.13: Evolution of $x(t, \chi)$ as in (6.86) with initial condition $x(0, \chi) = 0.1+3.5\cos(2\pi\chi)$ with heterogeneity as in (6.89) with internal model controller. Spatial homogenization occurs with spatially uniform oscillations.

a class of spatially and temporally-varying heterogeneities. Our controller has the advantage of not requiring knowledge of the initial conditions of the heterogeneities, and furthermore is amenable to heterogeneities that vary over multiple input and output channels. We have illustrated our results on systems with ring oscillator dynamics and bistable dynamics.

Chapter 7

Conclusion

Diffusively coupled spatially distributed models are an essential class of systems that lend crucial insight to understanding and improving the behavior of many engineered and biological systems. Diffusive coupling facilitates design and analysis of cooperative laws in multi-agent systems, oscillator synchronization in electrical and biological systems, and the spread of information in distributed systems. A good understanding of local network structure and dynamics of the individual agents is fundamental to achieving distributed control architectures to guarantee desired operation of the overall system in the absence of a centralized leader. Furthermore, it can lend insight into underlying vulnerabilities and potential for instabilities in the network.

In this dissertation, we have developed distributed algorithms that guarantee desirable behavior in diffusively coupled systems by making use of local network structure and agent dynamics. We have studied local behavior near a specific attractor as well as global behavior of the full nonlinear dynamics. The methods we have derived apply to systems coupled over graphs as well as systems defined over a spatial continuum. Additionally, we have derived analysis methodologies that can facilitate our understanding of coupling structure and interaction between agents. We next summarize our contributions.

7.1 Key Contributions

In Chapter 2, we considered the problem of designing distributed coordination laws for multi-agent systems coupled over a graph. We developed a convex optimization framework for determining optimal weights for the nodes and edges of the coupling graph. We applied the strategy to several graph design problems as well as a formation control problem, where the objective was fast convergence to a stable configuration with specified spacings between agents. We then outlined dual approaches for handling larger graphs.

In Chapter 3, we considered synchronization of oscillations in systems whose nominal dynamics admitted a stable limit cycle. We gave analytical and numerical conditions to determine whether diffusion homogenized limit cycle trajectories across the spatial domain. We highlighted a case of diffusion-driven instability wherein large enough diffusion coefficients indeed led to loss of synchrony.

We considered synchronization under space and component-dependent diffusive coupling in Chapter 4. We gave a condition that restricts the Jacobian of the vector field of the uncoupled dynamics as well as the Laplacian eigenvalues of each interconnection graph in order to guarantee synchrony. We then developed a sufficient condition that may be verified using linear matrix inequalities.

Using ideas developed in Chapter 4, in Chapter 5 we presented an adaptive algorithm for synchronization in which coupling weights were adjusted according to local disagreement between agents connected to the corresponding edges. The algorithm relied on the individual subsystems satisfying an incremental output-feedback passivity property. We demonstrated the effectiveness of the approach in reducing time to synchronization in multiple examples in both the spatially discrete and continuous settings.

In Chapter 6, we considered the case where individual agents no longer had identical dynamics. We proposed an internal model controller for agents satisfying an incremental output-feedback passivity property and subject to disturbances that guaranteed synchronization. We highlighted several examples in which the internal model controller successfully eliminated spatial inhomogeneities.

7.2 Future Work

The study of synchronization in diffusively coupled models is a rich and active research area, with increasing focus on designing robust algorithms that scale well to large networks. With respect to this dissertation, several avenues for future research exist. While the convex optimization framework developed in Chapter 2 is flexible and enables modifying various eigenvalues of the graph Laplacian matrix, the solution method using interior point algorithms limits the scale of graphs that can be considered. It would be interesting to explore efficient algorithms that exploit structural properties of specific networks to reduce the number of edges and nodes that must be considered. Also, recent progress in the development of first order methods to solve semidefinite programs [99][100] indicate the potential of developing algorithms that scale to large networks.

The adaptive algorithm developed in Chapter 5 is a step towards achieving robust network design in a completely distributed, dynamic fashion, in contrast to the static optimization proposed in Chapter 2. Additionally, the internal model controller in Chapter 6 addresses problems of robustness and heterogeneities between agents. We are also pursuing adap-

tively updating the weights of the coupling coefficients in the internal model controller in Chapter 6 as in Chapter 5. A key challenge is expanding the scope of dynamics to which these approaches are applicable, such as the case of nonminimum phase systems and systems with relative degree greater than one. Also, it would be useful to address robustness to broader classes of disturbances and heterogeneities with the goal of guaranteeing small residual synchronization errors.

The most promising direction is the application of the analysis and design tools developed in this dissertation to real systems. For instance, the techniques in Chapters 2 and 3 can lend insight to the design of coordination laws in multi-agent systems that take into account the possibility of diffusion-driven instabilities. Furthermore, we envision application of adaptive algorithm to numerical experiments that elucidate bottlenecks and other interesting structural features of a complex network or continuous domain. The algorithms may be able to assist in graph decomposition and community structure identification [47, 62] or spectral clustering and image segmentation [88]. Finally, the increasing deployment of distributed sensors and the development of the Internet of Things promise ever-expanding applications for which the methods described in this dissertation are well-suited and may be further refined.

Appendix A

Two-Time Scale Averaging

We state a lemma that follows from standard results in two-time scale averaging (see, e.g., [83], Thm. 4.4.3).

Lemma A1 *Let $w \in \mathbb{R}^p$ and $z \in \mathbb{R}^q$, and consider the linear time varying system:*

$$\begin{bmatrix} \dot{w} \\ \dot{z} \end{bmatrix} = \left(\begin{bmatrix} 0 & 0 \\ 0 & G \end{bmatrix} - \epsilon \begin{bmatrix} H_{11}(t) & H_{12}(t) \\ H_{21}(t) & H_{22}(t) \end{bmatrix} \right) \begin{bmatrix} w \\ z \end{bmatrix}, \tag{A.1}$$

where each $H_{ij}(t)$, $i,j \in \{1,2\}$ is a bounded piecewise continuous matrix-valued function of time such that $H_{ij}(t+T) = H_{ij}(t)$, $G \in \mathbb{R}^{q\times q}$, and $\epsilon > 0$. Define the associated averaged slow system:

$$\dot{w}_s = -\epsilon \bar{H}_{11} w_s, \;\; \bar{H}_{11} = \frac{1}{T} \int_{t_0}^{t_0+T} H_{11}(t)\, dt. \tag{A.2}$$

If $-\bar{H}_{11}$ and G are Hurwitz, then there exists ϵ^* such that $[w^T \;\; z^T]^T = 0$ is an exponentially stable equilibrium of (A.1) for $0 < \epsilon < \epsilon^*$. □

Proof: We provide a proof for completeness and to exhibit a procedure for obtaining ϵ^*. We begin by introducing a change of coordinates:

$$w = \left[I - \epsilon \int_0^t \left(H_{11}(\tau) - \bar{H}_{11} \right) d\tau \right] \hat{w}. \tag{A.3}$$

Upon substitution, we have:

$$\begin{aligned} &\left[I - \epsilon \int_0^t \left(H_{11}(\tau) - \bar{H}_{11} \right) d\tau \right] \dot{\hat{w}} \\ &\quad - \epsilon [H_{11}(t) - \bar{H}_{11}] \hat{w} \\ &= -\epsilon H_{11}(t) \left[I - \epsilon \int_0^t \left(H_{11}(\tau) - \bar{H}_{11} \right) d\tau \right] \hat{w} \\ &\quad - \epsilon H_{12}(t) z. \end{aligned} \tag{A.4}$$

Since each $H_{ij}(t)$ is bounded, we have $|H_{ij}(t)| \leq \hat{h}_{ij}$ for all t. Furthermore, since each $\int_0^t \left(H_{11}(\tau) - \bar{H}_{11}\right) d\tau$ is periodic, we have:

$$\left| \int_0^t \left(H_{11}(\tau) - \bar{H}_{11}\right) d\tau \right| \leq 2T\hat{h}_{11}. \tag{A.5}$$

Then for $\epsilon < \epsilon_1 := \frac{1}{2T\hat{h}_{11}}$, the change of coordinates is invertible. Rewriting, we have:

$$\begin{aligned} \dot{\hat{w}} = &- \epsilon \left[I - \epsilon \int_0^t \left(H_{11}(\tau) - \bar{H}_{11}\right) d\tau \right]^{-1} \\ &\times H_{11}(t) \left[I - \epsilon \int_0^t \left(H_{11}(\tau) - \bar{H}_{11}\right) d\tau \right] \hat{w} \\ &- \epsilon \left[I - \epsilon \int_0^t \left(H_{11}(\tau) - \bar{H}_{11}\right) d\tau \right]^{-1} H_{12}(t) z \\ &- \epsilon \left[I - \epsilon \int_0^t \left(H_{11}(\tau) - \bar{H}_{11}\right) d\tau \right]^{-1} \\ &\times [\bar{H}_{11} - H_{11}(t)] \hat{w}. \end{aligned} \tag{A.6}$$

With a similar change of coordinates, we have:

$$\begin{aligned} \dot{z} = &Gz - \epsilon H_{21}(t) \left[I - \epsilon \int_0^t \left(H_{11}(\tau) - \bar{H}_{11}\right) d\tau \right] \hat{w} \\ &- \epsilon H_{22}(t) z. \end{aligned} \tag{A.7}$$

Define the positive definite matrices P_w and P_z such that:

$$\begin{aligned} P_w \bar{H}_{11} + \bar{H}_{11}^T P_w &= I \\ P_z G + G^T P_z &= -I. \end{aligned} \tag{A.8}$$

We next consider the candidate Lyapunov function:

$$V = \hat{w}^T P_w \hat{w} + z^T P_z z. \tag{A.9}$$

Define the scalar $\gamma := \frac{1}{1 - 2\epsilon_1 T \hat{h}_{11}}$. Differentiating V, we have:

$$\begin{aligned} \dot{V} \leq &- (\epsilon\gamma - 2\epsilon^2 \gamma T \hat{h}_{11}^2) |\hat{w}|^2 + \epsilon\gamma \hat{h}_{12} |\hat{w}||z| \\ &- (1 - \epsilon \hat{h}_{22}) |z|^2 + \epsilon \hat{h}_{21} |z||\hat{w}| \\ &+ \epsilon^2 (2T \hat{h}_{21} \hat{h}_{11}) |z||\hat{w}|. \end{aligned} \tag{A.10}$$

Because $\epsilon < \epsilon_1$, the first term of (A.10) is negative. Similarly, choosing $\epsilon < \epsilon_2 := \frac{1}{\hat{h}_{22}}$ guarantees that the second term of (A.10) is negative. If the condition

$$\begin{aligned}
&\begin{bmatrix} M_{11} & M_{12} \\ M_{12} & M_{22} \end{bmatrix} \prec 0, \text{ with} \\
&M_{11} = -(\epsilon\gamma - 2\epsilon^2\gamma T\hat{h}_{11}^2) \\
&M_{12} = \frac{1}{2}\left(\epsilon\gamma\hat{h}_{12} + \epsilon\hat{h}_{21} + \epsilon^2(2T\hat{h}_{21}\hat{h}_{11})\right) \\
&M_{22} = -(1 - \epsilon\hat{h}_{22}),
\end{aligned} \tag{A.11}$$

is satisfied, then (A.10) is negative. Using the Schur complement, we rewrite the condition as:

$$\begin{aligned}
&-(\epsilon\gamma - 2\epsilon^2\gamma T\hat{h}_{11}^2) \\
&+\frac{1}{4}\left(\epsilon\gamma\hat{h}_{12} + \epsilon\hat{h}_{21} + \epsilon^2(2T\hat{h}_{21}\hat{h}_{11})\right)^2 (1 - \epsilon\hat{h}_{22})^{-1} \\
&< 0.
\end{aligned} \tag{A.12}$$

Therefore, there exists $\epsilon_3 > 0$ such that for $0 < \epsilon < \epsilon_3$, (A.12) holds. Thus, with $\epsilon^* = \min\{\epsilon_1, \epsilon_2, \epsilon_3\}$, $[w^T \ \ z^T]^T = 0$ is an exponentially stable equilibrium of (A.1). □

Appendix B

Structured Singular Value for Periodic Systems using Harmonic Balance

To justify the SSV analysis proposed in Section 3.3, in this appendix we extend the concept of structured singular value to periodic systems using a generalized Nyquist result and a classic result from robust control. We begin by reviewing the Nyquist criterion for periodic linear time varying systems studied by [51, 109]. We consider the system:

$$\begin{aligned} \dot{x} &= A(t)x + B(t)q \\ y &= C(t)x \\ q &= -\Delta y, \end{aligned} \tag{B.1}$$

with $A(t)$, $B(t)$, $C(t) \in \mathbb{R}^{n\times n}$. We assume that $A(t)$, $B(t)$, and $C(t)$ are periodic with period T and continuous with absolutely convergent Fourier series, and $\Delta \in \mathbb{R}^n$ with $|\Delta_{ij}| \leq 1$. The bi-infinite harmonic state space model of (B.1) is given by:

$$\begin{aligned} (s\mathcal{I} + \mathcal{N})X &= \mathcal{A}X + \mathcal{B}Q \\ Y &= \mathcal{C}X \\ Q &= -\tilde{\Delta}Y, \end{aligned} \tag{B.2}$$

where the matrix $\tilde{\Delta} = \text{blkdiag}(\Delta)$, and $\mathcal{N}$, $\mathcal{I}$, and $\mathcal{A}$ as in Section 3.3, and $\mathcal{B}$ and $\mathcal{C}$ defined similarly to $\mathcal{A}$. The (infinite-dimensional) harmonic open loop transfer operator of the system is:

$$G(s) = \mathcal{C}[s\mathcal{I} - (\mathcal{A} - \mathcal{N})]^{-1}\mathcal{B}. \tag{B.3}$$

We rewrite (B.2), substituting for Y:

$$\begin{bmatrix} I - (s\mathcal{I} + \mathcal{N})^{-1}\mathcal{A} & (s\mathcal{I} + \mathcal{N})^{-1}\mathcal{B} \\ \tilde{\Delta}\mathcal{C} & \mathcal{I} \end{bmatrix} \begin{bmatrix} X \\ Q \end{bmatrix} = \begin{bmatrix} 0 \\ 0 \end{bmatrix}. \tag{B.4}$$

Following [109], suppose $\mathcal{M}$ is a linear compact operator. Denote by $\lambda_i(\mathcal{M})$ and $\sigma_i(\mathcal{M})$ the i-th eigenvalue and singular value of $\mathcal{M}$, respectively. Denote by $C_p(l_2)$ the set of linear compact operators $\mathcal{M} : l_2 \to l_2$ that satisfy

$$||\mathcal{M}||_p = \left(\sum_i \sigma_i(\mathcal{M})^p \right)^{\frac{1}{p}} < \infty. \tag{B.5}$$

Elements in $C_1(l_2)$ are called trace-class operators, and the determinant

$$\det(\mathcal{I} + \mathcal{M}) := \Pi_{k=-\infty}^{\infty}(1 + \lambda_k) \tag{B.6}$$

of a trace-class operator is well-defined in the sense that it converges absolutely. Elements in $C_2(l_2)$ are called Hilbert-Schmidt operators, and may not have absolutely-convergent determinants.

We next apply the Schur determinant lemma to the left hand side of (B.4):

$$\begin{aligned} \psi_{cl}(\Delta) &:= \det \big(\mathcal{I} - (s\mathcal{I} + \mathcal{N})^{-1}\mathcal{A} \\ &\qquad - (s\mathcal{I} + \mathcal{N})^{-1}\mathcal{B}\tilde{\Delta}\mathcal{C} \big) \\ &= \det \left(\mathcal{I} - (s\mathcal{I} + \mathcal{N})^{-1}(\mathcal{A} - \mathcal{B}\tilde{\Delta}\mathcal{C}) \right). \end{aligned} \tag{B.7}$$

The operator $\mathcal{H}(s) = (s\mathcal{I} + \mathcal{N})^{-1}(\mathcal{A} - \mathcal{B}\tilde{\Delta}\mathcal{C})$ is not in $C_1(l_2)$, and in particular, $\psi_{cl}(\Delta)$ does not converge absolutely. Thus, it is not possible to develop a Nyquist criterion making use of the standard infinite determinant $\psi_{cl}(\Delta)$. To deal with this problem, [109] proposed an approach using the 2-*regularized determinant*. Since $\mathcal{H}(s) \in C_2(l_2)$, it holds that $R_2(\mathcal{H}) = (\mathcal{I}+\mathcal{H}) \exp(-\mathcal{H}) - \mathcal{I} \in C_1(l_2)$, and so the 2-regularized determinant $\det_2(\mathcal{I}+\mathcal{H}) := \det(\mathcal{I} + R_2(\mathcal{H}))$ is well-defined. We note that the Sylvester determinant lemma holds for the 2-regularized determinant: $\det_2(\mathcal{I} + \mathcal{K}\mathcal{H}) = \det_2(\mathcal{I} + \mathcal{H}\mathcal{K})$. Making use of the 2-regularized determinant, it can be shown that:

$$\begin{aligned} \psi_G(\Delta) &:= \det_2(\mathcal{I} + \tilde{\Delta}G(s)) \exp(-r(s+\rho)) \\ &= \frac{\det_2(\mathcal{I} - ((s+\rho)\mathcal{I} + \mathcal{N})^{-1}(\mathcal{A} - \mathcal{B}\tilde{\Delta}\mathcal{C} + \rho\mathcal{I}))}{\det_2(\mathcal{I} - ((s+\rho)\mathcal{I} + \mathcal{N})^{-1}(\mathcal{A} + \rho\mathcal{I}))}, \end{aligned} \tag{B.8}$$

with $r(s+\rho) = -\mathrm{tr}[((s+\rho)\mathcal{I} + \mathcal{N})^{-1}(\mathcal{A} + \rho\mathcal{I})(s\mathcal{I} + \mathcal{N} - \mathcal{A})^{-1}\mathcal{B}\tilde{\Delta}\mathcal{C}]$, and $\rho > 0$. The generalized Nyquist stability criterion for periodic linear time varying systems follows (see [109], Theorem 3.1):

Theorem B1 *Assume that $A(t)$, $B(t)$, and $C(t)$ are piecewise-continuously differentiable and have absolutely convergent Fourier series expansions. Let $\rho > 0$ be an arbitrary positive number, and let n_p be the number of unstable eigenvalues in the fundamental strip of the*

open loop operator $\mathcal{A}-\mathcal{N}$. The closed loop system (B.2) is asymptotically stable if and only if the Nyquist locus of $\psi_G(\Delta)$ is not zero for all points along the Nyquist contour about the closed right half plane intersected with the fundamental strip [51]:

$$S := \left\{ s \in \mathbb{C} : -\frac{\omega_p}{2} < Im(s) \leq \frac{\omega_p}{2} \right\}, \tag{B.9}$$

and $\psi_G(\Delta)$ encircles the origin n_p times in the counterclockwise direction. □

We now generalize a key result from MIMO robust control theory [108][31] to periodic time-varying systems, making use of Theorem B1:

Theorem B2 *Given a proper harmonic transfer operator $G(s) \in C_2(l_2)$ with no unstable poles and a bounded uncertainty set $\Phi \in \mathbb{R}^{n\times n}$ with a given sparsity structure, the closed loop system (B.2) is asymptotically stable if and only if $\det_2(\mathcal{I}+\tilde{\Delta}G(j\omega)) \neq 0$ for all $\Delta \in \Phi$ and $\omega \in \left(-\frac{\omega_p}{2}, \frac{\omega_p}{2}\right]$.* □

Proof: First, we shall prove necessity by contradiction. Suppose (B.2) is not asymptotically stable. By the Nyquist criterion in Theorem B.2, the Nyquist plot of $\psi_G(\Delta) = \det_2(\mathcal{I} + \tilde{\Delta}G(s)) \exp(-r(s+\rho))$ encircles or touches the origin for some $\omega \in \left(-\frac{\omega_p}{2}, \frac{\omega_p}{2}\right]$. Consider the homotopy:

$$h(\epsilon) = \det_2(\mathcal{I} + \epsilon\tilde{\Delta}G(s)) \exp(-r_\epsilon(s+\rho)), \tag{B.10}$$

with $\epsilon \in [0,1]$, $\mathrm{Im}(s) = \omega$, and $r_\epsilon(s+\rho) = -\mathrm{tr}[((s+\rho)\mathcal{I}+\mathcal{N})^{-1}(\mathcal{A}+\rho\mathcal{I})(s\mathcal{I}+\mathcal{N}-\mathcal{A})^{-1}\mathcal{B}\epsilon\tilde{\Delta}\mathcal{C}]$. Because $\psi_G(\Delta)$ is a meromorphic function (analytic except at a countable number of points) [109], it holds by Lemma A.1.18 [21] that if $h(\epsilon)$ vanishes nowhere, then $h(0)$ and $h(1)$ must have the same winding number, or Nyquist index. However, the curve at $\epsilon = 0$ is a point at 1, while the curve at $\epsilon = 1$ encircles or touches the origin. Thus $h(\epsilon)$ must vanish for some $\epsilon_0 \in (0,1]$. Now since $\Delta \in \Phi$ implies that $\Delta_0 := \epsilon\Delta \in \Phi$, and because $\exp(-r_\epsilon(s+\rho)) \neq 0$ since $r(s+\rho)$ is bounded (see [109], Lemma 2.3), it must hold that $\det_2(\mathcal{I}+\tilde{\Delta}_0 G(j\omega)) = 0$ for some $\Delta_0 \in \Phi$.

Next, we prove sufficiency, also by contradiction. Suppose that there exist $\omega \in \left(-\frac{\omega_p}{2}, \frac{\omega_p}{2}\right]$ and $\Delta \in \Phi$ such that $\det_2(\mathcal{I}+\tilde{\Delta}G(j\omega)) = 0$. Then (B.2) has a pole on the imaginary axis, and is not asymptotically stable. □

We now define the structured singular value for periodic linear time-varying systems in terms of the harmonic transfer operator:

$$\mu_{\mathbf{\Delta}}(G) := \frac{1}{\min\{\bar{\sigma}(\Delta) :\ \Delta \in \mathbf{\Delta},\ \det_2(\mathcal{I}+G(s)\tilde{\Delta}) = 0\}}, \tag{B.11}$$

where $\mathbf{\Delta}$ denotes a bounded structured uncertainty set and where we have invoked the Sylvester determinant lemma. Then Theorem B2 may be recast using the structured singular value:

Theorem B3 *Let* $\Phi = \{\Delta : \Delta \in \mathbf{\Delta}, \bar{\sigma}(\Delta) \leq \gamma\}$. *Then the closed loop system (B.2) is stable if and only if* $\mu_{\mathbf{\Delta}}(G(s)) < \frac{1}{\gamma}$ *for all* $s \in S$ *given in (B.9).* □

The final step of the analysis is developing a computationally tractable test, which requires a finite dimensional truncation of the infinite-dimensional operator $G(s)$. In [81], the authors showed that $G(s)$ could be approximated arbitrarily well by a finite truncated operator consisting of only the first N terms of the Fourier series expansion of $A(t)$, $B(t)$, and $C(t)$. We denote by $G_N(s)$ the truncated operator given by:

$$G_N(s) = \mathcal{C}_N[s\mathcal{I} - (\mathcal{A}_N - \mathcal{N})]^{-1}\mathcal{B}_N \tag{B.12}$$

where $\mathcal{A}_N$ is the $(N+1) \times (N+1)$ submatrix of $\mathcal{A}$ centered along the A_0 diagonal, and $\mathcal{B}_N$ and $\mathcal{C}_N$ defined similarly. In particular, it was shown that $||G - G_N||_2 \leq K(N) := O(N^{-1})$. From this fact and following the proof technique of Lemma 4.1 in [109], it then holds that:

$$\begin{aligned} &|\det_2(\mathcal{I} + G) - \det_2(\mathcal{I} + G_N)| \\ &\leq ||G - G_N||_2 \exp\left\{\frac{1}{2}\left[||G||_2 + ||G_N||_2 + 1\right]\right\} \\ &\leq K(N) \cdot M, \end{aligned} \tag{B.13}$$

where the second inequality follows from the boundedness of G and G_N. With the observation that the matrix Δ may be incorporated into the matrix $B(t)$ or $C(t)$, we see that the term $\det_2(\mathcal{I} + G\tilde{\Delta})$ appearing in Theorem B2 and (B.11) may be asymptotically approximated by $\det_2(\mathcal{I} + G_N\tilde{\Delta}_N)$, where $\tilde{\Delta}_N$ is the truncated version of $\tilde{\Delta}$.

Bibliography

[1] M. Arcak. "Certifying spatially uniform behavior in reaction-diffusion PDE and compartmental ODE systems". In: *Automatica* 47.6 (2011), pp. 1219–1229.

[2] M. Arcak. "Passivity as a design tool for group coordination". In: *IEEE Transactions on Automatic Control* 52.8 (2007), pp. 1380–1390.

[3] M. Arcak and E.D. Sontag. "Diagonal stability of a class of cyclic systems and its connection with the secant criterion". In: *Automatica* 42.9 (2006), pp. 1531–1537.

[4] M. Ashkenazi and HG Othmer. "Spatial patterns in coupled biochemical oscillators". In: *Journal of Mathematical Biology* 5.4 (1977), pp. 305–350.

[5] S. Assenza et al. "Emergence of structural patterns out of synchronization in networks with competitive interactions". In: *Scientific Reports* 1 (2011).

[6] H Bai and M. Arcak. "Instability mechanisms in cooperative control". In: *IEEE Transactions on Automatic Control* 55.1 (2010), pp. 258–263.

[7] He Bai, Randy A Freeman, and Kevin M Lynch. "Robust dynamic average consensus of time-varying inputs". In: *49th IEEE Conference on Decision and Control (CDC)*. IEEE. 2010, pp. 3104–3109.

[8] B. Bamieh et al. "A lifting technique for linear periodic systems with applications to sampled-data control". In: *Systems & Control Letters* 17.2 (1991), pp. 79–88.

[9] E. Biyik and M. Arcak. "Area aggregation and time-scale modeling for sparse nonlinear networks". In: *Systems & Control Letters* 57.2 (2008), pp. 142–149. ISSN: 0167-6911.

[10] Michael Böhm et al. "Model reference adaptive control of distributed parameter systems". In: *SIAM Journal on Control and Optimization* 36.1 (1998), pp. 33–81.

[11] S. Boyd, P. Diaconis, and L. Xiao. "Fastest mixing Markov chain on a graph". In: *SIAM Review* 46.4 (2004), pp. 667–689.

[12] S. Boyd et al. *Linear matrix inequalities in system and control theory*. Society for Industrial Mathematics, 1994. ISBN: 0898714850.

[13] Mathias Bürger and Claudio De Persis. "Internal Models for Nonlinear Output Agreement and Optimal Flow Control". In: *IFAC Symposium on Nonlinear Control Systems (NOLCOS)*. Vol. 9. 1. 2013, pp. 289–294.

[14] Richard G Casten and Charles J Holland. "Stability properties of solutions to systems of reaction-diffusion equations". In: *SIAM Journal on Applied Mathematics* 33.2 (1977), pp. 353–364.

[15] T. Chen and B.A. Francis. *Optimal sampled-data control systems*. Vol. 124. London: Springer, 1995.

[16] N. Chopra and M.W. Spong. "On exponential synchronization of Kuramoto oscillators". In: *IEEE Transactions on Automatic Control* 54.2 (2009), pp. 353–357.

[17] J.H. Chow, ed. *Time-Scale Modeling of Dynamic Networks with Applications to Power Systems*. Berlin Heidelberg: Springer-Verlag, 1982.

[18] F.R.K. Chung. "Spectral graph theory". In: *American Mathematical Society* (1997).

[19] E. Conway, D. Hoff, and J. Smoller. "Large time behavior of solutions of systems of nonlinear reaction-diffusion equations". In: *SIAM Journal on Applied Mathematics* (1978), pp. 1–16.

[20] M.C. Cross and P.C. Hohenberg. "Pattern formation outside of equilibrium". In: *Reviews of Modern Physics* 65.3 (1993), pp. 851–1112.

[21] R.F. Curtain and H.J. Zwart. *An introduction to infinite-dimensional linear systems theory*. Vol. 21. New York, NY: Springer, 1995.

[22] Claudio De Persis and Bayu Jayawardhana. "On the internal model principle in formation control and in output synchronization of nonlinear systems". In: *51st IEEE Annual Conference on Decision and Control (CDC)*. IEEE. 2012, pp. 4894–4899.

[23] Pietro DeLellis, Mario di Bernardo, and Giovanni Russo. "On QUAD, Lipschitz, and contracting vector fields for consensus and synchronization of networks". In: *IEEE Transactions on Circuits and Systems I* 58.3 (2011), pp. 576–583.

[24] Pietro DeLellis, Mario DiBernardo, and Francesco Garofalo. "Novel decentralized adaptive strategies for the synchronization of complex networks". In: *Automatica* 45.5 (2009), pp. 1312–1318.

[25] Michael A Demetriou. "Adaptation and optimization of synchronization gains in networked distributed parameter systems". In: *arXiv preprint arXiv:1305.7117* (2013).

[26] Michael A Demetriou. "Synchronization and consensus controllers for a class of parabolic distributed parameter systems". In: *Systems & Control Letters* 62.1 (2013), pp. 70–76.

[27] A. Demir, A. Mehrotra, and J. Roychowdhury. "Phase noise in oscillators: A unifying theory and numerical methods for characterization". In: *IEEE Transactions on Circuits and Systems I: Fundamental Theory and Applications* 47.5 (2000), pp. 655–674.

[28] L. DeVito et al. “A 52MHz and 155MHz clock-recovery PLL”. In: *38th ISSCC., 1991 IEEE International Solid-State Circuits Conference, 1991. Digest of Technical Papers.* IEEE. 1991, pp. 142–306.

[29] Andrew Dhawan, Abdullah Hamadeh, and Brian Ingalls. “Designing synchronization protocols in networks of coupled nodes under uncertainty”. In: *American Control Conference (ACC), 2012*. IEEE. 2012, pp. 4945–4950.

[30] F. Dörfler and F. Bullo. “Exploring Synchronization in Complex Oscillator Networks”. In: *arXiv Preprint: arXiv:1209.1335* (2012).

[31] J. Doyle and G. Stein. “Multivariable feedback design: Concepts for a classical/modern synthesis”. In: *IEEE Transactions on Automatic Control* 26.1 (1981), pp. 4–16.

[32] GE Dullerud and K. Glover. “Robust performance of periodic systems”. In: *IEEE Transactions on Automatic Control* 41.8 (1996), pp. 1146–1159.

[33] L.C. Evans. *Partial Differential Equations*. Vol. 19. Graduate Studies in Mathematics. American Mathematical Society, 1998.

[34] Makan Fardad, Mihailo R Jovanovic, and Bassam Bamieh. “Frequency analysis and norms of distributed spatially periodic systems”. In: *IEEE Transactions on Automatic Control* 53.10 (2008), pp. 2266–2279.

[35] M. Farkas. *Periodic motions*. New York, NY: Springer, 1994.

[36] J.A. Fax and R.M. Murray. “Information flow and cooperative control of vehicle formations”. In: *IEEE Transactions on Automatic Control* 49.9 (2004), pp. 1465–1476.

[37] M. Fiedler. “Algebraic connectivity of graphs”. In: *Czechoslovak Mathematical Journal* 23.2 (1973), pp. 298–305.

[38] Fulvio Forni and Rodolphe Sepulchre. “On differentially dissipative dynamical systems”. In: *9th IFAC Symposium on Nonlinear Control Systems*. IFAC. 2013.

[39] Fulvio Forni, Rodolphe Sepulchre, and Arjan van der Schaft. “On differential passivity of physical systems”. In: *52nd IEEE Conference on Decision and Control (CDC)*. IEEE. 2013.

[40] B. A. Francis and W. M. Wonham. “The internal model principle of control theory”. In: *Automatica* 12 (1976), pp. 457–465.

[41] Randy A Freeman, Peng Yang, and Kevin M Lynch. “Stability and convergence properties of dynamic average consensus estimators”. In: *45th IEEE Conference on Decision and Control*. IEEE. 2006, pp. 338–343.

[42] Avner Friedman. *Partial differential equations*. RE Krieger Publishing Company, 1976.

[43] F.R. Gantmacher. *The theory of matrices*. Chelsea Pub Co, 2000.

[44] X. Ge, M. Arcak, and K.N. Salama. "Nonlinear Analysis of Ring Oscillator and Cross-Coupled Oscillator Circuits". In: *Dynamics of Continuous, Discrete and Impulsive Systems, Series B: Applications and Algorithms* 17.6 (2010), pp. 959–977.

[45] Xiaoqing Ge and Murat Arcak. "A sufficient condition for additive D-stability and application to reaction–diffusion models". In: *Systems & Control Letters* 58.10 (2009), pp. 736–741.

[46] A. Ghosh, S. Boyd, and A. Saberi. "Minimizing effective resistance of a graph". In: *SIAM Review* 50.1 (2008), pp. 37–66.

[47] M.X. Goemans and D.P. Williamson. "Improved approximation algorithms for maximum cut and satisfiability problems using semidefinite programming". In: *Journal of the ACM* 42.6 (1995), pp. 1115–1145.

[48] M. Grant and S. Boyd. *CVX: Matlab Software for Disciplined Convex Programming, version 1.21*. `http://cvxr.com/cvx`. Oct. 2010.

[49] M. Grant and S. Boyd. "Graph implementations for nonsmooth convex programs". In: *Recent advances in learning and control* (2008), pp. 95–110.

[50] J.K. Hale. "Diffusive coupling, dissipation, and synchronization". In: *Journal of Dynamics and Differential Equations* 9.1 (1997), pp. 1–52.

[51] S.R. Hall and N.M. Wereley. "Generalized Nyquist stability criterion for linear time periodic systems". In: *Proceedings of the American Control Conference*. AACC. 1990, pp. 1518–1525.

[52] Abdullah Omar Hamadeh, G-B Stan, and Jorge Gonçalves. "Robust synchronization in networks of cyclic feedback systems". In: *47th IEEE Conference on Decision and Control*. IEEE. 2008, pp. 5268–5273.

[53] Jeff Hasty, David McMillen, and J. J. Collins. "Engineered gene circuits". In: *Nature* 420.6912 (Nov. 2002), pp. 224–230. URL: `http://dx.doi.org/10.1038/nature01257`.

[54] A. Henrot. *Extremum problems for eigenvalues of elliptic operators*. Basel: Birkhauser, 2006.

[55] Keum-Shik Hong and J. Bentsman. "Direct adaptive control of parabolic systems: algorithm synthesis and convergence and stability analysis". In: *Automatic Control, IEEE Transactions on* 39.10 (1994), pp. 2018–2033. ISSN: 0018-9286. DOI: `10.1109/9.328823`.

[56] R.A. Horn and C.R. Johnson. *Matrix analysis*. Cambridge Univ Pr, 1990.

[57] J. Hsia et al. "A Feedback Quenched Oscillator Produces Turing Patterning with One Diffuser". In: *PLoS Computational Biology* 8.1 (2012), e1002331.

[58] P.A. Ioannou and J. Sun. *Robust Adaptive Control*. Englewood Cliffs, NJ: Prentice Hall, 1996.

[59] A. Jadbabaie, J. Lin, and A.S. Morse. "Coordination of groups of mobile autonomous agents using nearest neighbor rules". In: *IEEE Transactions on Automatic Control* 48.6 (2003), pp. 988–1001.

[60] D.S. Jones, M.J. Plank, and BD Sleeman. *Differential Equations and Mathematical Biology*. Boca Raton, FL: CRC Press, 2010.

[61] M. R. Jovanović, M. Arcak, and E. D. Sontag. "A passivity-based approach to stability of spatially distributed systems with a cyclic interconnection structure". In: *IEEE Transactions on Automatic Control: Special Issue on Systems Biology* 53 (2008), pp. 75–86.

[62] G. Karypis and V. Kumar. "A fast and high quality multilevel scheme for partitioning irregular graphs". In: *SIAM Journal on Scientific Computing* 20.1 (1998), pp. 359–392.

[63] Eugenius Kaszkurewicz and Amit Bhaya. *Matrix diagonal stability in systems and computation*. Birkhauser Boston, 2000.

[64] H.K. Khalil. *Nonlinear Systems*. Englewood Cliffs, NJ: Prentice Hall, 2002.

[65] J. Kim, D.G. Bates, and I. Postlethwaite. "Robustness analysis of linear periodic time-varying systems subject to structured uncertainty". In: *Systems & control letters* 55.9 (2006), pp. 719–725.

[66] J.H. Kim et al. "Multiscale consensus for decentralized estimation and its application to building systems". In: *American Control Conference, 2008*. IEEE. 2008, pp. 888–893.

[67] Kwang-Ki K Kim and Richard D Braatz. "Continuous-and discrete-time D-stability, joint D-stability, and their applications: μ theory and diagonal stability approaches". In: *2012 IEEE 51st Annual Conference on Decision and Control (CDC)*. IEEE. 2012, pp. 2896–2901.

[68] Y. Kim and M. Mesbahi. "On maximizing the second smallest eigenvalue of a state-dependent graph Laplacian". In: *IEEE Transactions on Automatic Control* 51.1 (2006), pp. 116–120.

[69] Y. Kuramoto. "Self-entrainment of a population of coupled non-linear oscillators". In: *International Symposium on Mathematical Problems in Theoretical Physics*. Springer. 1975, pp. 420–422.

[70] L. Ma and P. Iglesias. "Quantifying robustness of biochemical network models". In: *BMC Bioinformatics* 3.1 (2002), p. 38.

[71] J.D. Murray. *Mathematical Biology*. Vol. 2. New York, NY: Springer, 2002.

[72] M. Negahban et al. "A two-chip CMOS read channel for hard-disk drives". In: *40th ISSCC., 1993 IEEE International Solid-State Circuits Conference, 1993. Digest of Technical Papers*. IEEE. 1993, pp. 216–217.

[73] R. Olfati-Saber and R.M. Murray. "Consensus problems in networks of agents with switching topology and time-delays". In: *IEEE Transactions on Automatic Control* 49.9 (2004), pp. 1520–1533.

[74] HG Othmer. "Current problems in pattern formation". In: *Lectures on Mathematics in the Life Sciences* 9 (1977), pp. 57–85.

[75] H.G. Othmer et al. "The intersection of theory and application in elucidating pattern formation in developmental biology". In: *Math. Model. Nat. Phenom* 4.4 (2009), pp. 3–82.

[76] A. Packard and J. Doyle. "The complex structured singular value". In: *Automatica* 29.1 (1993), pp. 71–109.

[77] Alexey Pavlov and Lorenzo Marconi. "Incremental passivity and output regulation". In: *Systems & Control Letters* 57.5 (2008), pp. 400–409.

[78] Louis M Pecora and Thomas L Carroll. "Master stability functions for synchronized coupled systems". In: *Physical Review Letters* 80.10 (1998), pp. 2109–2112.

[79] A. Pogromsky and H. Nijmeijer. "Cooperative oscillatory behavior of mutually coupled dynamical systems". In: *IEEE Transactions on Circuits and Systems I: Fundamental Theory and Applications* 48.2 (2001), pp. 152–162.

[80] G. Russo and M. Di Bernardo. "Contraction theory and master stability function: linking two approaches to study synchronization of complex networks". In: *IEEE Transactions on Circuits and Systems II: Express Briefs* 56.2 (2009), pp. 177–181.

[81] H. Sandberg, E. Mollerstedt, and B. Bemhardsson. "Frequency-domain analysis of linear time-periodic systems". In: *IEEE Transactions on Automatic Control* 50.12 (2005), pp. 1971–1983.

[82] S. Sastry. *Nonlinear systems: analysis, stability, and control*. Springer Verlag, 1999. ISBN: 0387985131.

[83] S. Sastry and M. Bodson. *Adaptive control: stability, convergence, and robustness*. Englewood Cliffs, NJ: Prentice-Hall, 1989.

[84] L. Scardovi, M. Arcak, and E.D. Sontag. "Synchronization of interconnected systems with applications to biochemical networks: An input-output approach". In: *IEEE Transactions on Automatic Control* 55.6 (2010), pp. 1367–1379.

[85] A. J. van der Schaft. *$\mathcal{L}_2$-gain and Passivity Techniques in Nonlinear Control*. Second. New York and Berlin: Springer, 2000.

[86] L.A. Segel and J.L. Jackson. "Dissipative structure: an explanation and an ecological example". In: *Journal of Theoretical Biology* 37.3 (1972), pp. 545–559.

[87] R. Sepulchre, M. Janković, and P. Kokotović. *Constructive Nonlinear Control*. New York: Springer, 1997.

[88] J. Shi and J. Malik. "Normalized cuts and image segmentation". In: *IEEE Transactions on Pattern Analysis and Machine Intelligence* 22.8 (2000), pp. 888–905.

[89] Hal L Smith. *Monotone dynamical systems: an introduction to the theory of competitive and cooperative systems*. Vol. 41. American Mathematical Society, 2008.

[90] J. Smoller. *Shock waves and reaction-diffusion equations*. Vol. 258. New York, NY: Springer, 1994.

[91] G.B. Stan and R. Sepulchre. "Analysis of interconnected oscillators by dissipativity theory". In: *IEEE Transactions on Automatic Control* 52.2 (2007), pp. 256–270.

[92] S.H. Strogatz. "From Kuramoto to Crawford: exploring the onset of synchronization in populations of coupled oscillators". In: *Physica D: Nonlinear Phenomena* 143.1 (2000), pp. 1–20.

[93] J. Sun et al. "The fastest mixing Markov process on a graph and a connection to a maximum variance unfolding problem". In: *SIAM Review* 48.4 (2006), pp. 681–699.

[94] A.R. Teel, L. Moreau, and D. Nešić. "A unified framework for input-to-state stability in systems with two time scales". In: *IEEE Transactions on Automatic Control* 48.9 (2003), pp. 1526–1544.

[95] K.C. Toh, M.J. Todd, and R.H. Tutuncu. "SDPT3—a Matlab software package for semidefinite programming". In: *Optimization Methods and Software* 11.12 (1999), pp. 545–581.

[96] A.M. Turing. "The chemical basis of morphogenesis". In: *Philosophical Transactions of the Royal Society of London. Series B, Biological Sciences* 237.641 (1952), pp. 37–72.

[97] Liancheng Wang and Michael Y Li. "Diffusion-driven instability in reaction–diffusion systems". In: *Journal of mathematical analysis and applications* 254.1 (2001), pp. 138–153.

[98] Wei Wang and Jean-Jacques E. Slotine. "On partial contraction analysis for coupled nonlinear oscillators". In: *Biological Cybernetics* 92 (1 2005), pp. 38–53. ISSN: 0340-1200.

[99] Z. Wen, D. Goldfarb, and W. Yin. "Alternating direction augmented Lagrangian methods for semidefinite programming". In: *Mathematical Programming Computation* (2010), pp. 1–28. ISSN: 1867-2949.

[100] Z. Wen et al. "Row by row methods for semidefinite programming". In: *Technical Report, Department of IEOR, Columbia University* (2009).

[101] N.M. Wereley and S.R. Hall. "Frequency response of linear time periodic systems". In: *Proceedings of the 29th IEEE Conference on Decision and Control*. IEEE. 1990, pp. 3650–3655.

[102] P. Wieland, Jingbo Wu, and F. Allgower. "On Synchronous Steady States and Internal Models of Diffusively Coupled Systems". In: *IEEE Transactions on Automatic Control* 58.10 (2013), pp. 2591–2602. ISSN: 0018-9286. DOI: 10.1109/TAC.2013.2266868.

[103] Peter Wieland, Rodolphe Sepulchre, and Frank Allgöwer. "An internal model principle is necessary and sufficient for linear output synchronization". In: *Automatica* 47.5 (2011), pp. 1068–1074.

[104] J.C. Willems. "Dissipative Dynamical Systems Part I: General theory; Part II: Linear systems with quadratic supply rates". In: *Archive for Rational Mechanics and Analysis* 45 (1972), pp. 321–393.

[105] Andrew Witkin and Michael Kass. "Reaction-diffusion textures". In: *ACM Siggraph Computer Graphics* 25.4 (1991), pp. 299–308.

[106] L. Xiao and S. Boyd. "Fast linear iterations for distributed averaging". In: *Systems & Control Letters* 53.1 (2004), pp. 65–78.

[107] Wenwu Yu et al. "Distributed adaptive control of synchronization in complex networks". In: *IEEE Transactions on Automatic Control* 57.8 (2012), pp. 2153–2158.

[108] G. Zames. "On the input-output stability of time-varying nonlinear feedback systems part one: conditions derived using concepts of loop gain, conicity, and positivity". In: *IEEE Transactions on Automatic Control* 11.2 (1966), pp. 228–238.

[109] J. Zhou and T. Hagiwara. "2-Regularized Nyquist criterion in linear continuous-time periodic systems and its implementation". In: *SIAM Journal on Control and Optimization* 44 (2005), pp. 618–645.

[110] J. Zhou and T. Hagiwara. "H_2 and H_∞ norm computations of linear continuous-time periodic systems via the skew analysis of frequency response operators". In: *Automatica* 38.8 (2002), pp. 1381–1387.